

Division of Solid Mechanics

ISRN LUTFD2/TFHF-11/5162-SE(1-104)

Numerical analysis of a BPHE channel plate section

Master thesis by
Björn Persson

Supervisors
M.Sc Lennie Liegnell, SWEP international AB
Prof. Per Ståhle, Div. of Solid Mechanics

Copyright ©2011 by Div. of Solid Mechanics, SWEP international AB
Björn Persson
Printed by Media-Tryck, Lund University, Lund, Sweden

For information, address:
Division of Solid Mechanics, Lund University, Box 118, SE-221 00 Lund, Sweden.
Homepage: <http://www.solid.lth.se>

Acknowledgment

This master's thesis was carried out at SWEP international AB and within the division of Solid Mechanics at Lund Institute of Technology during the autumn of 2010 and spring of 2011.

I would like to express my gratitude to my supervisors Per Ståhle, Lennie Liegnell and Tor Berggren, as well as Daniel Wallin, Vesna Trebjesanin and the rest of the personal at SWEP International AB for all their help and feedback.

I will also express my appreciation to Per Thilderqvist and Jörgen Hertzman at Industrielt UtvecklingsCentrum in Olofström for their support and help.

A special thanks Ulf Karlsson and Joakim Asklund from Simulia Scandinavia for the help with both the license and support of Abaqus.

Lund may 2011

Björn Persson

Abstract

The development of BPHE within SWEP is going towards larger formats, tougher patterns and thinner materials at the same time the performance must not be jeopardize. The material thinning of the channel plate is a critical part, in worse case even necking or a fracture will emerge due to the material thinning of the plate during pressing.

In this thesis the material thinning and the formability for a certain sheet metal at certain geometry will be treated, both with physical experiments and with a finite element analysis. The physical experiments will then be compared to the finite element analysis to confirm or dismiss the result. These finite element analyses are going to be the foundation for future investigation.

The physical test made for the comparison was divided into two separate test for measuring the thickness and formability for the channel plates. This was done with metallurgy and forming limit curves/diagrams. Metallurgy measure the actual thickness from a sliced channel plate. Forming limit curves measure the formability of the steel and forming limit diagrams measure the strain of geometry on the channel plat. The finite element analysis was made in Abaqus with an explicit, quasi-static code and hills 1948 yield criterion.

The result from the experiments showed that the material thinned out by approximate 9% locally in the most critical area. While the finite element analysis gave material thinned out by approximate 30%. Future investigation showed that in overall the experiments and the finite element analysis gave approximately the same result and thinning pattern over the geometry. It also showed the region where the possibility of material failure is prevalent, which is in the upper part of the scallop end as expected.

List of Abbreviations

BPHE - Brazed plate heat exchanger
ASTM – American Society for Testing Material
GL - Gage length
IUC - Industriellt utvecklingscentrum
FLC – Forming limit curve
FLD - Forming limit diagram
FEA - Finite element analysis
EDM - Electrical discharge machining

Table of Contents

Acknowledgment	i
Abstract	ii
List of Abbreviations	iii
1 Introduction	1
1.1 Background	2
1.2 Purpose	2
1.3 Objective	2
1.4 Delimitations	3
1.5 Disposition	3
2 Material Properties	4
2.1 Anisotropy	4
2.2 Determination of r-value	5
2.3 Surface Treatment	6
3 Sheet metal forming	8
3.1 Deep drawing & Stretch forming	8
3.2 Forming “window”	9
3.3 Failure	9
3.4 Measuring	10
4 Theory	11
4.1 Continuum Mechanics	11
4.2 Stress tensors	14
4.3 Plasticity	15
4.3.1 Yield criterion	15
4.3.2 Plasticity of large deformation	16

4.3.3 Hill 1948.....	17
4.4 Nonlinearity	19
5 FEA Theory	20
5.1 Time Integration Methods.....	20
5.1.1 Implicit	21
5.1.2 Explicit.....	22
5.1.3 Comparison Implicit/Explicit.....	24
5.2 Quasi-static	25
5.3 Mass scaling	25
5.4 Integration points	26
5.5 Contact.....	27
6 Experiments	29
6.1 Tensile test.....	29
6.2 Friction	32
6.2.1 Angle of friction	33
6.2.2 Dynamometer.....	34
6.3 Press settings	35
6.4 Forming limit curve and forming limit diagrams	36
6.4.1 Forming limit curve.....	36
6.4.2 Forming limit diagram (FLD) on a channel plate	37
Metallurgy.....	38
7 Sheet metal simulation	39
7.1 Geometry	39
7.2 General Set up.....	41
7.2.1 Material data	41
7.2.2 Time step and Increments	42
7.2.3 Velocity	42
7.2.4 Step.....	43
7.3 Finite Element Analysis (FEA).....	44
7.3.1 The 2D analysis	44

7.3.2 The 3D analysis	46
8 Results	51
8.1 Experiments	51
8.1.1 Metallurgy.....	51
8.1.2 Forming limit curve/diagram	54
8.2 Simulation	56
9 Comparison	59
9.1 Metallurgy.....	59
9.2 Forming limit curve/diagram	61
10 Discussion and future work	67
10.1 Conclusion.....	67
10.2 Reliability of the experiments	67
10.3 Future work.....	68
References	69
Appendix 1	70
Appendix 2	72
Appendix 3	80
Appendix 4	84

Chapter 1

Introduction

SWEP is a rapidly growing international company in the heat transfer field. SWEP is represented in more than 50 countries and has its own dedicated sales force in more than 20 countries. SWEP has production units in Sweden, Switzerland, USA, Malaysia, Slovakia and China.

SWEP International AB was founded 1983 in Sweden and is a part of the Dover Corporation.

SWEP is the world's leading supplier of Compact Brazed Heat Exchanger (BPHE). These products are used where heat needs to be transferred efficiently in air conditioning, refrigeration, heating and industrial applications. SWEP has annual sales of USD 250 million.

The BPHE is one of the most efficient ways to transfer heat from one medium to another. A BPHE consists of corrugated plates combined to create complex channels through which a hot medium and a cold medium can be distributed. The mediums come into close proximity inside the BPHE, on each side of the corrugated plate without mixing, where energy is transferred from one to the other as they flow side-by-side. The modular product concept, with totally customizable parts, means the right product solution for every application can always be found.

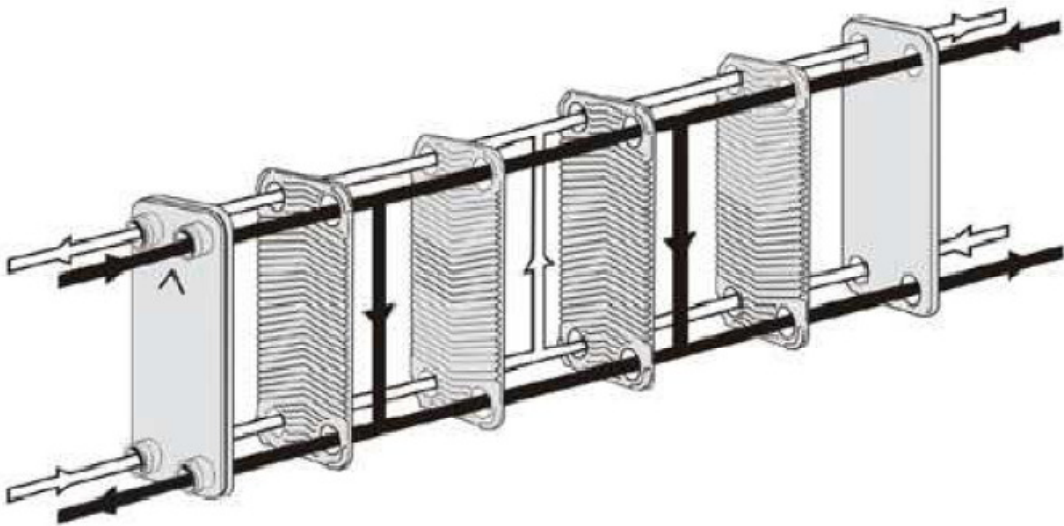


Figure 1.1. Exploded view of a BPHE

1.1 Background

The development of BPHE within SWEP is going towards larger formats, tougher patterns and thinner materials. The requirements for the products are increasing while margins are decreasing in pursuit of cost and competitiveness.

The latest plate designs are on the edge of what is possible in the existing process, in terms of press force, materials and tools.

By extreme drawing and stretching of the plate, the tension locally exceeds the ultimate tensile strength in critical areas so that thinning of the material occur, and in the worse cases even necking arises. This can be controlled by changing the geometry, press settings and/or lower the friction in the pressing operation.

How critical this thinning is depends on the material, if the geometry is tampered with to fit the need of the “worse” material then the properties of the BPHE will get changed as well. If instead the friction is decreased and/or the press setting is changed then the originally geometry can be used for all materials in use.

1.2 Purpose

To control what impact the different parameters have on the BPHE, a simulation of the pressing process is of great advantages. In the process of today the effect of a changed parameter are evaluated by a series of physical tests that both are time consuming and expensive.

The purpose of this master’s thesis is to create a starting point of such a tool, to shorten the time and cost in order to develop new designs and changes of the parameters.

1.3 Objective

This thesis will consist of preparation of physical test models in order to measure the tensions that arise and verifying the calculated material thinning from the physical tests.

Gathering parameters that describes the forming process to identify parameters like friction coefficient, loads and constrains, to set current state / baseline.

Develop a Finite element analysis (FEA) that will show material thinning of a critical area when pressing a channel plate.

Verify the FEA by physical tests

Construct a theoretical model for predicting the severity in the critical areas.

1.4 Delimitations

This project will be focus around SWEP's BPHE B80 (from here on referred as B80) which is one of the BPHE's that are most likely to have critical thinning of the material.

The mechanical properties of SWEP's presses differ from press to press due to different factors, because of this only B80 produced in press line 10 will be used for this project.

As early mentioned, the material plays a big part in to the likelihood of thinning of the material. SWEP is currently (2010-09-24) using 5 suppliers of 316 and 316L steel which is used in the B80. The material properties differ from supplier to supplier and how the material is stored before usage. To freeze the material properties a coil from one of the suppliers was blocked and stored at room temperature (20° C) before usage.

1.5 Disposition

The parameters in the current process were determined by a series of tests, which was preformed both internally by SWEP and externally.

The FEA were then preformed at different stages in Abaqus/Explicit both as 2D model and in 3D model for a small part of the BPHE.

Chapter 2

Material Properties

The material used in SWEP's BPHE is stainless steel of the type 316 and 316L according to the ASTM standard. Stainless steel is isotropic from the start but due to the rolling of the sheet metal the metal becomes anisotropic. 316 and 316L are almost identical, the mechanical properties are the same, which is shown in the table 2.1. The difference between 316 and 316L are that 316L has lower carbon content than 316. The material properties differs from supplier to supplier and because of that this thesis is looked to material from ThyssenKrupp with the steel type 316.

	Yield Strength 0.2 $R_{p0.2}$ [MPa]	Tensile Strength R_M [MPa]	Max. Elongation (A80) [%]
316	> 240	530 - 680	>40
316L	>240	530 - 680	>40

Table 2.1 Mechanical properties for 316 and 316 L steel
(Eube, J. Stahl – Tabellenbuch für die Auswahl und Anwendung)

2.1 Anisotropy

As the material gets rolled to sheet metal, the stainless steel change from isotropic to anisotropic, since the grains in the material gets stretched. Due to symmetry the metal becomes orthotropic with the three orientations: rolling direction (1), transverse direction (2) and normal direction (3), see figure 2.1. This anisotropy is measured by the materials anisotropy coefficient r-value, which is determined by uniaxial tensile test. For more information consult [1].

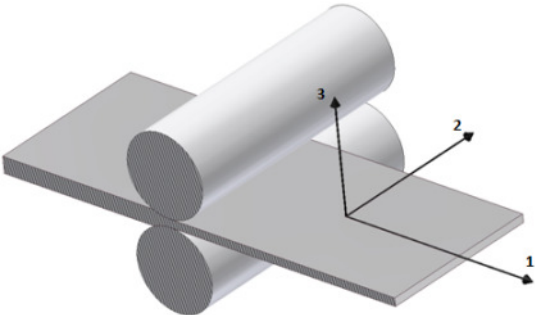


Figure 2.1 Sheet metal directions

2.2 Determination of r-value

As mention above the r-value is determined by uniaxial tensile test measuring the true strain in width direction and thickness direction, the r-value can then be calculated by equation 2.1. For isotropic material the r-value is equal to one. However due to that the thickness of the specimen is very small compared to its width, equation 2.1 can be replaced by equation 2.3. This can be done if the volume is assumed to be constant, equation 2.2 where figure 2.2 shows the orientation.

$$r = \frac{\epsilon_w}{\epsilon_T} \quad (2.1)$$

If the volume can be set as constant the strain can be written as:

$$\epsilon_w + \epsilon_T + \epsilon_L = 0 \quad (2.2)$$

$$r = -\frac{\epsilon_w}{\epsilon_L + \epsilon_w} = \frac{\ln\left(\frac{W}{W_0}\right)}{\ln\left(\frac{L_0 \cdot W_0}{L \cdot W}\right)} \quad (2.3)$$

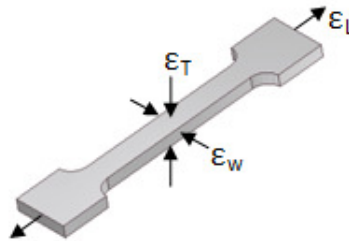


Figure 2.2 Width-, Thickness- and Length Strain ($\epsilon_w, \epsilon_T, \epsilon_L$)

The r-value is measured in different stages during the uniaxial tensile test, usually this is done in steps of 5% of the length strain (ϵ_L) until necking. How this measured in this thesis can be read in chapter 6.

As early mentioned the sheet metal is orthotropic, thereby samples are taken in three different directions in the plane: rolling, transverse and 45 degrees see figure 2.3. The coefficient of normal (also called average) anisotropy (r_n) is determined by equation 2.4.

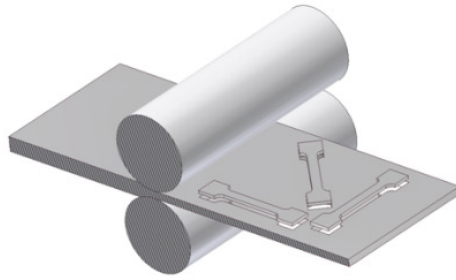


Figure 2.3 Tensile specimen in 0°, 45° and 90° to the rolling direction

$$r_n = \frac{r_0 + 2r_{45} + r_{90}}{4} \quad (2.4)$$

This can be used as a measure for thinning resistance as a large normal anisotropy indicates a domination in width is consequently restrict a thickness reduction.

A measure of variation of the normal anisotropy with the angle is given with planar anisotropy, the planar anisotropy (Δr) is determined by:

$$\Delta r = \frac{r_0 - 2r_{45} + r_{90}}{2} \quad (2.5)$$

A large planar anisotropy will result in ears during deep-drawing and uneven thinning of the material. The optimum combination for deep-drawing is high normal anisotropy and low planar anisotropy. For more information regarding the r-value consult [1].

2.3 Surface Treatment

The surface treatment is also an important part of the material properties, in table 2.2 the different types of surface treatment is shown.

Material code	Treatment	Surface condition
2H	Cold-worked	Blank
2C	Cold-rolled, heat-treated, not descaled	Clogged
2E	Cold-rolled, heat-treated, mechanically descaled	Rough and dull
2D	Cold-rolled, heat-treated, pickled	Clogged
2B	Cold-rolled, heat-treated, killed	Clogged
2R	Cold-rolled, bright-annealed	Clogged, shiny
2Q	Cold-rolled, hardened and tempered, scale-free	Scale-free

Table 2.2. Surface treatments of steels
(Eube, J. Stahl – Tabellenbuch für die Auswahl und Anwendung)

The material that SWEP use for its BPHE is 316/316L with surface treatment 2B and 2R which gives a R_a value according to table 2.3:

Surface finish	Surface Roughness R_a [μm]
2B	0.1 – 0.5
2R	0.05 – 0.1

**Table 2.3. The two types of surface treatments in use
(British Stainless Steel Association, 2010)**

According to material specification from ThyssenKrupp that followed that specific coil that is used for this master's thesis the surface finish is 2B.

Chapter 3

Sheet metal forming

The major manufacturing process at SWEP is sheet metal forming, that consist of a cutting operation and pressing operation. From here on a plate that is cut but not pressed will be known as a raw plate, see figure 3.1 and a plate that has been pressed a channel plate. This master thesis has its focus on pressing, moreover built in residual stress and strains in the raw plate from the cutting operation are neglected in this thesis. This residual stress and strains are expected to be low as the cutting operation is mostly pure shear.

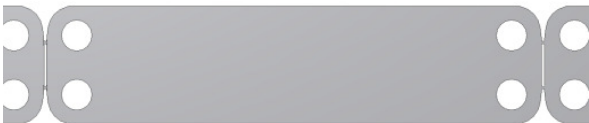


Figure 3.1. Raw plate

3.1 Deep drawing & Stretch forming

The sheet metal forming that is done by SWEP is a combination of both stretch forming and deep drawing (mainly stretch forming). This thesis is focused on stretch forming the reason of this is that it is under this type of operation that thinning of the material occurs.

To say exactly where the different types of drawing occurs is a bit hard, due to that it differ depending on where in the drawing process it is. In the first contact between the tool and the plate there is deep drawing but as the contact between the upper tool and the plate is made there will be stretch forming. Figure 3.4 illustrate how the plate “bends” in one direction in the final stage.



Figure 3.2. Stretch forming

Figure 3.3. Deep Drawing



Figure 3.4. Bended plate after forming

Stretch forming

As shown in figure 3.2 the stretch forming process reduces the thickness of the sheet metal which in worse case may lead to necking. The blank holder is holding the plate during the operation and by so stopping the material from flowing and making it stretch which leads to material thinning.

Deep drawing

In contrast to stretch forming the sheet metal thickness will be constant during the deep drawing operation as it is free to flow. The blank holder shown in figure 3.3 is mainly there to prevent wrinkles.

For more information consult [1].

3.2 Forming “window”

Sheet metal forming is performed in the plastic zone of the material there become a “window” of formability which is bounded by the yield stress and the ultimate stress, see figure 3.5. This factor is determined by tensile test, which will be done in chapter 6. Another way to express this window of formability is through a forming limit curve (FLC) which will be explained in chapter 6.

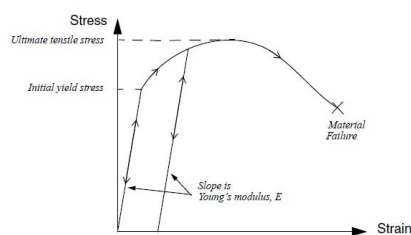


Figure 3.5. Stress Strain diagram
(Getting started with Abaqus)

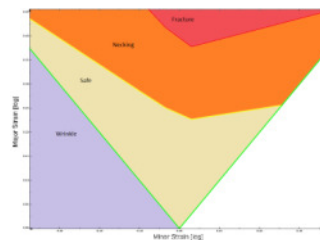


Figure 3.6. Forming limit curve

3.3 Failure

How severe the thinning of material in the channel plates can be difficult to determine and this is up to the experience of the operator. The severity of the thinning can differ from where in the roll of steel the material comes. Because of this some of the channel plates that are pressed in the beginning of the steel coil can be above acceptable thickness, nevertheless channel plates that are pressed from the same coil but from the middle of the coil can be under the acceptable thickness. This is something that is depending on the supplier and nothing that can be predicted by the operators. Thereby this can only be measured from random samples, this is measured by ocular inspection. The line between critical (necking) and accepted thinning is up to the experience of the operator.

When a BPHE with necking is brazed some of the brazing filler is melted in to the thinned out area, which gives the BPHE temporary strength. This will give a fatigue problem with great decreases of the BPHE lifespan. Figure 3.7 shows this “necking” and figure 3.8 shows a BPHE that has been claimed due to the necking.



Figure 3.7. Sever thinning that has started to neck

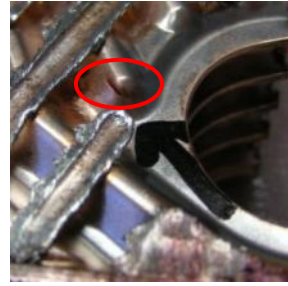


Figure 3.8. Failure due to fatigue/necking

3.4 Measuring

It is very difficult to measure how thin the material has become, but it can be done in two ways: one of them is with forming limit diagrams, another way is through metallurgy which gives us the actual thickness. This will be described in chapter 6.

These methods give us a hint about how the material acts due to different changes in parameters in the forming process.

Nevertheless this can only be done on channel plates that are not going to be used in an actual BPHE. The only way to measure the necking of the material in production today is by ocular inspection from the operator, what the operator is looking for is material thinning or necking that looks like figure 3.7.

Chapter 4

Theory

This chapter will explain the theory behind Continuum mechanics and solid mechanics. In the next chapter the theory behind the finite element analysis will be explained.

4.1 Continuum Mechanics

An un-deformed body at the time $t=0$ in a fix Cartesian coordinate system is used as a reference configuration which have a particle at the coordinate $\mathbf{X}^T=[X Y Z]$. With a displacement of the body the deformed configuration will have the same particle at the new coordinate $\mathbf{x}^T=[x y z]$.

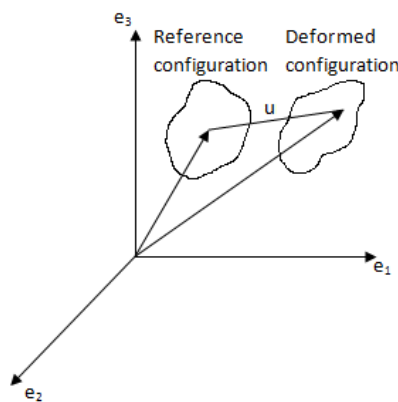


Figure 4.1. Configurations

This can be written as:

$$\mathbf{x} = \mathbf{x}(P, t) \quad (4.1)$$

Where P is the particle for which the coordinates describe at the time t . The relationship between the two bodies can be expressed as equation 4.2. Where \mathbf{X} is as early described refereeing to the reference configuration.

$$\mathbf{x} = \mathbf{x}(\mathbf{X}) = \mathbf{X} + \mathbf{u} \quad (4.2)$$

This description of the current description is called material or Lagrangian which describes the displacement for a certain particle. For more information consult [2] and [5].

Two neighboring particles are located apart from each other by the vector $d\mathbf{X}$, and in the deformed configuration as $d\mathbf{x}$. The relation between $d\mathbf{X}$ and $d\mathbf{x}$ is:

$$d\mathbf{x} = \mathbf{F}d\mathbf{X} \quad (4.3)$$

\mathbf{F} is called the deformation gradient tensor

$$\mathbf{F} = \begin{bmatrix} \frac{\partial x}{\partial X} & \frac{\partial y}{\partial X} & \frac{\partial z}{\partial X} \\ \frac{\partial x}{\partial Y} & \frac{\partial y}{\partial Y} & \frac{\partial z}{\partial Y} \\ \frac{\partial x}{\partial Z} & \frac{\partial y}{\partial Z} & \frac{\partial z}{\partial Z} \end{bmatrix} \quad (4.4)$$

The length of the vectors $d\mathbf{X}$ and $d\mathbf{x}$ is denoted by dS and ds , respectively, and is determined by equation 4.5 and 4.6.

$$dS^2 = d\mathbf{X}^T d\mathbf{X} \quad (4.5)$$

$$ds^2 = d\mathbf{x}^T d\mathbf{x} \quad (4.6)$$

From Green's strain it follows:

$$\varepsilon_G = \frac{ds^2 - dS^2}{2dS^2} \quad (4.7)$$

From equation 4.3, 4.5 and 4.7 it follows

$$\mathbf{E} = \frac{1}{2}(\mathbf{F}^T \mathbf{F} - \mathbf{I}) \quad (4.8)$$

This is known as Green-Lagrangian strain tensor. The velocity between the particles in question can be expressed as follow:

$$\mathbf{v} = \frac{d\mathbf{x}}{dt} \quad (4.9)$$

The velocity difference between the two neighboring particles for the deformed configuration can then be expressed as

$$d\mathbf{v} = \frac{d\mathbf{v}}{d\mathbf{x}} d\mathbf{x} \quad (4.10)$$

From this equation the gradient called the velocity gradient tensor can be extracted

$$\mathbf{L} = \frac{d\mathbf{v}}{d\mathbf{x}} \quad (4.11)$$

From equation 4.10 equation 4.11 can be written as

$$d\mathbf{v} = \mathbf{L}d\mathbf{x} = \mathbf{L}\mathbf{F}d\mathbf{X} \quad (4.12)$$

Another way to obtain the velocity difference is from equation 4.3 and 4.9

$$d\mathbf{v} = \frac{d}{dt}(\mathbf{F}d\mathbf{X}) = \dot{\mathbf{F}}d\mathbf{X} \quad (4.13)$$

Where

$$\dot{\mathbf{F}} = \frac{d\mathbf{F}}{dt} \quad (4.14)$$

Equation 4.3 and 4.13 then give

$$\mathbf{L} = \dot{\mathbf{F}}\mathbf{F} \quad (4.15)$$

\mathbf{L} can now be decomposed into one symmetric part \mathbf{D} and one antisymmetric part \mathbf{W}

$$\mathbf{L} = \mathbf{D} + \mathbf{W} \quad (4.16)$$

Where

$$\mathbf{D} = \frac{1}{2}(\mathbf{L} + \mathbf{L}^T) \quad (4.17)$$

And

$$\mathbf{W} = \frac{1}{2}(\mathbf{L} - \mathbf{L}^T) \quad (4.18)$$

\mathbf{D} is the rate of deformation tensor and \mathbf{W} is called the spin tensor

Equation 4.12 can now be rewritten as:

$$d\mathbf{v} = (\mathbf{D} + \mathbf{W})d\mathbf{x} \quad (4.19)$$

From this it can easily be seen that if \mathbf{D} is equal to zero, then the motion is a pure rigid body motion. Likewise if \mathbf{W} is equal to zero, then the motion is a pure deformation without any rigid body motion. For more information consult [2], [5] and [6]

4.2 Stress tensors

To get a deeper understanding about how the stress is connected to continuum mechanics the relation between the stress for the current configuration and the reference configuration must be sorted up. This is done by the Cauchy and Kirchhoff stress tensors. For more interested read consult [5] and [6]

Traction vector

The traction vector contains the normal force and the shear stress acting on an arbitrary point in the cross-section. To get the complete description of the arbitrary point in the cross-section, three orthogonal cross-section through the point has to be made. For small deformations this state is fully described by Cauchy stress tensor.

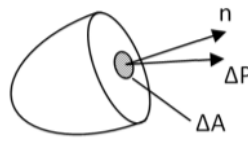


Figure 4.2. Arbitrary body

$$\tau = \frac{\Delta P}{\Delta A} \quad (4.20)$$

Cauchy stress tensor

The Cauchy stress tensor also known as the true stress tensor is referred to the current configuration.

$$\sigma = \frac{F}{A} \quad (4.21)$$

Where F is the applied force and A is the current area.

The Cauchy stress (also known as the true stress) relates to the traction vector by equation 4.22.

Where n is normal vector to the boundary point.

$$\tau = n\sigma \quad (4.22)$$

Kirchhoff stress

Kirchhoff stress on the other hand refers to the reference configuration and are frequently used in finite strain plasticity. Kirchhoff stress relates to Cauchy stress tensor by

$$\mathbf{T} = J\sigma \quad (4.23)$$

Where

$$J = \det(\mathbf{F}) \quad (4.24)$$

For an incompressible material the volume ratio (J) is equal to 1 i.e. the two stress tensors Cauchy and Kirchhoff is equal.

4.3 Plasticity

When the initial yield stress is exceeded, plastic strain will develop and permanent deformations will occur. There is no unique relation between the stress and strain as for the elastic part that can be expressed by Hookes law. For more information regarding plasticity consult [3] and [8]

4.3.1 Yield criterion

Yield criterion describes how the material reacts during the transition from elastic to the plastic phase, which means that the yield stress is the minimum stress needed to permanently deform a material. After this transition every stress higher than the last will give a new permanently deformation. This change of the yield surface is called hardening. The transition is described by the yield surface which is defined as:

$$F(\sigma, K^\alpha) = 0 \quad (4.25)$$

Where K^α are hardening parameters that decides how the current yield surface change size, position and shape with plastic loading. These hardening parameters depend on internal variables k^β . These internal variables memorize the plastic loading history. There is a unique relation between the hardening parameter K^α and the internal variable k^β .

$$K^\alpha = K^\alpha(k^\beta) \quad (4.26)$$

For isotropic hardening the yield surfaces can be described by von Mises criterion in the deviatoric plane, where a cylinder goes through an octahedral plane (a plane that has equal angles to the three principal stress directions see figure 3). The diameter of the cylinder is equal to the yield surface.

If $F(\sigma, K^\alpha) < 0$ i.e. inside the circle only elastic response occurs. In the current yield surface $F(\sigma, K^\alpha) = 0$.

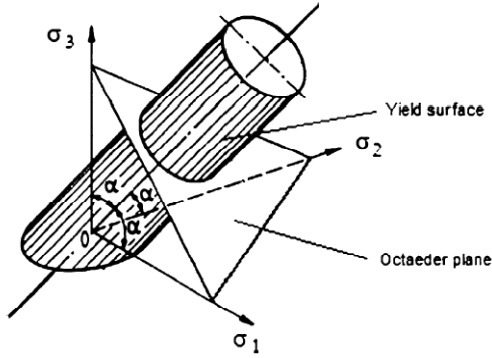


Figure 4.3. Octahedral plane

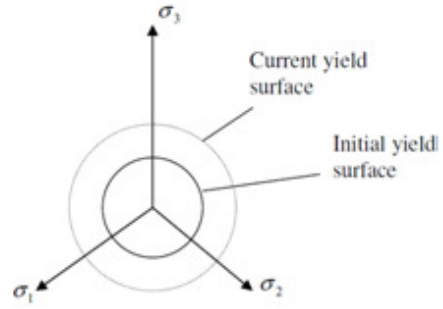


Figure 4.4. Yield surfaces

4.3.2 Plasticity model for large deformation

When considering large deformations the rate of deformation (equation 4.17) is used to determine how the yield surface moves. Just as for the strain the rate of deformation can be divided into elastic and a plastic part according to equation 4.27.

$$\mathbf{D} = \mathbf{D}^e + \mathbf{D}^p \quad (4.27)$$

The plastic part of the rate of deformation is the outwards normal to the yield surface, this can be expressed by the associated flow rule, equation 4.28.

$$\mathbf{D}^p = \dot{\lambda} \frac{\partial f}{\partial \boldsymbol{\sigma}} \quad (4.28)$$

Where $\dot{\lambda}$ is the effective plastic rate of deformation according to equation 4.29. The direction of the normal is given by the gradient $\frac{\partial f}{\partial \boldsymbol{\sigma}}$.

$$\dot{\lambda} = D_{eff}^p = \sqrt{\frac{2}{3} (\mathbf{D}^p)^T \mathbf{D}^p} \quad (4.29)$$

If strain hardening is assumed, the hardening parameter can be described by equation 4.30.

$$k = \int D_{eff}^p dt \quad (4.30)$$

4.3.3 Hill 1948

Hill is an extension of von Mises yield criterion that handles anisotropy (orthotropic symmetry planes) and is widely used in the industry do to its simplicity. Mainly because all you need to determined the input parameters is a uniaxial tensile test.

If the material is isotropic i.e. the r-value is equal to one hill 1948 reduce von Mises yield criterion.

The yield surface is described by:

$$F(\sigma, K^\alpha) = \sqrt{\sigma_{y0}^2 \mathbf{s}^T \mathbf{P} \mathbf{s}} - \sigma_{y0} - K^\alpha (k^\beta) \quad (4.31)$$

Where

$$\sigma_{y0} = \sqrt{\frac{3}{2(F + G + H)}} \quad (4.32)$$

And \mathbf{s} is the deviatoric stress:

$$\mathbf{s} = \boldsymbol{\sigma} - \frac{1}{3} \boldsymbol{\sigma} \delta \quad (4.33)$$

Alternative:

$$\bar{\sigma} = \sqrt{F(\sigma_{22} - \sigma_{33})^2 + G(\sigma_{33} - \sigma_{11})^2 + H(\sigma_{11} - \sigma_{22})^2 + 2L\sigma_{23}^2 + 2M\sigma_{31}^2 + 2N\sigma_{12}^2} \quad (4.34)$$

If F=G=H=L=M=N=1 then equation 4.34 is equal to von Mises criterion as earlier mentioned.

When the anisotropy is orthotropic the P tensor from equation 4.31 takes the following shape.

$$\mathbf{P} = \begin{bmatrix} A & -F & -G & 0 & 0 & 0 \\ -F & B & -H & 0 & 0 & 0 \\ -G & -H & C & 0 & 0 & 0 \\ 0 & 0 & 0 & 2L & 0 & 0 \\ 0 & 0 & 0 & 0 & 2M & 0 \\ 0 & 0 & 0 & 0 & 0 & 2N \end{bmatrix} \quad (4.35)$$

Where

$$A = F + G \quad B = F + H \quad C = G + H \quad (4.36)$$

$$F = \frac{1}{2} \left(\frac{1}{(\sigma_{y0}^{11})^2} + \frac{1}{(\sigma_{y0}^{22})^2} - \frac{1}{(\sigma_{y0}^{33})^2} \right) \quad G = \frac{1}{2} \left(\frac{1}{(\sigma_{y0}^{11})^2} + \frac{1}{(\sigma_{y0}^{33})^2} - \frac{1}{(\sigma_{y0}^{22})^2} \right) \quad H = \frac{1}{2} \left(\frac{1}{(\sigma_{y0}^{22})^2} + \frac{1}{(\sigma_{y0}^{33})^2} - \frac{1}{(\sigma_{y0}^{11})^2} \right) \quad (4.37)$$

$$L = \frac{3}{2(\sigma_{y0}^{23})^2} \quad M = \frac{3}{2(\sigma_{y0}^{13})^2} \quad N = \frac{3}{2(\sigma_{y0}^{12})^2}$$

In sheet metal forming the anisotropy for the material is described by the r-values instead of the yield stress, see equation 4.38. By using equation 4.38 and the parameters F,G,H and N can now be used to describe the r-values, see equation 4.39.

$$F = \frac{r_0}{r_{90}(1+r_0)} \quad G = \frac{1}{(1+r_0)} \quad H = \frac{r_0}{(1+r_0)} \quad N = \frac{(r_0+r_{90})(1+2r_{45})}{2r_{90}(1+r_0)} \tag{4.38}$$

$$r_0 = \frac{H}{G} \quad r_{90} = \frac{H}{F} \quad r_{45} = \frac{N}{F+G} - \frac{1}{2} \tag{4.39}$$

How this is implemented in Abaqus can be read in chapter 7. In which way the different r-values effect the yield surface can be seen in figure 4.5-4.8, where r is the average r-value (see chapter 2). For more information regarding Hill 1948 consult [3], [A2],[A5] and [6].

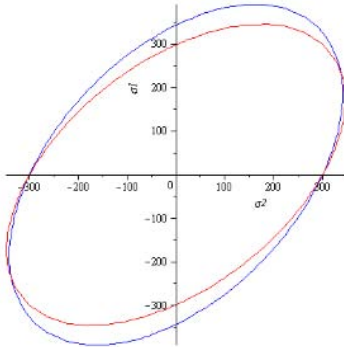


Figure 4.5. Comparison between von Mises and Hill (blue-Hill Red-von Mises)

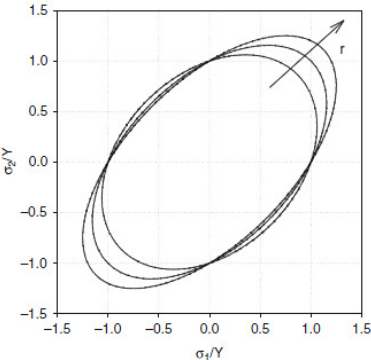


Figure 4.6 r-values impact on the yield surface (Banabic D. Sheet Metal Forming Processes)

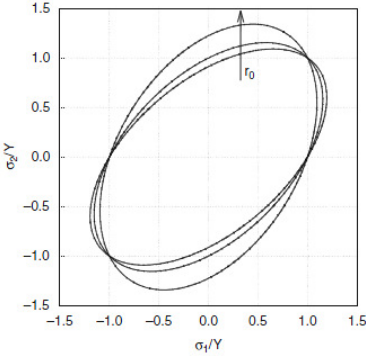


Figure 4.7. r₀ impact on the yield surface (Banabic D. Sheet Metal Forming Processes)

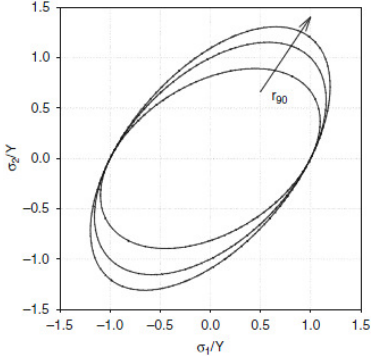


Figure 4.8. r₉₀ impact on the yield surface (Banabic D. Sheet Metal Forming Processes)

4.4 Nonlinearity

Depending on how the structures geometry, boundary conditions and/or material are it will become nonlinear at some point if it is not already nonlinear from the start.

Material nonlinearity

Material nonlinearity is the type of nonlinearity most people think of when they hear nonlinearity, and is when the material shows nonlinear properties which could be the material enter the plastic zone after initial yielding (figure 4.9). Or if the material like rubber is reversible elastic see figure 4.10.

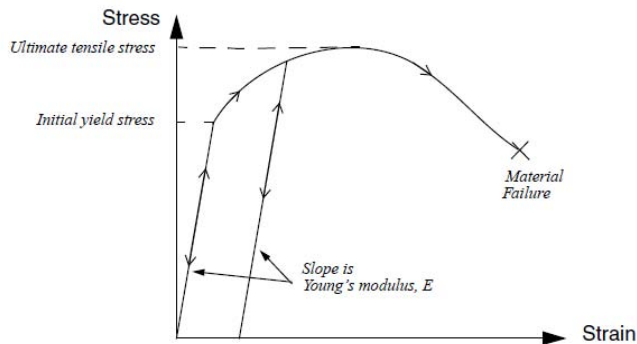


Figure 4.9. Typical stress strain diagram for a metal
(Getting started with Abaqus)

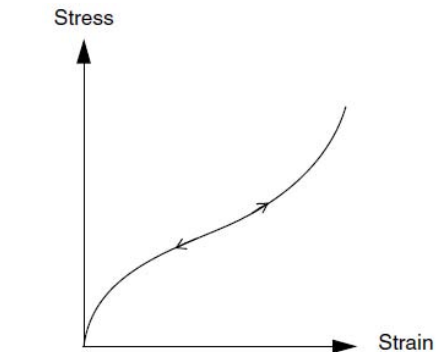


Figure 4.10. Stress strain for reversible elastic
(Getting started with Abaqus)

Boundary nonlinearity

Occur when a structures boundary conditions changes during the analysis, for example when the blank meets the die. This is approximately true for all sorts of contacts.

Geometric nonlinearity

Depending on how the geometry changes during the analysis it may become nonlinear. This may be cause by:

- Large displacements
- “Snap through/back”
- And so on

When considering sheet metal forming, all of above types of nonlinearity is meet, thereby the problem is highly nonlinear.

Chapter 5

FEA Theory

5.1 Time Integration Methods

Sheet metal forming is a dynamic problem, and due to this time integration needs to be performed. There are two ways to perform time integration, explicit and implicit.

The dynamic problem can be explained by Newmark as:

$$\mathbf{M}\ddot{\mathbf{u}} + \mathbf{g}(\mathbf{u}, \dot{\mathbf{u}}) = \mathbf{f}(t) \quad (5.1)$$

Where \mathbf{M} is the mass matrix and \mathbf{g} the internal force which depends on the displacement \mathbf{u} , \mathbf{f} is the external force as a function of time.

Abaqus use Hilber-Hughes-Taylor (HHT) which is α method (i.e. a generalization of the Newmark time integration scheme) there by equation 5.1 become:

$$\mathbf{M}\ddot{\mathbf{u}} + (1 + \alpha) * \mathbf{g}(\mathbf{u}, \dot{\mathbf{u}}) = (1 + \alpha) * \mathbf{f}(t) \quad (5.2)$$

To calculate the differential both the Newmark and the HHT time integration scheme, use:

$$\mathbf{a}_{n+1} = \mathbf{a}_n + \Delta t \dot{\mathbf{a}}_n + \frac{\Delta t^2}{2} [(1 - 2\beta)\ddot{\mathbf{a}}_n + 2\beta\ddot{\mathbf{a}}_{n+1}] \quad (5.3)$$

$$\dot{\mathbf{a}}_{n+1} = \dot{\mathbf{a}}_n + \Delta t [(1 - \gamma)\ddot{\mathbf{a}}_n + \gamma\ddot{\mathbf{a}}_{n+1}] \quad (5.4)$$

Where's $0 < \beta < 1/2$ and $0 < \gamma < 1$, the value of β and γ differ between implicit and explicit, what effect this has will be discussed later in this chapter.

These parameters are controlled by the α parameter in the HHT. If α is equal to zero then the HHT and Newmark is the same. These parameters are chosen according to what method (type of problem) that's going to be used see table 5.1. Later in this chapter it's shown that by choosing method from this table you also choose if the time integration is going to be explicit or implicit.

METHOD	γ	β	δ	$\frac{\Delta t}{T_{MSR}}$	ACCURACY
Central Difference	1/2	0	0	0.3183	Excellent for small Δt Unstable for large Δt
Linear Acceleration	1/2	1/6	0	0.5513	Very good for small Δt Unstable for large Δt
Average Acceleration	1/2	1/4	0	∞	Good for small Δt No energy dissipation
Modified Average Acceleration	1/2	1/4	$\frac{\Delta \Gamma}{\pi}$	∞	Good for small Δt Energy dissipation for large Δt

**Table 5.1. Parameters for Newmark/HHT
(Dynamic Analysis by Integration)**

5.1.1 Implicit

The implicit scheme is the most common solver and gives a correct solution with the help of iteration, and is used for long load durations.

A widely used method to solve the implicit algorithm is to linearise the equation at a given point, for obvious reasons this may give a false result to non linear function, this procedure is repeated until a correct result is located. Newton-Rahpson is method that is iterates every increment this is a method that is often used for implicit solvers.

In the implicit method the weight function goes backwards there by the parameters β and γ differs from zero there by giving the equation 5.3 the following look:

$$\ddot{\mathbf{a}}_{n+1} = \frac{1}{\beta \Delta t^2} (\mathbf{a}_{n+1} - \mathbf{a}_n) - \frac{1}{\beta \Delta t} \dot{\mathbf{a}}_n - \frac{1 - 2\beta}{2\beta} \ddot{\mathbf{a}}_n \quad (5.5)$$

Here the step and the current parameters are known at the time t_n . The equation 5.1 can now be calculated by inserting equation 5.5, which then give:

$$\mathbf{M} \left[\frac{1}{\beta \Delta t^2} (\mathbf{a}_{n+1} - \mathbf{a}_n) - \frac{1}{\beta \Delta t} \dot{\mathbf{a}}_n - \frac{1 - 2\beta}{2\beta} \ddot{\mathbf{a}}_n \right] + \mathbf{g}(\mathbf{a}_{n+1}) - \mathbf{f}(\mathbf{a}_{n+1}) = 0 \quad (5.6)$$

The value of the next increment (\mathbf{a}_{n+1}) is first approximated then it is control and recalculated by the iteration steps until de residual is acceptable, see figure 5.1.

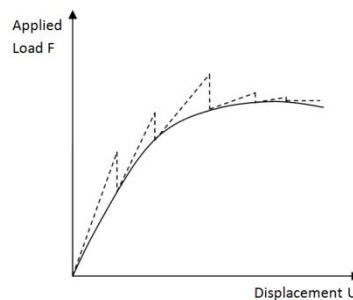


Figure 5.1. Implicit curve

5.1.2 Explicit

Explicit schemes are often used for problems with: high-speed dynamics, complex contact problems, material failure etc.

In general, explicit schemes are used for short duration of load like crash test, shock loads etc.

The explicit method is based on the current configuration and calculates the configuration on a later time from the current configuration by the equation of motion in equation 5.1. The explicit scheme is a full forward Euler scheme and by choosing the Central Difference method presented in table 5.1 the parameters β , γ and α become 0, $\frac{1}{2}$ and 0 respectively, Equations 5.3 and 5.4 can now be written:

$$\mathbf{a}_{n+1} = \mathbf{a}_n + \Delta t \dot{\mathbf{a}}_n + \frac{\Delta t^2}{2} \ddot{\mathbf{a}}_n \quad (5.7)$$

$$\dot{\mathbf{a}}_{n+1} = \dot{\mathbf{a}}_n + \frac{\Delta t}{2} (\ddot{\mathbf{a}}_n + \ddot{\mathbf{a}}_{n+1}) \quad (5.8)$$

Equation 5.7 and 5.8 can be rewritten as:

$$\ddot{\mathbf{a}}_n = \frac{2}{\Delta t^2} (\mathbf{a}_{n+1} - \mathbf{a}_n) - \frac{2}{\Delta t} \dot{\mathbf{a}}_n \quad (5.9)$$

For the next increment equation 5.9 can be written:

$$\ddot{\mathbf{a}}_{n+1} = \frac{2}{\Delta t^2} (\mathbf{a}_{n+2} - \mathbf{a}_{n+1}) + \frac{2}{\Delta t} \dot{\mathbf{a}}_{n+1} \quad (5.10)$$

From this equation 5.8 can be written as:

$$\dot{\mathbf{a}}_{n+1} = \frac{1}{2\Delta t} (\mathbf{a}_{n+2} - \mathbf{a}_n) \quad (5.11)$$

For the current increment equation 5.11 can be written as:

$$\dot{\mathbf{a}}_n = \frac{1}{2\Delta t} (\mathbf{a}_n - \mathbf{a}_{n-1}) \quad (5.12)$$

By inserting equation 5.12, equation 5.10 can now be written as:

$$\ddot{\mathbf{a}}_n = \frac{1}{\Delta t^2} (\mathbf{a}_{n+1} - 2\mathbf{a}_n + \mathbf{a}_{n-1}) \quad (5.13)$$

By inserting equation 5.13 into equation 5.1:

$$\mathbf{M}\mathbf{a}_{n+1} = \mathbf{M}(2\mathbf{a}_n - \mathbf{a}_{n-1}) - \Delta t^2(\mathbf{g}(\mathbf{a}_n) - \mathbf{f}(\mathbf{a}_n)) \quad (5.14)$$

This is the explicit algorithm from this the next step can be calculated. This is has a great advantage when the mass matrix is lumped, then the equation can be divided into separate independent parts that can be calculated in for example a cluster.

Explicit methods require a small time increment to get an accurate result, see figure 5.2. For the entire problem the number of increments is generally in the order of 10,000 to 1,000,000 increments. However this increment has a very low cost per increment, due to that no iteration is needed, thus the overall cost in form of disk space are smaller than for the implicit scheme. The explicit scheme is depending of the speed of wave propagation in the material this regulate the time step. For more information about the explicit scheme consult [3]

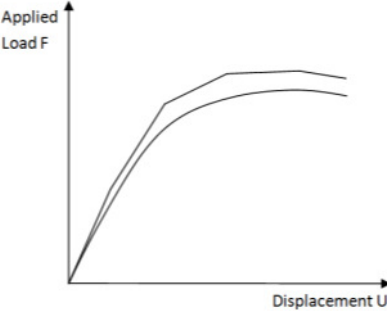


Figure 5.2. Explicit curve

5.1.3 Comparison Implicit/Explicit

The main difference between Implicit and Explicit algorithm is the way it calculate the increments. The major difference is that the implicit scheme uses an iteration method (for example Newton-Raphson) and needs to calculate the stiffness matrix for every iteration, while the explicit scheme does this once per increment. Below some pros and cons is shown for the implicit/explicit scheme.

Implicit

Pros

The Implicit scheme is very stable and can take large time steps due to that it iterates every step. Because of this the implicit algorithm is well suited for long loading problems. If the implicit scheme converges the correct solution has been found.

The implicit scheme is suitable for small deformations.

Cons

As implicit iterates every increment it can be both time consuming and become large files when there is advance contact problem, large deformation etc. If the Implicit resolution doesn't converge it is a good idée to go over to an explicit scheme.

Explicit

Pros

The Explicit scheme has a handles short load duration and contact problems better then implicit scheme. Another advantage of the explicit scheme is that see solution to the equation of motion can be divided to different computer cores or sent into a cluster there by reducing the computation time. The file size is smaller than for the implicit scheme. The explicit scheme is suitable for large deformations.

Cons

When the load time is long the explicit scheme is slower than the implicit scheme.

When converges has been reach it not necessary correct and must be controlled.

For more information on Implicit /Explicit schemes consult [3],[5],[6], [7] and [A1].

5.2 Quasi-static

Quasi-static is a form of a mixture between static and dynamic analysis, where some or all forces are induced from physical motion from a body. The quasi-static analysis should not be confused with the dynamic analysis. The major difference of the quasi-static and the dynamic analysis is the moment of inertia. In a quasi-static analysis the force is applied with a certain speed but not so fast that it affects the inertia. For more information regarding quasi-static consult [7]

Imagine a person entering a crowded elevator. If he enters the elevator with a relative low speed the people in front of him have time to move and make room, the people on the side of the elevator are also going to move to make room. But if he instead runs into the elevator the same people do not have the time to move and they are going to get hurt, the people on the sides are now not affected by this change.



Figure 5.3. Quasi-static elevator example (Quasi-static to the left dynamic to the right)
(Getting started with Abaqus)

5.3 Mass scaling

Mass scaling is done by increasing the density locally in an element there by reducing the time step according to the equation 5.15:

$$\Delta t = \frac{L^e}{C_d}, c_d = \sqrt{\frac{E}{\rho}} \quad (5.15)$$

Where L^e is the minimum element length and c_d is the wave speed of the material.

As seen from equation 5.15 by increasing ρ by a factor of f^2 decrease the wave speed by a factor of f . This is done to get a smaller time step. This is done due to if the time step is too large the smallest elements will be unaffected by the sound wave.

Mass scaling is used to get a more economical solution from the explicit quasi-static solver i.e. get a shorter calculation time. This can also be done by scaling down the natural time but for strain rate sensitive material can't be done and mass scaling is used instead.

A drawback of this is that as a large mass is added locally the dynamic effects will be affected which might give a corrupt solution. For more information consult [7]

5.4 Integration points

To get a solution from the elements a numerical integration need to be solved, see figure 5.4. This numerical integral can be represented such as equation 5.16, where $f(\xi)$ is an arbitrary function and ξ is integration points in the interval $-1 \leq \xi \leq 1$. This is equation might be very complicated or impossible to solve analytical.

$$I = \int_{-1}^1 f(\xi) d\xi \quad (5.16)$$

To solve this integration numerically the area under the curve can be represented by bars, depending on the numbers of bars used to represent the curve the more accurate result is achieved, see figure 5.5. This can be calculated by equation 5.17, where H is the weight parameter and R is called the reminder, n is the number of integration points. By making R as small as possible equation 5.17 can be written as equation 5.18.

$$I = \sum_{i=1}^n f(\xi)H_i + R \quad (5.17)$$

$$I \approx \sum_{i=1}^n f(\xi)H_i \quad (5.18)$$

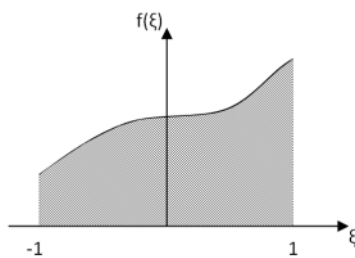


Figure 5.4. $I = \int_{-1}^1 f(\xi) d\xi$

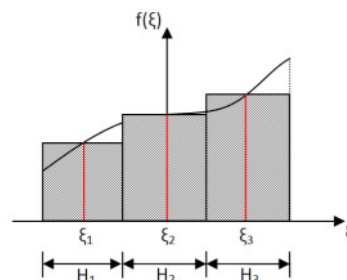
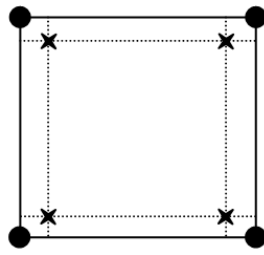


Figure 5.5. $I \approx \sum_{i=1}^3 f(\xi)H_i$

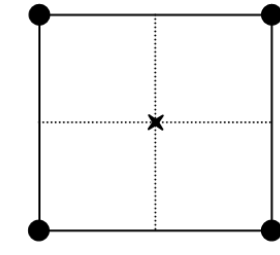
The integration points and weight parameter can be chosen by Gauss integration points. When a four node isoparametric element is used there are four gauss integration points as well, see figure 5.6, this is called full integration or an element of a higher order. If there are a fewer Gauss integration point this is called a reduced integration or lower order element, see figure 5.7. When using reduced integration there might be a problem with hourglassing, figure 5.8.

The hourglass problem is an effect of some elements deformations has become energyless (zero strain and zeros stress at the integration point). The reason of this is that the length and the angle between the dotted lines in figure 5.7 and 5.8 are the same, i.e. the integration points sees the element in figure 5.8 to be the non-deformed. This means that element is unable to resist some types of deformation as it has no stiffness in this mode. This problem is compensated in Abaqus by introducing a artificial "hourglass stiffness" in first-order reduced integration.

For more information consult [4],[7] and [A4].



Figur 5.6. Fully integrated



Figur 5.7. Reduced integration

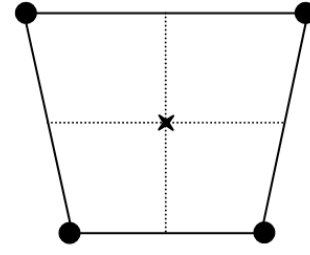


Figure 5.8. Hourglassing

5.5 Contact

The contact problem has a very complicated nature and is “depending” on both friction and adhesion, and plays an important role since the contact determines the dynamic property of the system. The contact in FEA can be illustrated in different ways depending on the problem and on the solver, this is both for the contact method that is used and how this is represented.

Contact representation

There are different ways to represent the contact between two bodies, this is depending on the problem, solver and what method that is used. Two ways to represent the contact are briefly presented below. For more information consult [7].

Node-to-surface

Here the contact is represented from one master surface and one that is represented by a slave surface. The master surfaces boundaries are the surfaces itself and the slave surfaces boundaries are the nodes for the surface. This means that the slave surface are allowed to penetrate the master surface until a node from the slave surface come into contact with the master surface, see figure 5.9. To achieve a good result the slave surface should have a finer mesh if this is not possible or the mesh are similar the slave surface should have the softer material.

Surface-to-surface

Here both bodies boundaries are represented by their surfaces i.e. when the two surfaces come into contact there are no penetration allowed, see figure 5.10.

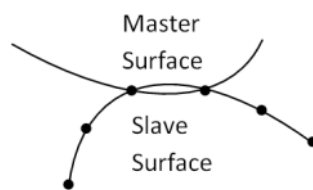


Figure 5.9. Node-to-surface contact

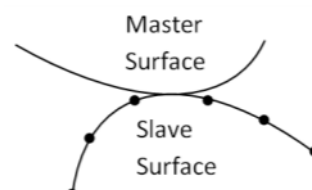


Figure 5.10. Surface-to-surface contact

Contact methods

There are different ways to calculate the contact between two bodies that gives the different strength and make the solution converge easier. Below two contact methods is going to briefly be described. For more information consult [7].

Penalty

The penalty method uses a stiff approximation of hard contact. In theory this method uses bar element that have no initial stiffness until they are compressed to the final location of the contact surface, then they becomes extremely stiff, see figure 5.11. When using elastic-slip the stiffness of the bar elements become gradually stiffer according to the angel of the dotted line in figure 5.12.

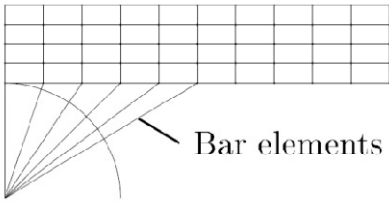


Figure 5.11. Bar elements in the penalty method

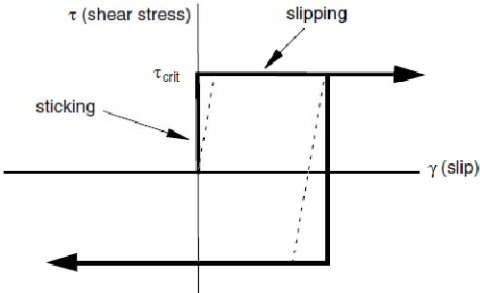


Figure 5.12. Shear/slip relationship (Abaqus user's manual)

Augmented Lagrange

This method has the same kind of stiff approximation as the penalty method however the augmented Lagrange also uses extension of iterations to improve the accuracy of the approximation. For the first iteration it's the same as the penalty method but for each iteration the Lagrange multiplier λ is changed to make a better approximation. The augmented Lagrange makes the convergence easier for the implicit solver and works well together with Newton-Rahpson. Once again the more interested reader are asked to consult [7].

Chapter 6

Experiments

To get correct in data and to verify that if the FEA were correct or not a number of experiments were carried out. Most of the experiments that were carried out were with SWEP’s own equipment but one of the tests was made by an external company (Indutirellt utvecklingscentrum center). This chapter starts with the in data test and be followed by the experiments for the comparison. Only the result from the in data test will be presented in this chapter, the result from the experiments will be presented in chapter 8.

6.1 Tensile test

In chapter 4 and chapter 2 the material model respectively the in parameters was described. To determine these material data, a number of tensile tests were needed to be done.

Due to that the tensile test machine was recently acquired the knowledge of its functions were limited. This meant that a series of test and trials had to be done before an acceptable result could be found.

One of the issues was the speed of which the specimen should be tested. Another problem was that for the standard specimen used to day the necking occurred outside of the extensometer when using the smallest extensometer with a gage length (GL) of 25 mm. There are three different settings for the GL: 25, 50 and 80 mm but due to the large displacement of the specimen only the 25 mm is working for this type of steal. There were even concerns about if the extensometer was adding a bending force to the specimen.

SWEP follow the standard SS-EN ISO 6892-1:2009 the different parameters for a flat specimen are shown in table 6.1 and the parameters are shown in figure 6.1.

Dimensions in millimetres

Test piece type	Width b_0	Original gauge length L_0	Parallel length L_c		Free length between the grips for parallel sided test piece
			Minimum	Recommended	
1	12,5 ± 1	50	57	75	87,5
2	20 ± 1	80	90	120	140
3	25 ± 1	50 ^a	60 ^a	—	Not defined

^a The ratio L_c/b_0 and L_0/b_0 of a type 3 test piece in comparison to one of types 1 and 2 is very low. As a result the properties, especially the elongation after fracture (absolute value and scatter range), measured with this test piece will be different from the other test piece types.

Table 6.1. Specimen sizes according to ISO standard SS-EN ISO 6892-1:2009

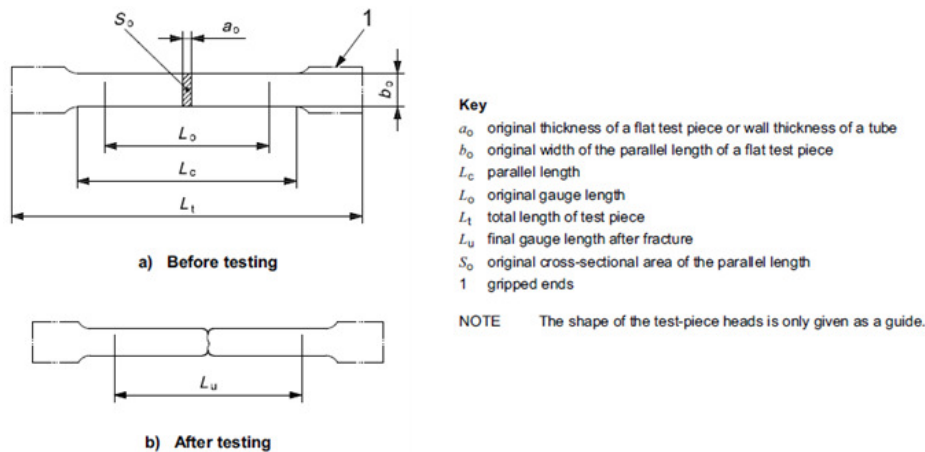


**Figure 6.1. Specimen's parameters
(SS-EN ISO 6892-1:2009)**

Final specimen size and tensile parameters

The width for SWEPS specimens are 12.5 mm and the final parallel length (L_c) of the specimen followed the recommended parallel length of 57 mm. One should observe that the gauge length L_o in this case is not 50 mm but 25 mm.

After consulting LTH technician Zivkovic Zivorad regarding a way to control in what area the necking accure, a very light grinding with an 1200 sandpaper were applied in the center of extensometer. However it is important to control the width (b_0) afterward to control if the width change is measurable if so this became the new b_0 . This solved the problem with making the specimen work with the extensometer with the GL 25 mm.

The velocity of the tensile test was another issue this was sorted out with the help of the ISO standard and with help from Per Thilderkvist at Industriellt utvecklingscentrum (IUC) in Olofström Sweden. The tensile test machine uses two different velocity's one for the elastic zone and one for the plastic zone, this were calculated from equation 6.1.

$$v_c = L_c * \dot{\epsilon} \quad (6.1)$$

According to the ISO standard the strain rate should be in the span:

$$0.00025 \text{ s}^{-1} < \dot{\epsilon} < 0.0025 \text{ s}^{-1}$$

In the plastic zone the strain rate must not exceed 0.0025 s^{-1} .

Equation 6.1 uses the parallel length (L_c) but after consulting Per Thilderkvist this were change to the length between the clamps (L_g), see figure 6.2 and 6.3. The reason of this is that, if the velocity of the machine is calculated from the extensometer and this slip or fall of (not that uncommon) the tensile machine will run out of control and might get damage. If the length between the clamps is used instead to calculate the velocity this will no longer be an issue.

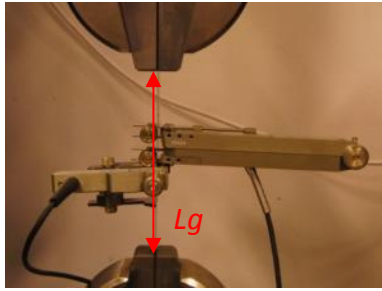


Figure 6.2. Length between the clamps L_g

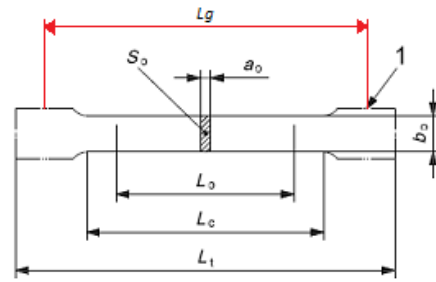


Figure 6.3. Length between the clamps L_g

Tensile Testing

Before every specimen was used the width (b_0) and thickness in the area inside the extensometer were measured with a sliding caliper and a micrometer respectively. These values were then inserted in the tensile test machine for every specimen.

The velocity is calculated as earlier described from the length between the clamps for this type of specimen the length were set to 80 mm, which gave of velocity of 1.2 mm/min up to yielding and then the velocity increased to 12 mm/min. In figure 6.2 the two extensometers can be seen, one can observe that the width extensometer is not measuring on the same area as the length extensometer in lack of room. This might seem like problem but as the r -value is measured at 5% elongation and this happens quite early in the process this should not be a worry for that problem. However, how and when the r -value is measured is quite important.

r -value

As mentioned in chapter 2 the r -values are calculated by equation 2.3. But to get a correct r -value the strain should be determined when the length strain has been subjected to 20% of strain according to [A3]. The supplier on the other hand measure the r -value in steps of 5% up to A_g , see figure 6.4, where the last measurement are the one that is used.

For the metal used in this thesis the A_g values are between 48-55% engineering length strain (ϵ_L) deepening on the orientation of the specimen.

However, the specimens r -value is only measured up to 15-28% engineering length strain deepening on the orientation of the specimen. The reason of this is that the width extensometer was set to stop recording after a reduction of 1mm as default i.e. 8% width engineering strain (ϵ_w). This was unfortunately discovered to late in the process after all tensile tests already were made.

As default the tensile test machine is set to calculate the r -value at 5% length engineering strain.

The r -value should be determined from the true plastic strain (ϵ^p), but in this thesis as well as in some industrial applications the r -value is calculated on the true strain ($\epsilon = \epsilon^e + \epsilon^p$).

The reason of this is that a deeper understanding of how this is done must be known and with the limitation of this thesis this is left out for now. However, as the elastic zone for this material is very small the difference between ϵ and ϵ^p should be very low.

As can be seen from the results below the r -value at 5% gives a value close to the “ A_g ” value that ThyssenKrupp has supplied. For more information consult [A3]

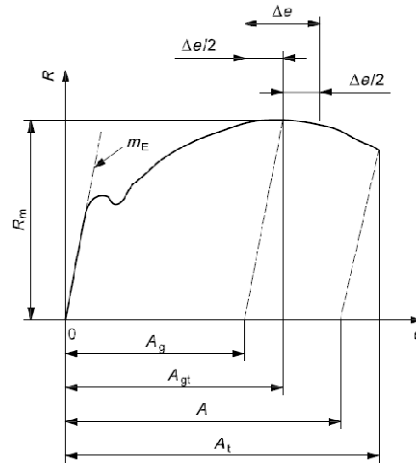


Figure 6.4. Stress strain diagram explanation

Tensile Testing Result

From the tensile test result only the r -value is extracted and used. There were of course other data that could have been used as well, for example the yield stress. But as the FEA uses true stress and strain this were needed to be recalculated from engineering stress and strain before usage (that the tensile test machine has as the default setting). The reason why this was not done is the lack of time. In future work a way to extract more data might be used, where the flow curve is one example. Instead data from the supplier were used for the missing in data in this thesis. The r -value from the supplier's data however was compared to the r -value from the tensile test and they matched up within 5%. Except for the r_{90} value where the difference were 39.8%, why this is are going to be investigated from both the supplier and from SWEP.

6.2 Friction

To determine the friction coefficient (μ) between the raw plate and the tool two tests was carried out, the angle of friction and by using a dynamometer, the tool to measure this is shown in figure 6.5. The result from these two tests was then inserted into the FEA. The material parameter that steers the friction is the surface finish that is 2B for ThyssenKrupp.



Figure 6.5. Dynamometer (top) and angle ruler (bottom)

6.2.1 Angle of friction

This method is often called the simplest method due to that you basically do not need any measuring equipment besides a ruler. The testing rig is setup as figure 6.6 shows then the angle φ is increased until the body starts to slide. When the body starts to slide φ is calculated from equation 6.2. Then the equilibrium of the forces is set up as equation 6.3.

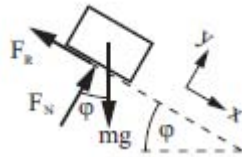


Figure 6.6. Force acting on the body

$$\tan(\varphi) = \frac{Y}{X} \quad (6.2)$$

$$\begin{aligned} x: mg * \sin(\varphi) - \mu F_N &= 0 \\ y: F_N - mg * \cos(\varphi) &= 0 \end{aligned} \quad (6.3)$$

From equation 6.3 it follows:

$$\tan(\varphi) = \mu \quad (6.4)$$

I.e. by either calculating the angle φ or by as in this case measuring it directly the friction coefficient can be calculated.

Result from the angle test

The test was carried out by making a slope out of a pallet collar on which a piece of the actual sheet metal was ducked taped on. Then a piece of the same material and coating as the tool were placed directly on this area, see figure 6.7. By inclining and measure the angle of the slope until the piece started to slip the friction coefficient was calculated.

The piece started to glide at 13° (stick - slip) and at 16° it achieved fully developed slip, the result is presented in table 6.2.



Figure 6.7. Angle of friction test rig

Angle	μ
13° (stick - slip)	~0,23
16° (fully developed)	~0,29

Table 6.2. Result from angle of friction

6.2.2 Dynamometer

Another way that is a bit more straightforward is to place the body on a flat surface, and using a dynamometer to drag the body. The force need to move the body (F_b) is then equal to the friction force (F_r). From this friction coefficient then can be calculated using equation 6.5. Where's N is equal to the mass times the gravitation and as earlier mention the force needed to move the body is equal to friction force there by equation 6.5 can be rewritten as equation 6.6.

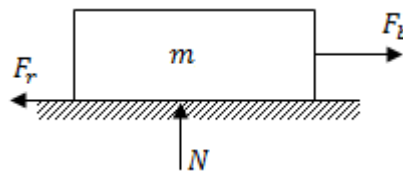


Figure 6.8. Forces over the body

$$F_r = N * \mu \quad (6.5)$$

$$\mu = \frac{F_b}{mg} \quad (6.6)$$

Result from the dynamometer test

Using the same sheet metal plate and tool piece but now taped on to a flat surface the coefficient of friction was determined by the force needed to move the piece, see figure 6.9. The dynamometer was actually a precision luggage/fish scale. The friction coefficient is calculated from equation 6.6. Where m for the piece was measured to 2.14 kg and the force needed is shown in table 6.3.



Figure 6.9. Dynamometer test rig

Force (kg)	μ
0,5 (stick - slip)	~0,23
0,6 (fully developed)	~0,28

Table 6.3. Result from the dynamometer test

6.3 Press settings

Due to that the finite element analysis (FEA) will be set as displacement controlled (see chapter 7) it was of highest importance that the speed and stroke for one cycle were established, such cycle are presented in figure 6.10.

Fortunately there are two presses at SWEP that have a control system that is built up around this type of curve, press line 10 is one of them, see figure 6.11. The crucial parameters was set according to table 6.4 during all test, this gave a relative certain value to go on for the FEA.

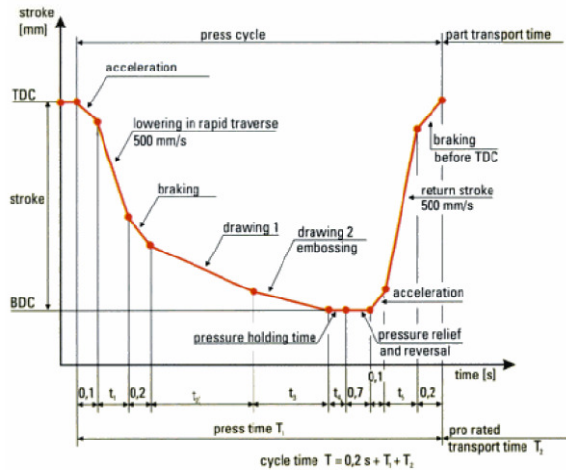


Figure 6.10. Typical press curve (Schuler-Metal Forming Handbook)

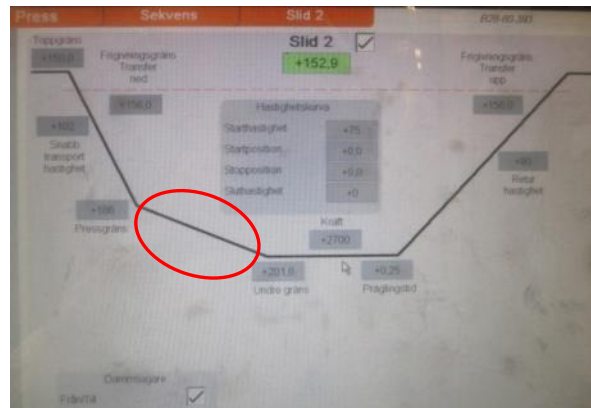


Figure 6.11. Press curve for PL 10

Velocity	75 mm/s
*Press Depth	51 mm
Embossing time	0,25 s
Press force	270 ton

Table 6.4. Press settings

Note that the press depth is when the “final” velocity starts (the marked line in figure 6.11). The “actual” press depth that is simulated, is when the press meets the sheet metal and until it reaches its lowest position (2,04 mm).

When the pressing the channel plate the copper and raw plate are pressed at the same time (see figure 7.1 in next chapter). Because the FEA is done without copper the test had to be done without copper. That meant that the actual press depth got changed by 0.05 mm. However, this is too small change for the press to detect this, which means that the parameters stayed the same regardless if there is copper or not. The fact that the copper works like a lubricant for the steel can’t be neglected and there by the result from with and without copper plays an important role, this is the reason why no copper was used during the pressing of the channel plates for the tests.

To ensure that all pressed BPHE plates are pressed with the same geometry they were pressed at the same time with the B80 tool nr 393 that has made approximately 500,000 strokes (506,792 strokes at 2011-01-24) i.e. is in the middle of the lifecycle for a tool (normal life-span for a tool is 1 million strokes)

6.4 Forming limit curve and forming limit diagrams

Forming limit diagrams (FLD) is a way to detect forming defects such as tearing or wrinkling, there by the FLD describes the formability of the geometry. But before this can be done a forming limit curve (FLC) is need for the metal in question i.e. the formability of the material, both of this is build around the same principle.

Both FLD and FLC are done by pre printing circles on to piece of sheet metal before pressing, this piece is then pressed. As the piece get pressed the circles deforms and change shape to an ellipse. The major and minor strain is then calculated from the deformation of pre printed circles, see figure 6.12 were the black circle is before pressing and the red ellipse is after.

The major strain is represented by the major axis of an ellipse, major strain is always positive due to that the material stretches.

The minor strain is represented by the minor axis of an ellipse, major strain can both be positive and negative.

Both the major and minor strain is calculated as engineering strain. If the major strain is becomes smaller than the minor strain, they simply change place and the minor strain becomes the major strain. Each of these points is then inserted to a diagram and in figure 6.13 it is shown how a typical FLC looks like. For more information consult [1].

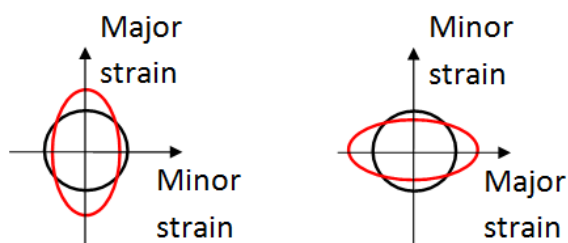


Figure 6.12. Major and minor strain axis

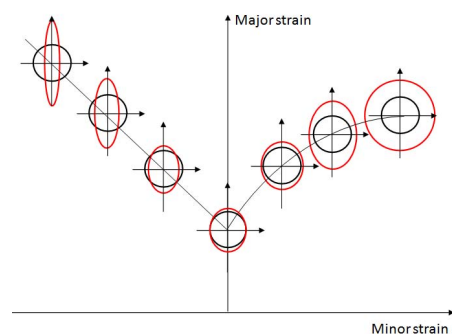


Figure 6.13. Major and minor strain for a FLC

6.4.1 Forming limit curve

To determine how the material in question behaves during sheet metal forming, a stretch forming of the material was done during measuring, how this is done can be read in the appendix 2.

Because the material size for the specimens was too large for the B80 sheet metal coil (125x0.3) a large sheet metal coil was needed. After some investigation a similar sheet metal with almost the same material properties (see appendix 1) was found, but unfortunately this also meant that the thickness was change to 0.4 instead of 0.3 (25% thicker). Nevertheless after consulting Per Thilderkvist at IUC this wasn't considered an issue in this case. The result from this measuring should look something like in figure 6.13. The shape of the FLD is approximate the same for all steels but the curve is moved up or down depending of the material.

To get more information from the FLC it is divided into different zones see figure 6.14, as earlier mention there is a "window" or zone that is optimum for the forming process. In figure 6.14 there are other zones marked. How these curves are extracted can be read in appendix 2.

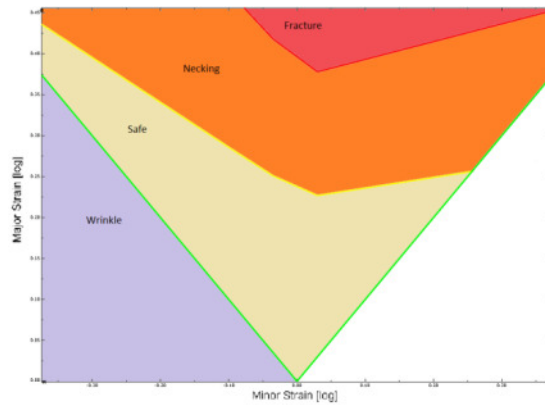


Figure 6.14. Forming limit curves (FLC)

6.4.2 Forming limit diagram (FLD) on a channel plate

To determine how good or bad a geometry is for this material, a FLD for an actual channel plate was done. This was done as explained in section 6.4 by a number of dots printed onto the raw plate before pressing, see figure 6.15. These were then measured after pressing see figure 6.16. For more information consult appendix 2.

These points were then inserted to the final FLC and by controlling in which zone there are in, an approximation can be said about how the formability is for this geometry.

In chapter 2 it was explained how the strain in the thickness direction was calculated when a constant volume is assumed. From the strain in the thickness direction the thickness then can be calculated through equation 6.7 assuming the original thickness was 0.3 mm. The result of this will be presented in chapter 8.

$$\varepsilon_{Th} = \ln\left(\frac{Th}{Th_0}\right) \Rightarrow Th = Th_0 * e^{\varepsilon_{Th}} \quad (6.7)$$



Figure 6.15. Pre printed dots on a raw plate



Figure 6.16. Pressed plate with deformed dots

Metallurgy

Another way also mention earlier is to use metallurgy to physical measure the thickness of the sheet metal. Just as for the FLD raw plates was pressed using the presetting earlier described, then the BPHE plate was cut in to section, se figure 6.17 and 6.18 and finally it was analyzed in SWEPs claim lab. For more information about how this were done see appendix 3.



Figure 6.17. Scallop cut in 90°



Figure 6.18. Scallop cut in 0°

Chapter 7

Sheet metal simulation

In this chapter the steps and in parameters for the simulation will be presented. The simulation is divided into 2D and 3D geometry and is built around the same scallop thereby the simulations has the same criteria's.

For this simulation the upper and lower tools are set to be rigid and the gravity is neglected i.e. the only part that can be deformed is the blank. Another general criterion is the material parameters and contact criteria's, which are mention earlier in the material chapter 2 and the experiment chapter 6.

7.1 Geometry

The tool design is provided by SWEP and the complete B80 tool is shown in the figure 7.1 below. Where the part where the raw plate lays against in figure 7.1 is the lower tool (Note not visible in figure 7.1 due to the raw plate).

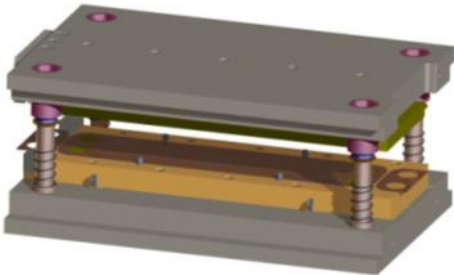


Figure 7.1. B80 Tool with raw plate

As mention, this simulation is divided into 2D and 3D geometry and focus at the most troubling spots shown in figures 7.2, 7.3 and 7.4. This thesis was focused around one of these spots as can be seen in figure 7.5.



Figure 7.2. Troubling spots on the lower tool



Figure 7.3. Troubling spots on the upper tool

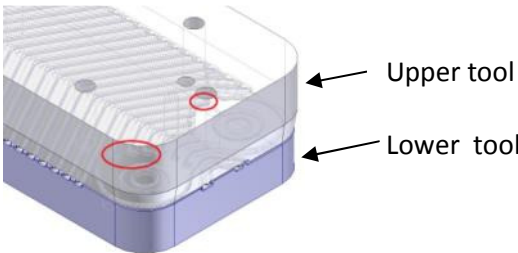


Figure 7.4. Troubling spots on in the assembled tool

The 2D geometry

To make the starting simulations as simple as possible the scallop end is divided into two 2D geometry areas as mentioned earlier. These were taken in an angle of 0° and 90° according to the “pattern”, see figure 7.5, 7.6 and 7.7. In figure 7.6 and 7.7 the grey “line” is the channel plate. This geometry was model directly in Abaqus CAE.

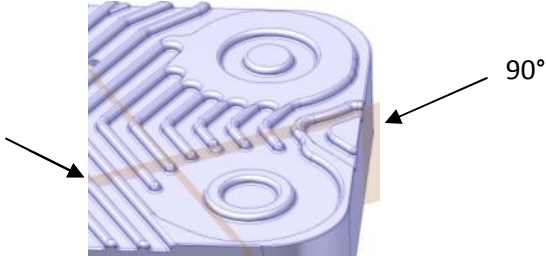


Figure 7.5. The section cuts shown in the lower tool



Figure 7.6. The 0° section cut



Figure 7.7. The 90° section cut

The 3D geometry

The 3D geometry is built around the same scallop end as the 2D geometry i.e. one of the scallops is cut out from the rest of the tool and smoothen out to get rid of unwanted geometries that just take up computing time, see figure 7.8 and 7.9. The upper and lower tool was taken from CAD files while the blank was model in Abaqus CAE.

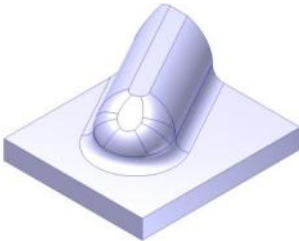


Figure 7.8. Lower tool

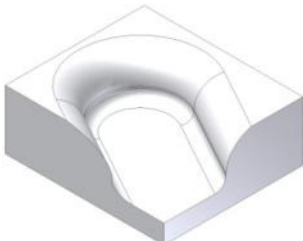


Figure 7.9. Upper tool

7.2 General Set up

The major difference between the 2D and 3D is the geometry otherwise they share the same problem setup and material parameters.

The calculation time is depending of the size of the model i.e. mesh and boundary condition etc.

7.2.1 Material data

As earlier mention the tool parts were model as rigid bodies which meant that no material data for these parts were needed. The blank however used the following material data input:

Density	$\rho = 8000 \text{ kg/m}^3$
Young's modulus	$E = 200 \text{ GPa}$
Poisson's ratio	$\nu = 0.30$
Yield strength (0.2%)	$R_{p0.2} = 220 \text{ MPa}$
Flow curve	

ϵ^p	σ
0.02	383 MPa
0.049	444 MPa
0.068	481 MPa
0.095	533 MPa
0.140	608 MPa
0.182	671 MPa
0.223	724 MPa
0.262	770 MPa
0.300	810 MPa
0.336	845 MPa

Table 7.1. Flow curve

r-values

$$r_0 = 0.50680714$$

$$r_{45} = 1.649644$$

$$r_{90} = 1.63562769$$

When using hills anisotropy material model in Abaqus the stress ratio R is used. This is calculated by the following equations. As the "one-one" direction is the same as the "zero" direction the R_{11} becomes equal to 1 i.e. the rolling direction.

$$R_{11} = \frac{\bar{\sigma}_{11}}{\sigma_0} \quad R_{22} = \frac{\bar{\sigma}_{22}}{\sigma_0} \quad R_{33} = \frac{\bar{\sigma}_{33}}{\sigma_0}$$

$$R_{12} = \frac{\bar{\tau}_{12}}{\tau_0} \quad R_{13} = \frac{\bar{\tau}_{13}}{\tau_0} \quad R_{23} = \frac{\bar{\tau}_{23}}{\tau_0} \quad (7.1)$$

However when using sheet metal the stress ratio is calculated from the r-value instead as mentioned in chapter 4.3.2. The stress ratio is now calculated according to:

$$R_{22} = \sqrt{\frac{r_{90}(r_0 + 1)}{r_0(r_{90} + 1)}}, R_{33} = \sqrt{\frac{r_{90}(r_0 + 1)}{(r_{90} + r_0)}}, R_{12} = \sqrt{\frac{3r_{90}(r_0 + 1)}{(2r_{45} + 1)(r_{90} + r_0)}} \quad (7.2)$$

There are still two values that aren't defined R_{13} and R_{23} . After consulting Simulia regarding these values they were set to one as well. The final values are shown below:

Stress ratio (R-value):

$$\begin{aligned}R_{11} &= 1 \\ R_{22} &= 1.3583 \\ R_{33} &= 1.0725 \\ R_{12} &= 1.4404 \\ R_{13} &= 1 \\ R_{23} &= 1\end{aligned}$$

All values that are used here are taken from the material supplier except the r-values which is taken from a tensile test earlier explained. Note this is not the same as the stress ratio, however the stress ratio is calculated from the r-value according to equation 7.2. For more information consult [6] and [7]

The contact condition was set as general contact and the friction was set to $\mu=0.28$. Where general contact works as a surface-to-surface contact, this can be read about in chapter 5.

7.2.2 Time step and Increments

Abaqus automatically choose the time step from equation 5.15. When using Abaqus explicit the increments are chosen automatically as well.

7.2.3 Velocity

The velocity of the model is set as the total time of the step not as a velocity. There by it must be calculated. The press velocity is set to 75mm/s and the press depth in this step is 2.04mm which gives:

$$t=0.0272s$$

To make it easier for the explicit calculation the on loading and off loading was set to a smooth curve shown in figure 7.10. Where the x-axle is the time of the pressing operation and y-axle is the press depth (reversed curve) i.e. the slope of the curve is the velocity in during the pressing operation. This represents the real forming operation rather good as well if we compare it to figure 6.10.

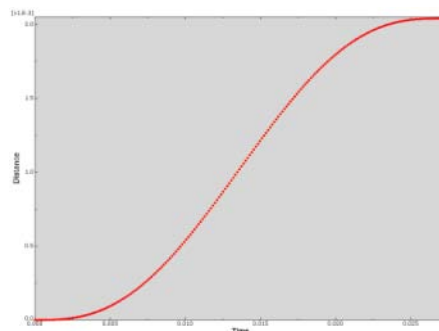


Figure 7.10. Velocity of curve of the upper tool

The velocity can be speed up to reduce the calculation time. However, this will affect time dependent materials. This is why mass scaling is used instead to speed up the calculation time. How this mass scaling works can be read about in the chapter 5.

7.2.4 Step

The step is how Abaqus symbolize in which order different stages will be carried out during the simulation. In this simulation only one step besides the initial step is needed as there is only one operation that will be carried out i.e. the upper tool moves down.

If the forming operation for example had have an blank holder that should hold the blank with a certain force before the forming operation were carried out then two step would be needed, not including the initial step.

In the explicit step it is here the time of the forming are specified as the step time i.e. the velocity of the tool. It is also here we specify if any time scaling or mass scaling should be used.

The setup for increments are also done here for both of this analysis the increment type were set to automatic and a global stable increment were used. The max time increment was set to unlimited.

7.3 Finite Element Analysis (FEA)

The finite Element analysis (from here on out FEA) is done in two independent simulations where the first 2D analysis is a starting point to resolve the initial problems and to discover potential problems for the 3D analysis. It is only the 3D analysis result that is going to be used for comparison.

7.3.1 The 2D analysis

This is the starting simulation which is used to solve the initial problems before a 3D attempt is made. As this is just a start up phase and that it will not be included in the result, the setup will only briefly be described.

For this operation the upper - and lower tool was set as analytical rigid bodies.

The mesh used here was a solid quad mesh (CPS4R), the mesh had 20 elements over the thickness of the plate and 4040 elements in total see figure 7.11.

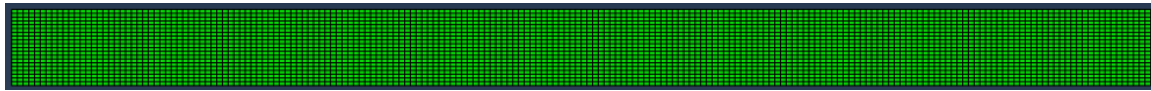


Figure 7.11. 2D mesh (CPS4R)

To speed up the process a series of mass scaling were made which are shown in Figure 7.12. The different mass scaling that was used was 100, 400, and 1600 which means that the speed of the process was 10, 20 and 40 times faster respectively. This speed up meant that instead of 6.35 hours calculation time the fastest calculation time with 1600 mass scaling were done in 5 min for the same calculation.

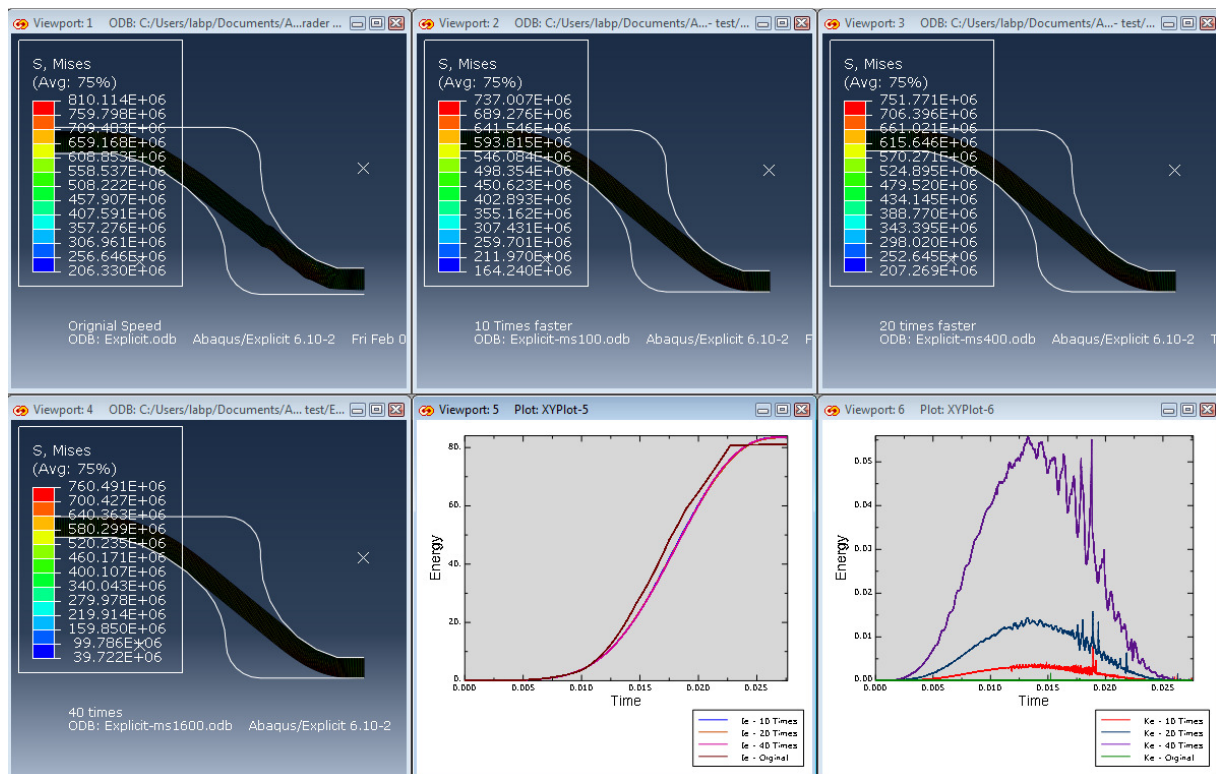


Figure 7.12. Comparison of mass scaling 0-1600

There might be a tendency of snagging as shown in the figure 7.13 below. Snagging is when a node gets stuck behind another one, as in this case the blanks node might get stuck behind the lower tools node.

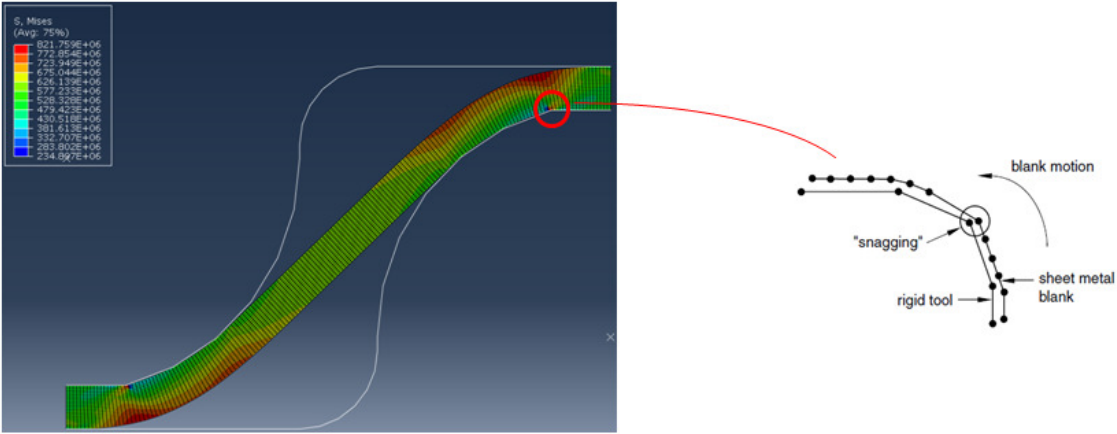


Figure 7.13. Risk for snagging

A way to get rid of this is to smoothen out the sharp edges but by doing so the geometry won't be 100% correct (however the actual tool that the simulation was compared to is by all likelihood worn down to a certain radius). This will be left as it is for now but it will be looked out for in the 3D model.

7.3.2 The 3D analysis

Most of the initial problems with the sheet metal forming were solved during the 2D analysis, when it was time for the 3D model it was mostly just to use the settings made for the 2D model. As learned from the 2D model a mass scaling of 400 were used to speed up the calculation (the mass scaling of 1600 were too large for this simulation).

Material definition

As the sheet metal is anisotropic the model had to be oriented correctly according to the sheet metal direction the direction is shown in figure 7.14 and 7.16.

Where's as earlier mention the "one" direction is the same as the rolling direction, as can be seen in the figure 7.16 the normal to the channel plate is oriented down towards the lower tool.

The input material parameters that are depending on this direction are the stress ratio earlier described in this chapter.

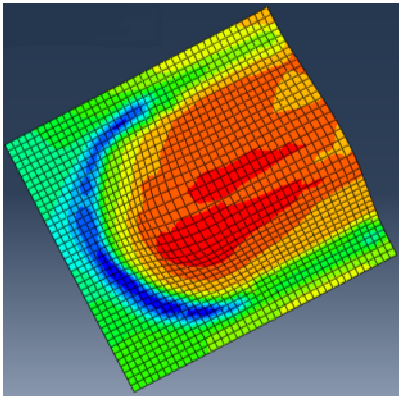


Figure 7.14. Scallop end correct oriented

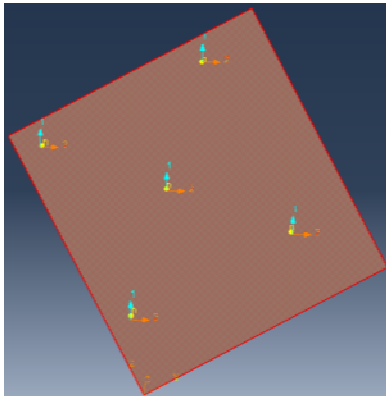


Figure 7.15. Material orientation of the scallop end

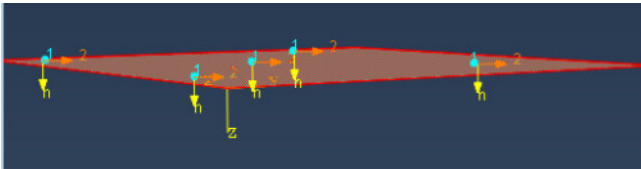


Figure 7.16. Normal to the sheet metal

Boundary conditions and loads

In this forming operation no load were applied due to there is no holding force and this forming operation is displacement controlled, there are however several of boundary conditions.

For the blank a symmetry boundary condition (BC) is around the edges while the upper and lower tool initial are encastred, but as the upper tool must move down to form the blank the BC in U3 direction (normal to the plain see figure 7.16) for the step is changed to a new location, see table 7.2.

BC name	Initial BC	Step BC
Blank x-direction	XSYM	Propagated
Blank y-direction	YSYM	Propagated
Lower tool	ENCASTRE	Propagated
Upper tool	ENCASTRE	U3=2.04mm

Table 7.2. Boundary condition

Mesh

In the 3D analysis the tool could not be analytical rigid anymore but needed to be discrete rigid, this meant that a mesh was needed to represent the geometry of the parts shown in figure 7.17 and 7.18. As this is a rigid geometry this mesh (R3D4) is just there to express the geometry.

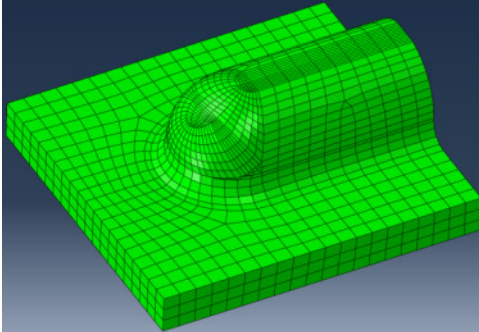


Figure 7.17. Discrete rigid mesh for the lower tool

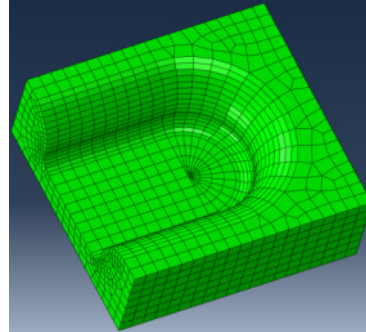


Figure 7.18. Discrete rigid mesh for the upper tool

As there were concerns that an adaptive mesh may be needed the first 3D simulation was made with solid elements (C3D8R). With the mesh size that were used it was shown that this was not an issue. But when the mesh was refined it showed that an adaptive mesh might be needed, more about this in the mesh convergence.

When it came to extract data from the post processor it showed that shell elements were needed to give the results that were asked for.

The final mesh used for the blank was a shell element (S4R) with 1599 elements, see figure 7.19.

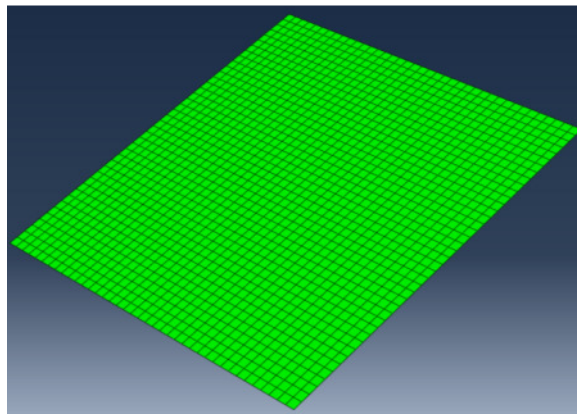


Figure 7.19. Final mesh for the blank (S4R)

Convergence

To control if the simulation has been set up correct a series of convergence control has to be made. This is an important step if this is not done then the result might show a result that is completely wrong. How important these convergence controls are by themselves vary from case to case. In this case as the plate is exposed to large deformation and explicit scheme it is of great importance to control the convergences discussed below.

Mesh convergence

To control if the mesh was fine enough two different methods was used, both refinement of the mesh and by controlling the discontinuities. As a control a hex element (S3R) was used as well, see appendix 4 to see the comparison.

The refinement of the mesh showed that the difference between the mesh were locally around 1-3%.

The discontinuities looks good overall but in the area were the thinnest region are, there is a maximum discontinuity of about 30 μm . This sounds large but after consulting Simulia this was accepted and the original mesh was kept.

When the mesh was refined the concern for the need of adaptive mesh were confirmed, see figure 7.20 due to large deformations. But because of that it had been shown that Abaqus can't deliver the results in the post processor that was need with solid elements and the adaptive mesh can't be used with shell elements, the adaptive mesh were left out. As can be seen in the chapter 8 this area is not a critical area and because of that this problem area was overlooked for this thesis. This is also a reason why there is a strain peak in this area that will be shown in chapter 8.

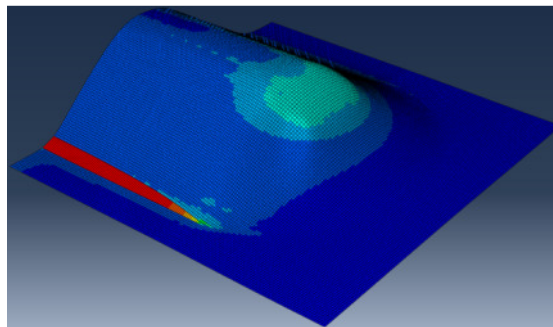


Figure 7.20. Large deformed elements

The reason why the original mesh were used were that it made it much easier to extract the result for the comparison to the metallurgy and the large deformation of the elements (shown in figure 7.20) didn't have that large of an impact to the surrounding elements.

Explicit/Quasi-static convergence

As this is the forming analysis uses an explicit scheme that is quasi static it is important to compare the internal- and kinetic energy's.

If the explicit scheme is correct the internal and external energy are well separated due to that most of the energy should go to forming the blank not to move it, see figure 7.21.

It is also important to control this graphs individually to control if the kinetic energy contains large oscillations, if it does the result might be inadequate, see figure 7.22 and 7.23.

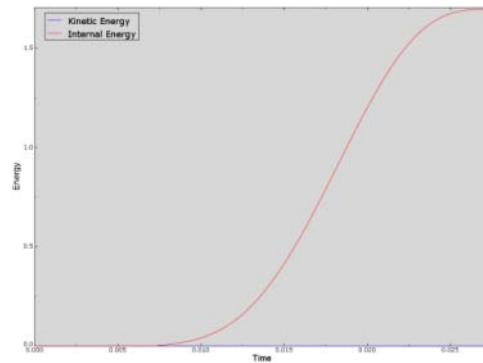
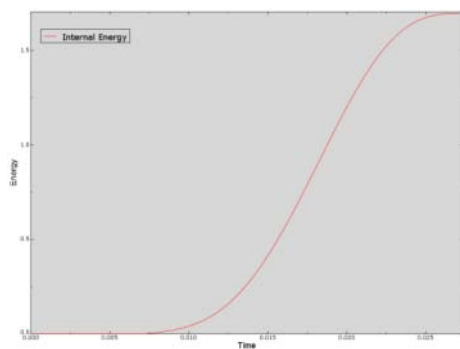
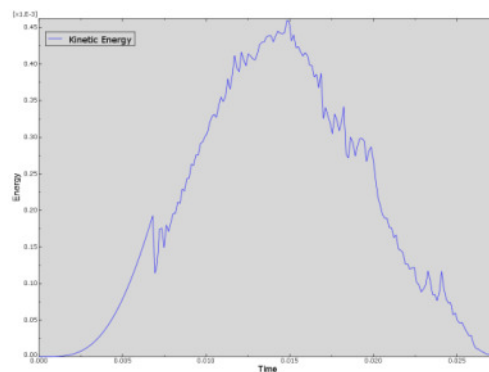


Figure 7.21. Internal vs Kinetic energy plot



Figur 7.22. Internal energy plot



Figur 7.23. Kinetic energy plot

As can be seen in figure 7.21 the kinetic energy is just a small fracture of the internal energy, in figure 7.23 it can be seen that there is only a small oscillation. This meant that both criteria's for the quasi-static analysis are met and the explicit solution can be used without worries.

Post processor

The result from this simulation are directly compared to the test and as shell elements are used there are commands available to measure the thickness, from this the thickness reduction can be calculated.

A FLD is also of interest and for shell elements there are a command for this as well. However, this command can only use one forming limit curve which meant that either you know how the model while behave or you need to solve your model at least three times. To overcome this, a python script had to be made that could use three or more forming limit curves at the same time instead of the already existing FLRCRT. This script was written by Joakim Asklund at Simulia after a very rough "initial code" was written by the author of this thesis. in addition to the result from FLRCRT the "home made" script made a FLD for the geometry that was analyzed .

Chapter 8

Results

In this chapter both the result from the experiments and the result from the simulation will be presented. This result will then be compared in the next chapter.

8.1 Experiments

The result from the tensile test and friction test is already presented and used. The result that will be presented here are the experiments that are used for comparison to the simulation i.e. the metallurgy and FLD tests. How these tests were made has already been explained in chapter 6.

8.1.1 Metallurgy

As earlier mentioned this test was divided into two parts 0° and 90° degrees cuts according to the pattern. When these tests were measured they were grinded 5 times and measured between every grinding. Nonetheless it is difficult to tell where the different grinding depths are in the model as the grinding depth are described in the appendix 3 this make the first grinding more suitable to use for the upcoming comparison.



Figure 8.1 Scallop cut in 90°



Figure 8.2. Scallop cut in 0°

The 90° cut

In the 90° cut the thinnest part for the first grinding were in the lower end and around 0.26 mm in figure 8.3 below the thickness of the plate for the first grinding are shown in μm . This cut was made in the 90° direction to the scallop and depending on how close it is to the scallop end, the values should be consistent through the grinding. But as been shown in the appendix 3 there is quite a difference between the grindings, this might indicate that the grinding is close to the end and are affected by the stretching of the end of the scallop.

Assumed that the plate were exactly 0.3 mm (the tolerance is +0.005 -0.022) from the start the thickness reduction can be calculated as follow from the figure 8.4. The thinnest area dose not consist with were the experiences would indicate it will be for this cut, if it's close to the scallop end. However, if the distance to the scallop end is far enough this area might be where the thinnest part can be found.

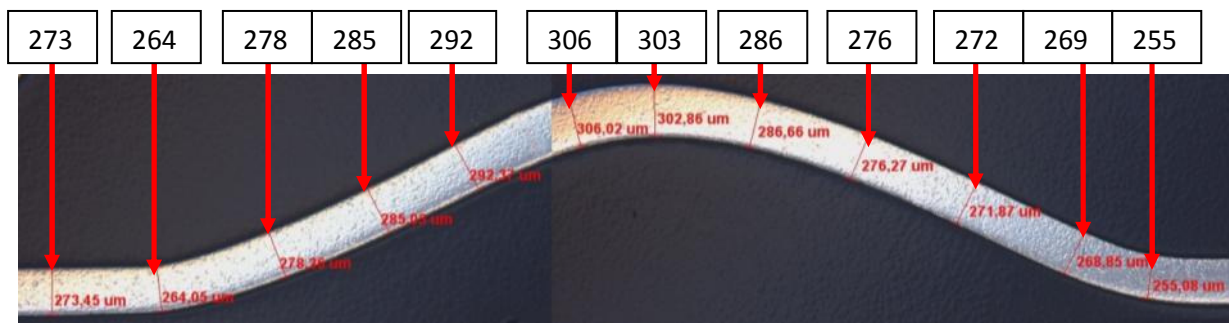


Figure 8.3. Measured values from the metallurgy in 90° cut for the first grinding in μm

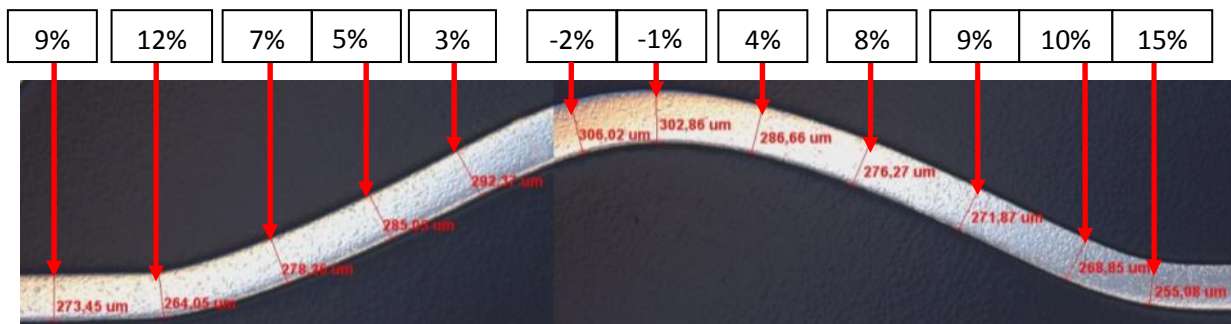


Figure 8.4. Thickness reduction in the 90° cut

In figure 8.3 and 8.4 it can be seen that there is an area that has become “thicker” than the original plate. The reason of this might depend on the source of error discussed in appendix 3, this together with tolerances for the plate might give an explanation to why the plate is “thicker” than what was expected.

The 0° cut

As for the 90° cut the measurements were taken for the first grinding as hopefully if the specimen are cut right will be in the exact middle of the scallop. In figure 8.5 it can be seen that the thinnest area are in the upper part where the plate meets the blank first, which gave the thinnest part a value of about 0.26 mm. As for the 90° the thickness reduction is calculated assuming that the plate from the beginning is exactly 0.3 mm this is shown in figure 8.6. This result adds up with what was expected.

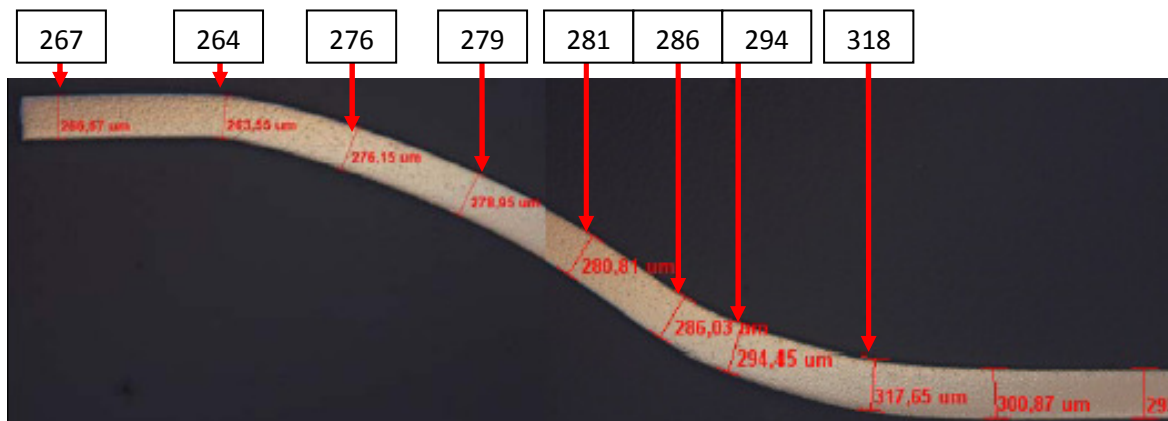


Figure 8.5. Measured values from the metallurgy in 0° cut for the first grinding in µm

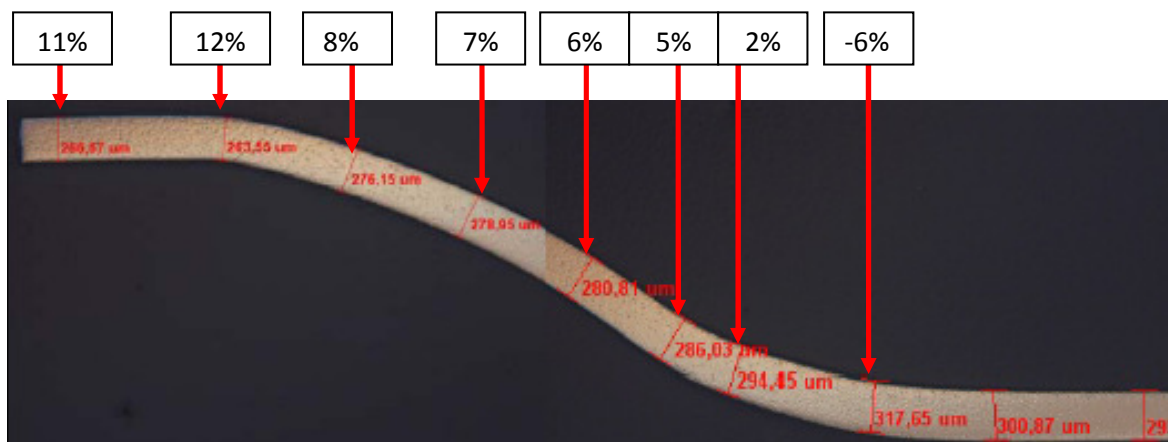


Figure 8.6. Thickness reduction in the 0° cut

These values can later be used to compare to the FLD measuring and simulation. One shall keep in mind that metallurgy is very difficult to get exact values due to the source of error. For the more interested reader consult appendix 3.

8.1.2 Forming limit curve/diagram

These experiments are two individual experiments that are combined. The forming limit curves (FLC) as described in chapter 6 are made not for comparison but for interpretation of the forming limit diagram (FLD) results. The FLD on the other hand is strictly for comparison to the simulation. As a bonus from the FLD the thickness can be calculated from the major and minor strain.

Thickness reduction

The major and minor strain is used to calculate the thickness of the plate this are measured on the top surface and then recalculated down to the middle surface all this can be read in chapter 6 and in appendix 2. To make it easier for the reader only the thickness from the different planes of the plate are shown, see figure 8.7-8.10.

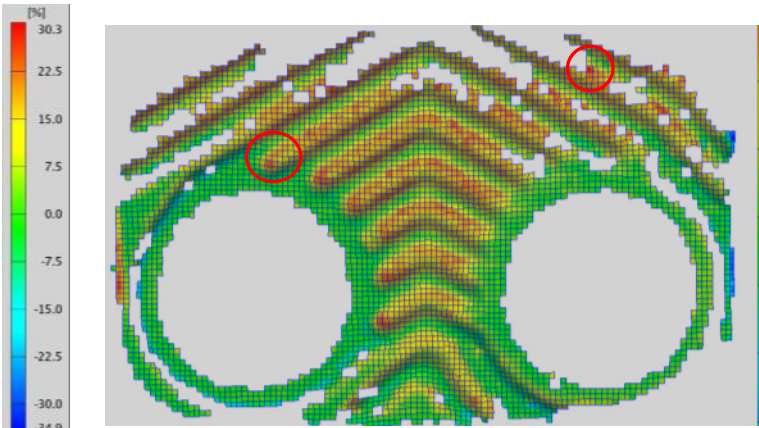


Figure 8.7. Top surface thickness reduction

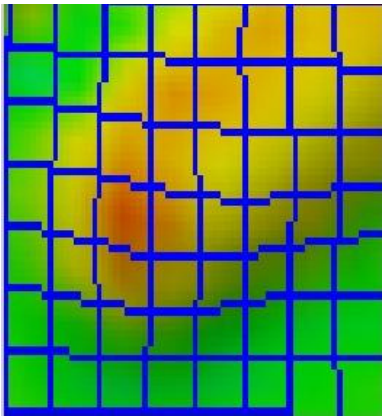


Figure 8.8. Top surface scallop end zoomed

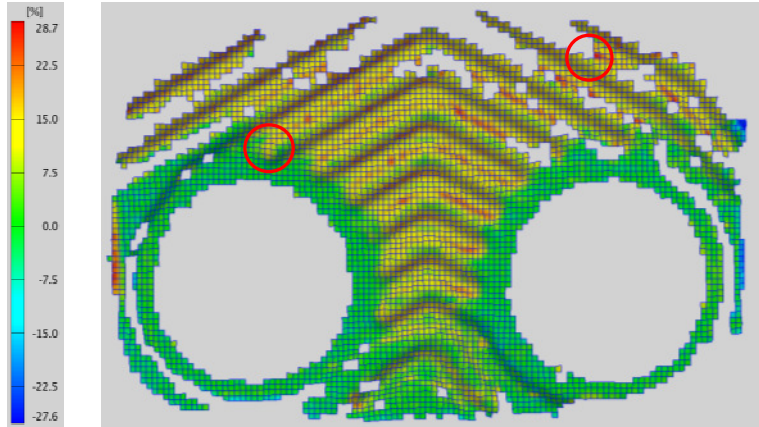


Figure 8.9. Middle surface thickness reduction

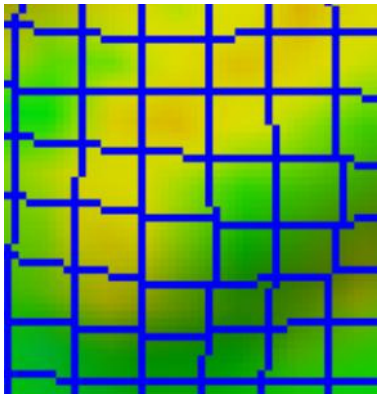


Figure 8.10. Middle surface scallop end zoomed

Observe that in Figure 8.7 and 8.9 it can be shown that the maximum thickness reduction for the top surface are 30.3 % while for the middle surface it is 28.7% . This is however not in the scallop end but in the area marked in figure 8.7 and 8.9, the other marking in figure 8.7 and 8.9 are the scallop end in question that are enlarged in figure 8.8 and 8.10.

From figure 8.8 and 8.10 it can be seen that the largest thickness reduction for the scallop in question is about 25% for the top surface and 17% for the middle surface.

Forming limit curve/diagram

A way to control how critical different areas are on this plate the major and minor strain were put into a FLD shown in figure 8.11. In the figure 8.11 it can be seen that majorities of the dots are in the “safe” zone but there are also some in the “wrinkling” and “necking” zone. The ones in the “wrinkling” zone are disregarded in this thesis as this are in the outer areas which not are of interest. Where this “necking” area is can be hand calculated from the major and minor plot but for now this is left out in lake of time.

This FLD is a good way to compare the formability of this plate to the formability result from the simulation later on.

Note that the FLD in figure 8.11 is for a much larger area and for the scallop end that were simulated.

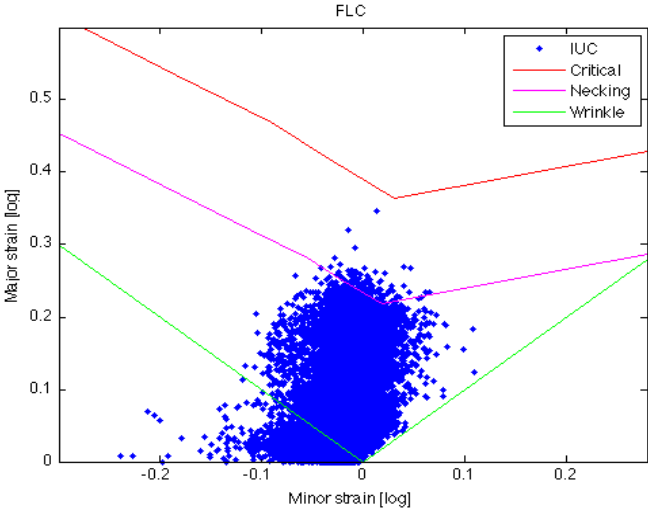


Figure 8.11. FLD based on the middle surface

8.2 Simulation

The goal of the simulation was to get result that could match the experimented values and because of this the result that was taken from the simulation was the thickness and thickness reduction of the final pressed scallop end. Moreover as how formable the current setup is, an FLD were made as well. In chapter 9 a comparison between the experiment data and the simulated data will be made. Note that it's only the 3D models result that will be presented due that the 2D result can be extracted from the 3D.

Thickness

From the start the plate was 0.3 mm thick but as the plate stretches during the forming the plate gets thinner. In figure 8.12 and 8.13 the thickness are presented, STH stands for section thickness and is a pre installed command in the post processor for shell elements.

The average thickness, figure 8.12 is calculated from the average value of the integration points. The thickness shows that in the thinnest area the plate are around 0.21 mm for both the average and actual STH.

The average thickness gives a higher value than the actual thickness of the lowest thickness. This difference is about 0.6%.

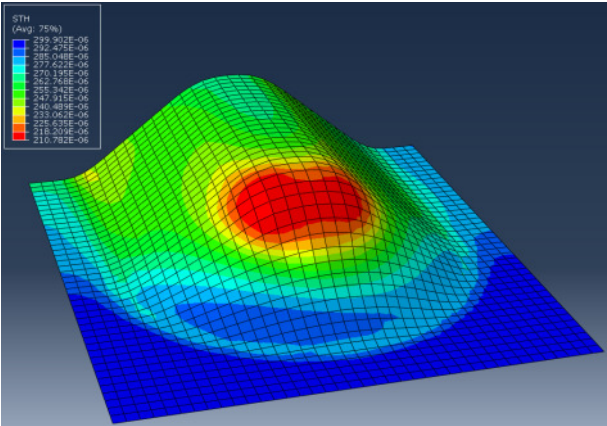


Figure 8.12. Average thickness

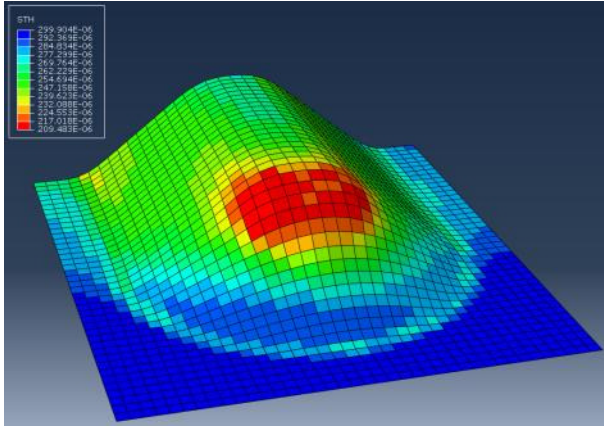


Figure 8.13. Actual thickness

Another way to control the thickness of the plate is to calculate it from the true out of plain strain. This is done by equation 8.1 as the palate where 0.3mm from the start l_0 was set to $0.3E-3m$ in equation 8.1. By calculating the thickness from the true strain the different surfaces result can be compared.

As earlier mention the middle surface is the one that FEA uses when comparing FLD, when comparing the calculated result from different surfaces it can be seen that the thickness calculated with the middle surface gives the same result as the STH function, see figure 8.14 and 8.15. This means that it is the middle surface that gives the correct result and thereby the middle surface from the FLD is the one that is going to get used for comparison.

$$l = e^{\epsilon_3} * l_0 \tag{8.1}$$

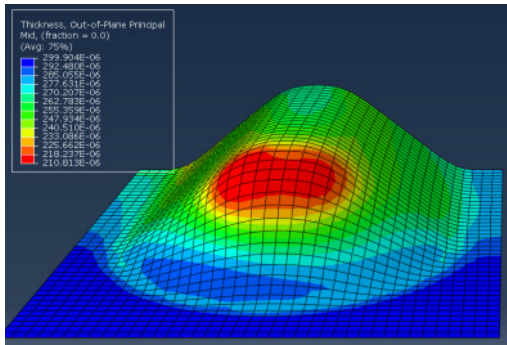


Figure 8.14. Calculated Average thickness

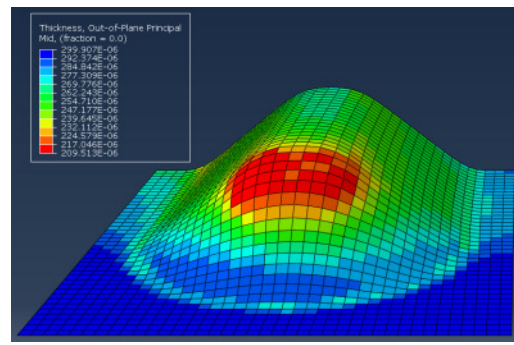


Figure 8.15. Calculated actual thickness

Thickness reduction

The thickness reduction is calculated by inserting the equation 8.2 into Abaqus. The input parameter STH are explained above and this is divided by the plates starting thickness l_0 that once again was set to $0.3E-3m$, the result from this can be seen in figure 8.16 and 8.17.

From figure 8.16 and 8.17 it can be seen that the thickness is around 30% (the average thickness are 29.7% and the actual thickness is 30.2%).

$$Th\ Reduction\ (\%) = \left(1 - \frac{STH}{l_0}\right) * 100 \quad (8.2)$$

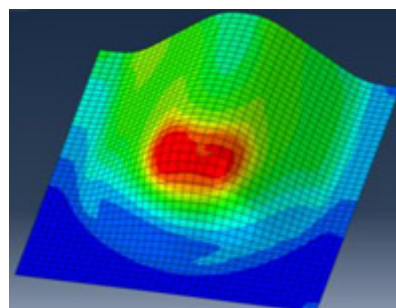


Figure 8.16. Average thickness reduction

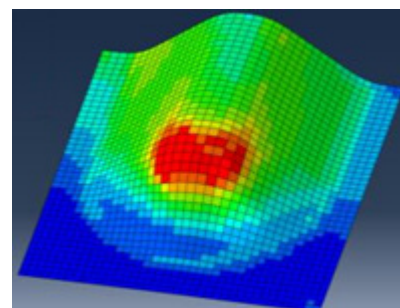


Figure 8.17. Actual thickness reduction

Forming limit diagram

Another interesting result are the forming limit diagram as explained in previous chapter a new script were made to calculate this. This is however is depending on which plane the major and minor strain are taken on, normally the mid plane are used for FEA and therefore all result presented for this simulation are based on the mid plane, once again the more interested reader may consult appendix 2.

The script includes both a fringe plot and a FLD graph, see figure 8.18 and 8.19. A way to ensure that this were correct calculated it were compared to the already built in routine FLDCRT, As the only curve that is exceed are the necking curve this curve were used for the FLDCRT function.

For this diagram every point represents an element however this diagram can't tell which element

belongs to which point. Just by looking at the diagram itself can only tell what risk there is for the geometry in question not where these problems areas are. This is the reason why the script was needed to show where the problem areas are. As can be seen in the figure 8.19 and 8.20 are in the same spots and it seems to match.

The areas where the figure 8.19 and 8.20 shows that the necking may occur are the same area where this problem has been expected to be i.e. in the upper radius for the scallop end.

In chapter 7 the large deformation of the elements were discussed and it was mention that this is a reason of large strain and as the FLD is built upon the major and minor strain it can be shown in figure 8.17 and 8.18 that there are an increase in the FLD in the same area.

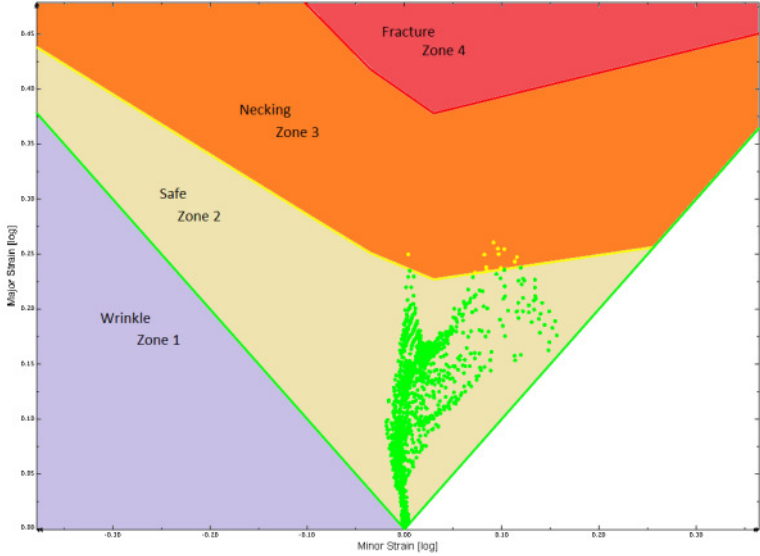
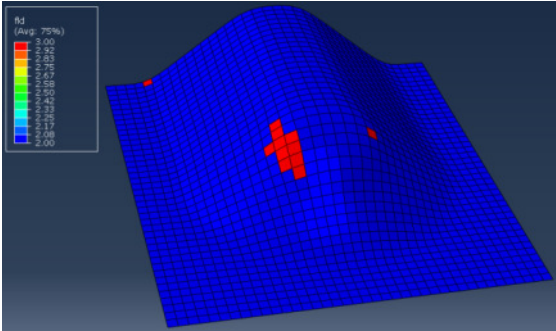
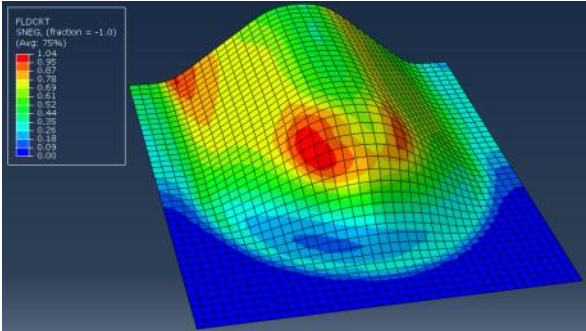


Figure 8.18. FLD based on the middle surface for the simulation



Figur 8.19. "Home made" FLDCT



Figur 8.20. Pre instal FLDCT

Chapter 9

Comparison

The result by them self might look good on paper but without comparing those, both the two experiments and the FEA may not be used. This is partly because the FEA must be confirmed or denied but also to control if the experiments are accurate enough by themselves.

In this chapter a comparison between the results from the FEA and the experiments will be carried out, as well as a comparison between the two experiments.

9.1 Metallurgy

In the last chapter the metallurgy results were presented to get an accurate result for the comparison the section cut from the FEA had to be taken on the same “spots”. How these “spots” were found are described under respectively cut.

The comparison between the FEA and the metallurgy where made by taking one element that are approximately in the same place as a end measurement from the metallurgy, then the value of every other element was taken.

The 90° cut

For the 90° cut it was a bit difficult to find where the cut was made. To get approximately where the cut where made. A measurement of the picture were taken and at the same time a reference measurement where taken, then the distance from the scallop end to the cut was calculated and a section cut in the FEA scallop were made, see figure 9.1.

This section cut is in the middle of two elements which meant that the values from both elements were need. The average of this values where used, the arrows in figure 9.1 shows which elements that were used for this comparison.

This average value where compared to the result from metallurgy in 90°, this can be seen in figure 9.2. Where the green boxes are the values from the FEA and the white boxes are from the metallurgy measurements. There is a large difference between these values but, to make it easier to compare the difference in percentage are shown in figure 9.3. The largest difference of 23% is close to that area where’s the experience tells the highest thinning should be if this cut is taken close to the scallop end as earlier discussed. But in the other region it seems to be comparable.

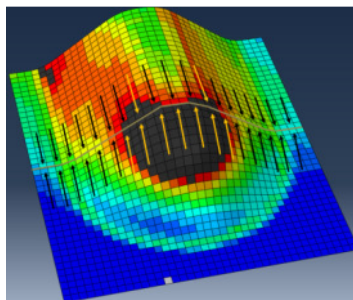


Figure 9.1. The 90° cuts position in the FEA



Figure 9.2. Comparison of the 90° cut for the thickness between metallurgy and FEA in μm

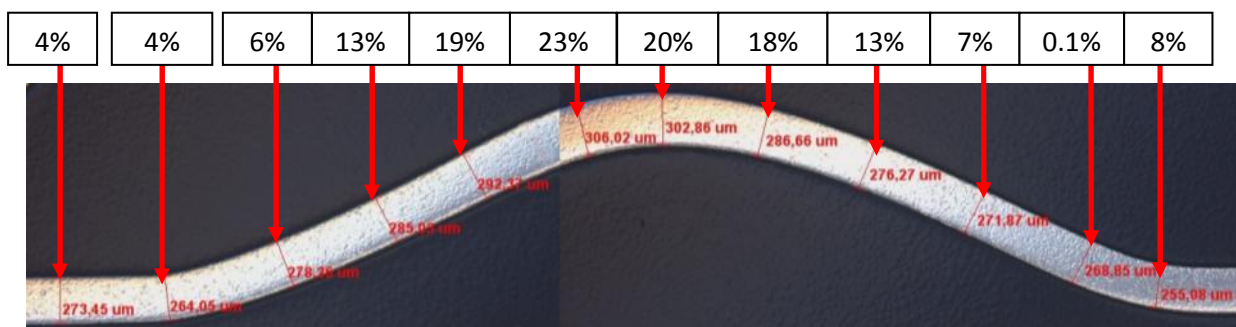


Figure 9.3. Difference in percent between the FEA and metallurgy for the 90° cut

The 0° cut

The 0° cut where pretty simple to get in the same area, as it was cut in the middle of the scallop. Assuming that the cut were made exactly in the middle the section cut for the FEA would be in the middle of the element shown in figure 9.4 once again the arrows shows which elements that values were taken from. As this section is in the middle of an element there is no need to get any extra data from adjoining elements. Just as before these values are compared to those taken from metallurgy, which is shown in figure 9.5. The green boxes are the simulated value and the white boxes are from the metallurgy. Just as for the 90° cut the percentage difference were calculated and is shown in figure 9.6. The largest difference between the FEA value and the measured value from the metallurgy is in the upper region, where the FEA shows the largest thickness reduction. But in the other regions it's not that far off.

This far it can't be confirm if this is because the source of error for the metallurgy or this is an error in the FEA or maybe both.

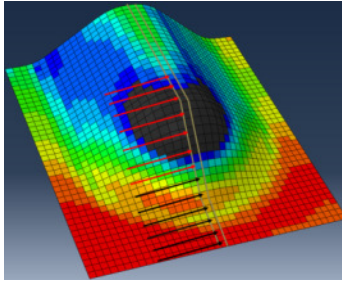


Figure 9.4. The 0° cuts position in the FEA

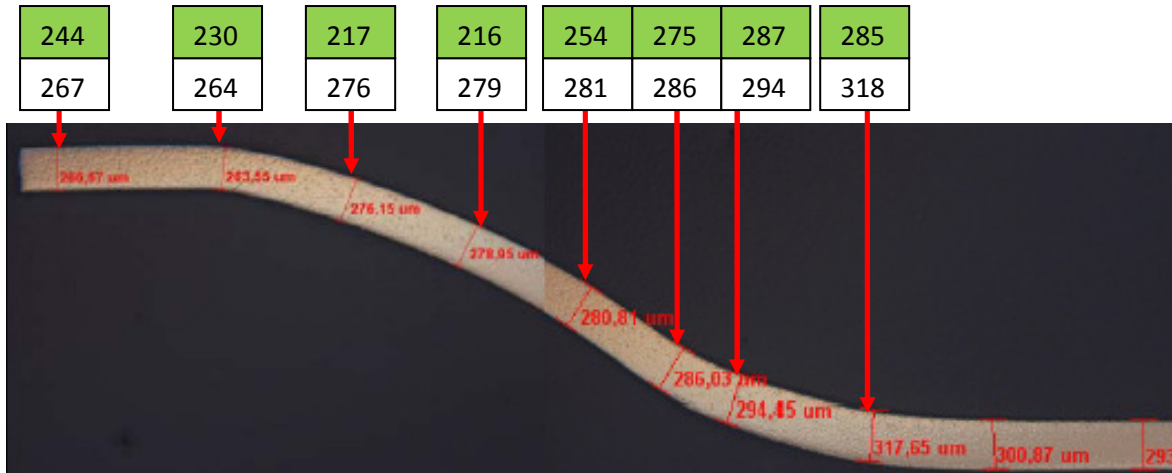


Figure 9.5. Comparison of the 0° cut for the thickness between metallurgy and FEA in μm

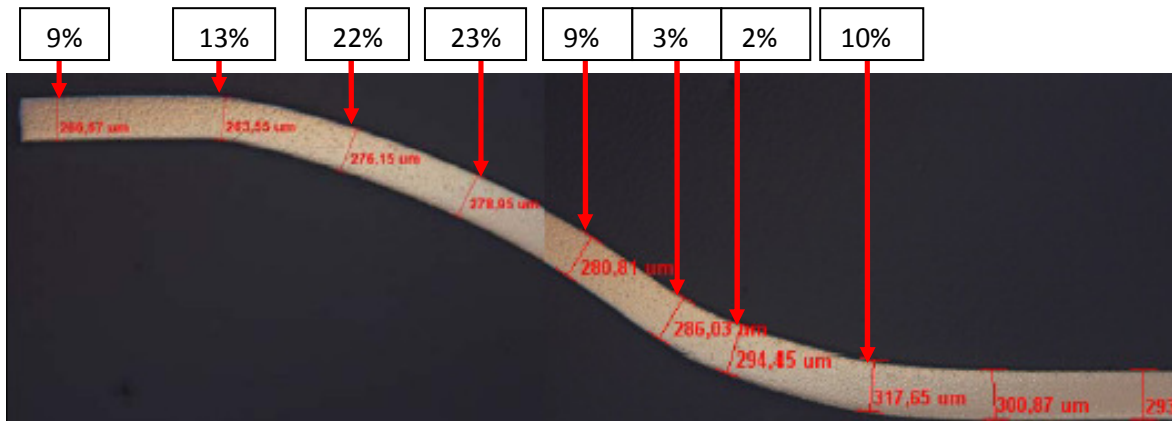


Figure 9.6. Difference in percent between the FEA and metallurgy for the 0° cut

9.2 Forming limit curve/diagram

The comparison between the FLD and FEA might seem pretty straight forward. But before any comparison can be done, it must be confirmed that it is the middle surface that are going to be used. For the FLD it's evident that it's the middle surface due to that this is what the FEA scripted FLD were calculated on. This comparison is also a good way to control that the two experiments results match each other.

Thickness reduction

In the result in chapter 8 it was shown in the simulated values that the middle surface gives the same value as the thickness and in this case STH, which confirms that it's the middle surface that is going to be used for the thickness reduction.

The percentage for the middle surface and top surface for the FLD are taken from the approximately center of the scallop end, this can be a bit hard to see and the values might differ not be 100% accurate. The FLD values are taken from figure 9.7 and 9.8 which is an enlargement of the scallop end. Figure 9.9 shows the comparison between this three, the brown boxes are from the FLD where the darker brown boxes is the middle surface furthermore the light brown boxes is for the top surface and white boxes are from metallurgy.

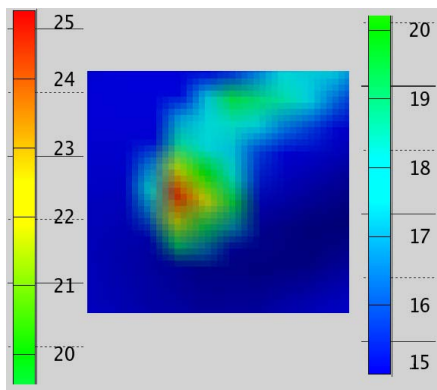


Figure 9.7. Thickness reduction of the scallop end for the top surface

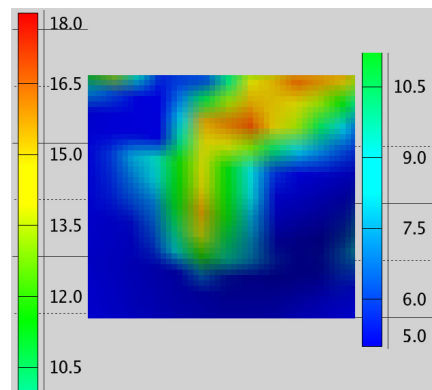


Figure 9.8. Thickness reduction of the scallop end for the middle surface

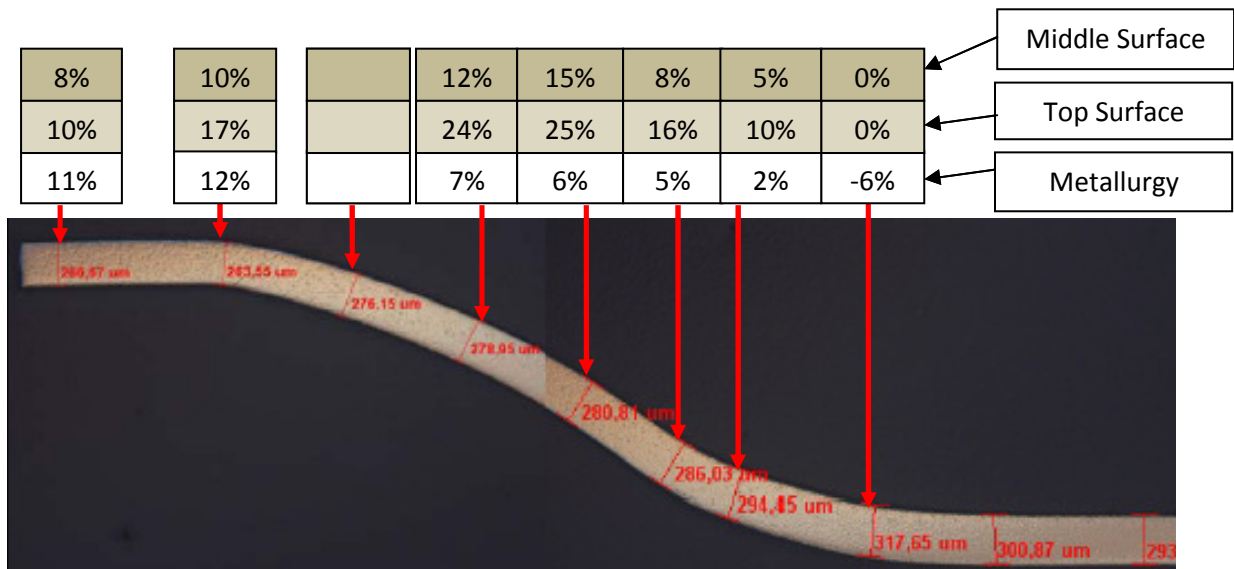


Figure 9.9. Comparison between FLD and metallurgy

Note this percent is referring to the original thickness not to the FEA values as for the metallurgy above i.e. assuming that the original thickness was 0.3mm.

The top surface (light brown boxes) is as earlier mention higher and are not direct comparable to the metallurgy.

Furthermore when moving the cut a bit more the thickness reduction percent for the FLD gets lower and by this the value gets more like the result from the metallurgy.

There by the conclusion can be made that the middle surface and the metallurgy are good enough to use as a correct thickness reduction.

When comparing the FEA thickness reduction, see figure 9.10- 9.12. It can be seen that it seems to be comparable depending on which area that is compared. To make it easier the scallop end has been divided into 3 regions: bottom, middle and top. Where the bottom region is the one that is closes to the lower tool and the top region is the top surface on the scallop end i.e. closes to the upper tool. In the area were the most thickness reduction can be seen the FEA value is greater than the one from the FLD.

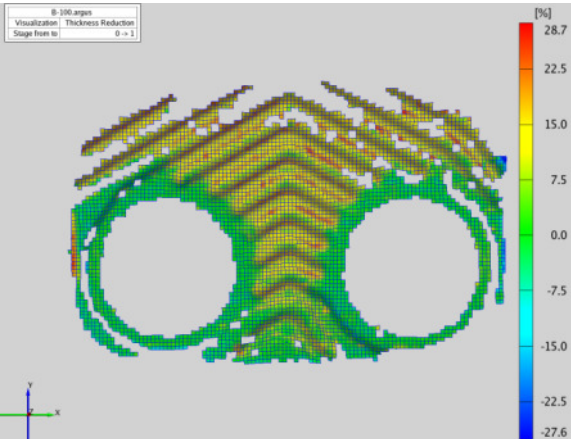


Figure 9.10. Original legend for the experimental middle surface

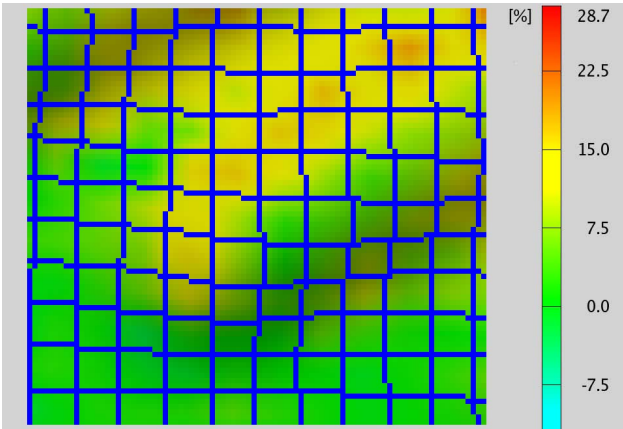


Figure 9.11. Scallop end with the original legend

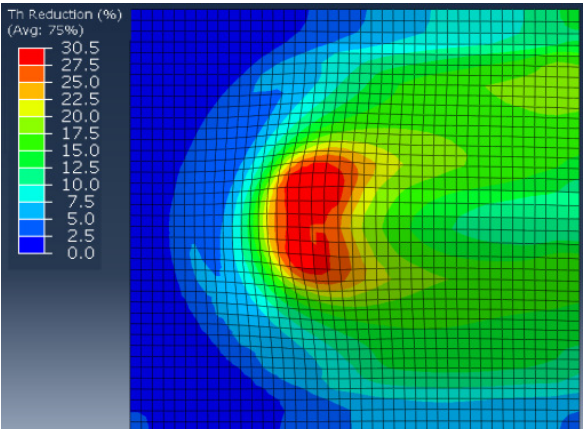


Figure 9.12. Thickness reduction calculated from the FEA

In the bottom area there is a thickness reduction around 0-8% in both the FEA and in FLD model. In the middle area (except the dark red area in the simulated model) the value is around 10-22.5% but the difference is a bit larger between the models. On the top of the scallop the thickness reduction is between 5-10% in both models.

However the thickness reduction spans in these areas are quite larger. The legend was refined for both the FLD model and the FEA model to make these spans smaller and to control if these models are comparable or not. In figure 9.13-9.15 a comparison between the same scallop end as above is made but with a more detailed legend.

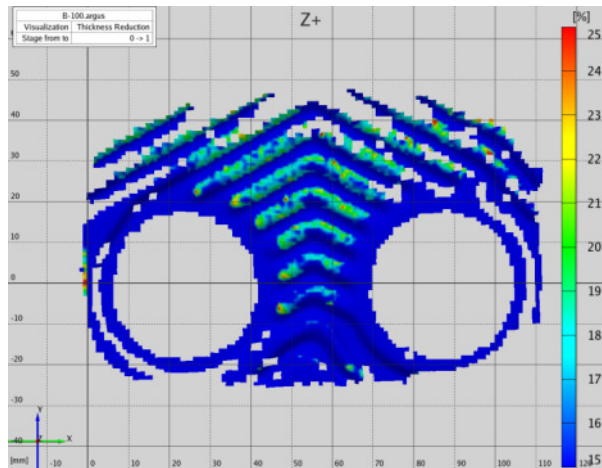


Figure 9.13. Refinement of the legend for the experimental middle surface

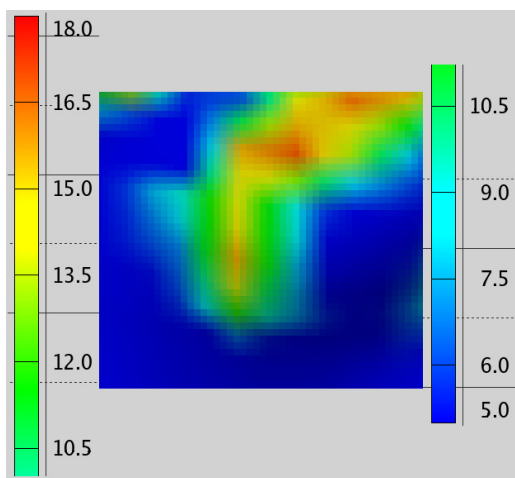


Figure 9.14. Scallop end with refined legend

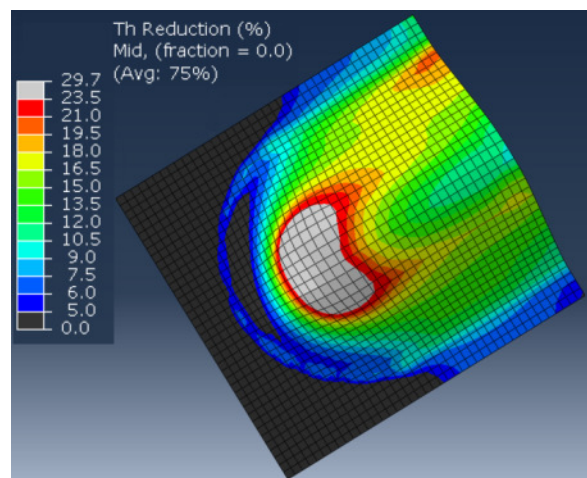


Figure 9.15. Refined legend for the FEA calculated thickness reduction

The lower area is still the same as for the original legend i.e. between 0-8% for both models. As the biggest span was in the middle area it is expected that the largest difference are in this region. On the side it can be seen that thickness reductions location area adds up with models and are between 12-18% once again the area that shows the largest thickness area are in the middle, see grey area in figure 9.15.

The top region of the scallop end is shows a little bit more difference as the FLD shows the same value (0-7.5%) but the simulation gives a larger thickness reduction of 7.5-13.5%

In section 9.1 the comparison between the metallurgy and FEA was done for certain points along the scallop end. Earlier in this section the value from the FLD for the same point were extracted. In figure 9.16 the values from this extraction are compared, the green boxes are the FEA values, the brown boxes are from FLD and the white are from metallurgy.

The FEA values are taken from figure 9.16 and are probed for the same elements as for the comparison to the metallurgy above. It can be seen that the values for the simulation from the middle of the scallop end to the lower end are pretty similar for the FLD measurements. This is the same result as the earlier comparison showed.

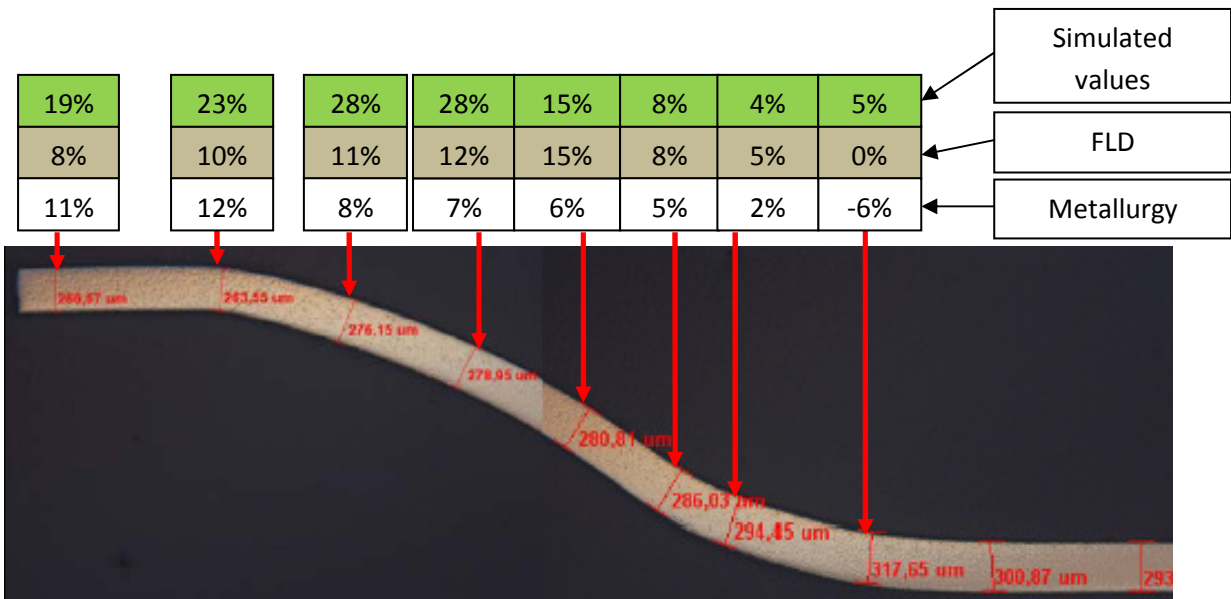


Figure 9.16. Comparison of the thickness reduction between the simulated value and the FLD a long with the metallurgy

When inserting these values into a diagram the tendencies between the three methods are more foreseeable, see figure 9.17. As already noticed the FEA are a bit more aggressive but overall the tendencies are similar.

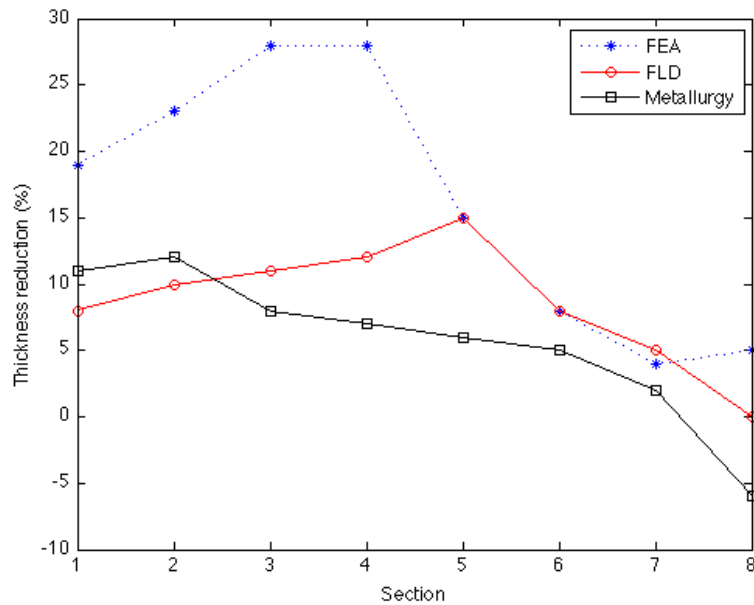


Figure 9.17 Diagram of the thickness reduction

Forming limit diagram

The comparison with the FLD is done only for the scallop end and as discussed in the last chapter the material thinning where shown for a larger area than the one simulated. However if the FEA values are in the same area it can be seen that they are comparable and as can be seen from figure 9.10 – 9.15 this is in fact the case. Figure 9.18 shows the results from the middle surface.

Note that Abaqus uses about 5 times more control points than IUC's physical measurements and because of this there a higher resolution that can describe why some of the points are outside the measurements done by IUC. This together with the source of error for FLD can explain the variation between these two.

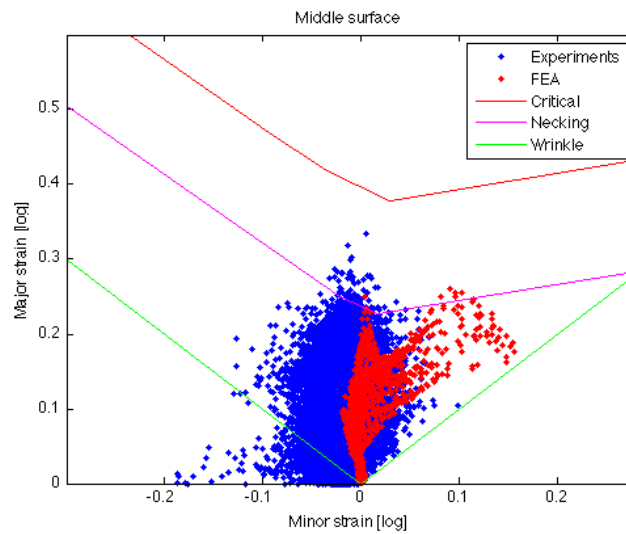


Figure 9.18. FLD comparison between experiment and FEA

Chapter 10

Discussion and future work

In this chapter the conclusion and the reliability of the result will be discussed. Further on the impact of this thesis and ideas on how SWEP can carry on with this thesis as a starting point for future work.

10.1 Conclusion

The result and comparison showed that the two experiments were comparable and gave a final material thickness of about 0.26 mm for this deposition.

It has also been shown that there were a large difference between to experiments and FEA in one region, but overall they gave the same results.

Experiments

It was shown that both of these experiments are useable on their own and can be used separately as they give more or less the same result within the source of error. However both of these are destructive testing i.e. they must be carried out on a channel plate that then can't be used to build a BPHE.

Both methods have benefits and drawbacks that make them more or less use full for the purpose they intended for.

The FLD gives more information as it both covers a larger area and gives more data but takes longer time and is expensive.

While the metallurgy can be made on site and gives a fast result but gives a limited data.

FEA

The reason on why the FEA showed more material thinning in one region might depend on the boundary condition that was used. One big issue is that this FEA could be any scallop end as the area that is simulated is too small to take any specific boundary into a count. Nevertheless the simulation is just a starting phase for future work and gives a good approximation for the thickness over all and is a good base for future work.

10.2 Reliability of the experiments

There were shown that the simulation were more accurate to the FLD measurements over the entire surface, but are this correct or just a coincident that this are similar? Both the metallurgy and the FLD were done on one channel plate, to control if these values are correct more test would have been needed both for the FLD and metallurgy. Because of lack of time and expenses this was left for future work. The sources of error are explained in appendix 2 and appendix 3 for the FLC/FLD and the metallurgy respectively. The impacts of these sources of errors are discussed below.

Metallurgy

There are quite a few sources of errors from the metallurgy which can affect the outcome for the result and jeopardizes the reliability. With more investigation and more measurements this can be overlooked for and reduces giving a more accurate result as earlier mention.

Forming limit curve/diagram

This is a new method for SWEP and may need some work to fully understand and fine tune for SWEP's products, especially the forming limit curves (FLC) as for this thesis these were taken from what Volvo and IUC have specified for their products. As mentioned before the result from the FLD consist with the FEA and from the sources of error it looks a bit more reliable than the metallurgy.

10.3 Future work

This is as earlier mentioned a stating phase for this type of work at SWEP and the future work is endless. The future work that can be done is both reading the topic of this thesis and work that this thesis can be modified to do in general.

Future work on this FEA

This thesis has just scratched the surface for this type of FEA and there are allot of future work to be done to fine tune this FEA and the experiments for example:

- Expand the geometry
- material models (Ex barlat)
- Antistrophe friction
- Tensile test machine
- Adapted the FLC
- Springback

General future work

When and if the FEA is considered good enough, it can be used to control and investigate future works to name a few:

- Lubrication
- Heated raw plates
- Press settings
- Thinner material
- New scallop design
- Narrowing of the MQS and material testing

References

Books

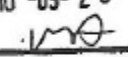

- [1] Kalpakjian S, Schmid R.S. *Manufacturing Engineering and Technology* (2006)
- [2] Ahadi A. *Continuum Mechanics*, rapport, Avdelningen för mekanik, Lund Universitet (2011)
ISRN LUTFD2/TFME-11/1005-SE(1-152).
- [3] Ottosen N.S., Ristinmaa M. *The Mechanics of Constitutive Modeling* (2005)
- [4] Ottosen N.S., Petersson H. *Introduction to the Finite Element Method* (1992).
- [5] Krenk S. *Non-linear Modeling and Analysis of Solids and Structures* (2009)
- [6] Banabic D. *Sheet Metal Forming Processes - Constitutive Modeling and Numerical Simulation* (2009)
- [7] Abaqus documentation reference, Vol 6.10 (2010)
- [8] Ottosen N.S, Ristinmaa M, Ljung C. *Hållfasthetslära* (2007)

Articles

- [A1] Dynamic Analysis by Integration .
- [A2] Investigation of anisotropy problems in sheet metal forming using finite element method.
- [A3] Determination of the plastic anisotropy r in sheet metal using automatic tensile test equipment
- [A4] Global mode hourglassing control
- [A5] Sheet metal forming analyses with an emphasis on the springback deformation

Appendix 1

Hersteller / Manufacturer's works / Usine productrice		Art der Prüfbescheinigung / Type of inspection document / Type du document		Bescheinigungs-Nr. / 30.11.2010 Document number / Numéro de document 1000256229 /						
SWEP INTERNATIONAL AB Bävergatan 9 SE-26122 LANDSKRONA		ABNAHMEPRUEFZEUGNIS INSPECTION CERTIFICATE CERTIFICAT DE RECEPTION nach / according to / suivant EN 10204-3.1		Seite / Page / Page: 1 / 1						
		Besteller/Empfänger / Customer/Consignee / Acheteur/Destinataire SWEP INTERNATIONAL AB, LANDSKRONA		Kundenbestell-Nr. / Customer's order number / Numéro de la commande du client PO						
		Webauftrags-Nr. / Manufacturer's work order no. / N° de la commande de l'usine productrice		Lieferanzeige Nr. / Delivery Note No. / Avis d'expédition n° 87257855 / 010 203607001						
Ezeugnis / Product / Produit BAND/COIL/ROULEAU										
Lieferbedingungen / Terms of delivery / Conditions de livraison EN 10028-7 AD 2000 W2 Richtlinie 97/23/EG EN 10088-2 ASTM A 240/A 240M ASME SA 240/SA 240M Sec. II Part A Ed. 2010 MOS C000011S /17 Inkl. vereinbarter Abweich.		Stahlsorte und Gütegruppe / Steel grade and quality / Numéro de l'acier TYPE 316								
Kundenmaterial-Nr. Customer's material number N° de matière du client		Masse des Erzeugnisses (Dicke / Breite / Länge) Product dimensions (Thickness / Width / Length) Dimensions du produit (Epaisseur / Largeur / longueur)		Herstellart Manufacturing proc. Mode d'fabric.						
		0,3 mm x 125,0 mm		AOD						
Ausführung Finish Fin		IIIco/ZBB								
Paket-Nr. Packing No N° Paquets	Stückzahl No of pieces N° de pièces	M-Gewicht Actual weight Masse effective	Ident-Nr. Erzeugnis Ident. No of product Ident. N° du produit	Schmelz-Nr. Cast number N. de la coulée	Proben-Nr. Sample No. Épl. du prélèvement					
5231984	2	1267 KG	409983	519732	1002377650					
5231991	2	1267 KG	409983	519732	1002377650					
5232011	2	1367 KG	409983	519732	1002377650					
5232016	2	1367 KG	409983	519732	1002377650					
5232463	2	1370 KG	409983	519732	1002377650					
5232472	2	1370 KG	409983	519732	1002377650					
12		8008 KG								
Chemische Zusammensetzung / Chemical composition / Composition chimique										
Schmelz-Nr. Cast no.	% C	% Si	% Mn	% P	% S	% Cr	% Mo	% Ni	% N	
519732	0,028	0,54	0,90	0,034	0,0010	16,54	2,01	10,51	0,024	
Prüfart/Inspection let. Essai de contrôle Proben-Nr./Lage Sample No./Position Épl./empl. du prélèvement						QUER				
	Rp0,2%	Rp1%	Rm	A80	A2*	HV	KO			
	MPa	MPa	MPa	%	%					
1002377650	292	304	661	55,5	55,5	148	9,0			
1002378662	300	315	674	53,8	53,8	151	9,0			
Beständig gegen Interkrist.-Korros. / Resistant to intercryst. corros. / Résistant à la corros. intercryst.						EN ISO 3651-2 O.B.				
Messe-Charakteristika/Dimensions-Surface/Dimensions-Surface:						I.O.				
Verwechslungsprüfung (Beobachtungsanalyse)/Test of identity/spectrom analysis/Certificat d'identification (analyse spectrale)						I.O.				
WÄRMEBEHANDLUNG : 1050 GRAD C / LUFT										
TRAITEMENT THERMIQUE : 1050 GRAD C / AIR										
HEAT - TREATMENT : 1050 DEGREE / AIR										
Komplöße nach ASTM E 112										
REGISTRERAD				ARRIVAL DEPT						
2010-12-06				2010-12-06						
Sign. <i>[Signature]</i>				SWEP INT. AB						
Aussteller der Bescheinigung / Originator of the document / Auteur du document		Stempel des (der) Abnahmebeauftragten Receiving agent's stamp Règlement de l'agent réceptionnaire		QA						
Abnahme		Datum der Ausfertigung und Bestätigung Date of issue and validation date d'émission et validation		30.11.2010						

Herstellernr. / Manufacturer's code / Usine productrice		Art der Prüfbescheinigung / Type of inspection document / Type du document ABNAHMEPRUEFZEUGNIS INSPECTION CERTIFICATE CERTIFICAT DE RECEPTION nach / according to / suivant EN 10204-3.1		Bescheinigungsnummer / Document number 1000238158 / Seite / Page / Page: 1 / 1	
SWEP INTERNATIONAL AB Bävergatan 9 SE-26122 LANDSKRONA		Besteller/Empfänger / Customer/Consignee / Acheteur/Destataire SWEP INTERNATIONAL AB, LANDSKRONA		Kundenbestellnr. / Customer's order number / Numéro de la commande du client PO 107263	
Lieferbedingungen / Terms of delivery / Conditions de livraison EN 10028-7 AD 2000 W2 Richtlinie 97/23/EG EN 10088-2 ASTM A 240/A 240M ASME SA 240/SA 240M Sec.II Part A Ed.07 MOS 000014S /10 inM. vereinbarter Abweich.		Stahlsorte und Gütegruppe / Steel grade and quality / Marque de l'acier TYPE 316		195804006	
Kundenmaterial-Nr. Customer's material number N° de matière du client		Maße des Erzeugnisses (Dicke / Breite / Länge) Product dimensions (Thickness / Width / Length) Dimensions du produit (Epaisseur / Largeur / Longueur) 0,4 mm x 375,0 mm		Herstellert. Steinlösung spez. Mode d'élabor.	
Part.-Nr. Packing-No. N° Palette		Ist-Gewicht Actual weight Masse effective		Merk-Nr. Erzeugnis Ident. No of product Ident. N° du produit	
Stückzahl No of pieces N° de pièces		Schmelzanne. Cast number Id. de la coulée		Proben-Id. Sample Id. Echant. n°	
5205712		1536 KG		517985	
5205715		1536 KG		517985	
2		3072 KG		1002321807	
				1002321808	
Chemische Zusammensetzung / Chemical composition / Composition chimique					
Stahlnummer / Steel no.					
517985					
Profilart/Inspektionort Lot de contrôle Proben-Id./Lage Sample Id./Position Echant./emplacement					
QUER					
Rp0,2% N/mm ²					
Rp1% N/mm ²					
Rm N/mm ²					
A80 %					
A2" %					
HV					
KO					
1002321807					
287					
314					
637					
53,6					
53,6					
164					
9,0					
1002321808					
286					
309					
643					
57,4					
57,4					
166					
9,0					
Beständig gegen Inerzgas, Wasser/Resistant to intercryst. corrosion/Resistant à la corrosion intercryst.					
EN ISO 3651-2 O.B.					
Maße/Charaktere/Dimensions-Substanz/Dimensions-Surface					
I.O.					
Vergleichsprüfung (Spektralanalyse)/Test of identity (spectrum analysis)/Contrôle d'identification (analyse spectrale)					
I.O.					
WÄRMEBEHANDLUNG : 1050 GRAD C / LUFT					
TRAITEMENT THERMIQUE : 1050 DEGREE C / AIR					
HEAT - TREATMENT : 1050 DEGREE C / AIR					
Korngröße nach ASTM E 112					
REGISTRERAD					
2010-09-29					
Sign. 					
ARRIVAL DEPT					
2010-09-29					
SWEP INT. AB					
Aussteller der Bescheinigung / Originator of the document / Auteur du document		Stempel des Stab-Abnahmebeauftragten Receiving Agent's stamp Patouin de l'agent réceptionnaire			
Abnahme		Datum der Ausstellung und Bestätigung Date of issue and validation date d'emission et validation		24.09.2010	

Appendix 2

Forming limit curve (FLC)

The FLC is made from seven discs with different mid sizes, see figure 1, which were in the span from 200mm to 25mm. This disc were then painted with white paint and painted a seconded time with graphite paint, see figure 2.

To eliminate the impact of friction between the stamp and the bottom side of the disc, two layers of oil were applied as well as a PVC and Teflon disc. Starting with oil between the metal disc and the Teflon then an oil layer was applied between the Teflon and the PVC, the bottom part of the PVC was left clean (this is the part that is in contact with the punch), see figure 3 to figure 6.



Figure 1. The sizes of the test specimens



Figure 2. Painted metal disc

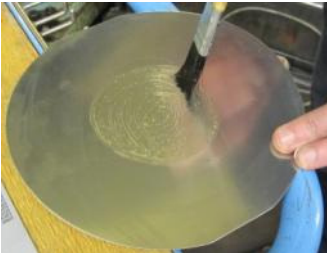


Figure 3. Step 1, Oil applied to metal disc

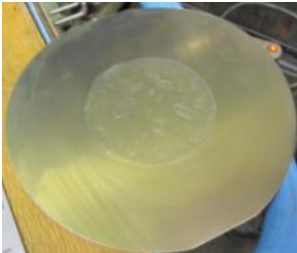


Figure 4. Step 2, Teflon disc placed on top of the oil



Figure 5. Step 3, Oil applied onto one side of the PVC



Figure 6. Final prepared test specimen

The metal discs were then pressed starting with the largest dimension, during the pressing two cameras were taking pictures of the disc with a frequency of 20 Hz, see figure 7 and 8 the press settings is presented in table 1. The computer program keeps track of the different paint dots that were made from the graphite paint, however it is important that the camera take pictures continually otherwise the program can't keep track of the random dots. This is the difference between pre etched dots that was made for measuring thinning of the material in actual BPHE plates (B80) more about this later. The reason why the paint is sprayed on instead of etched is that the resolution is grater do to the dots a smaller.

Velocity	25mm/s
Press depth	Untill it cracks
Press force	200 ton

Table 1. Press settings

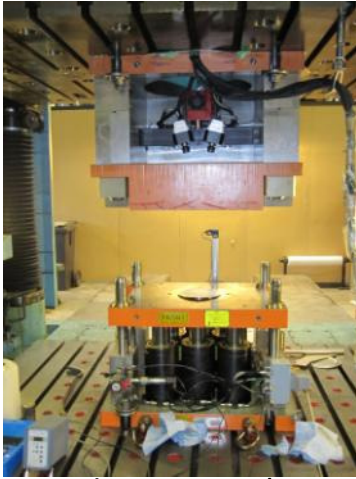


Figure 7. Press tool

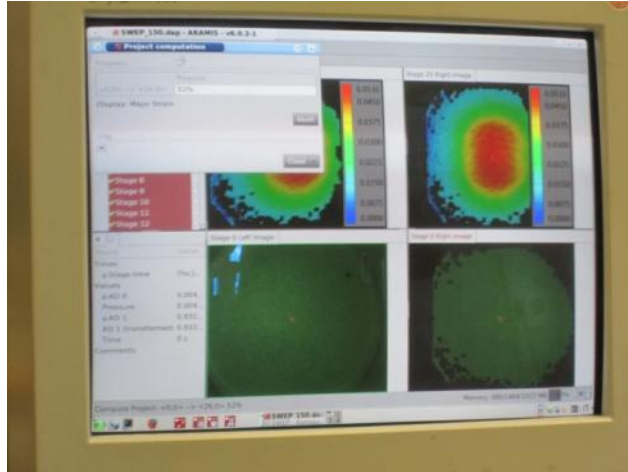


Figure 8. Analysis of the press pictures

The result of this pressing is analysed by the computer program ARAMIS (by Gom) and then inserted in to a diagram according to figure 9 and 10. Where the bigger metal discs is in the right side of the curve and farther to the left you come the smaller the mid size is.

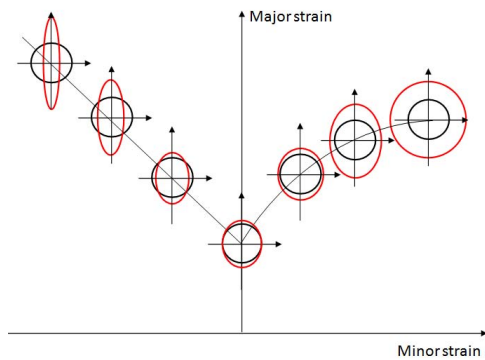


Figure 9. Strain distribution in FLC

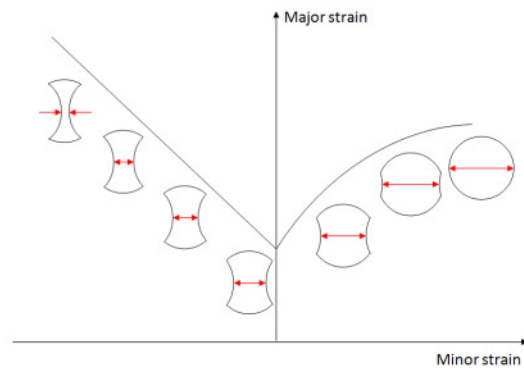


Figure 10. Metal disc sizes in the FLC

The FLC is done by taking a three close cross-sections that is orthogonal to the crack, see figure 11. These are then analysed both at the picture just before the crack and at the picture when the disc has cracked see figure 12 to figure 13.

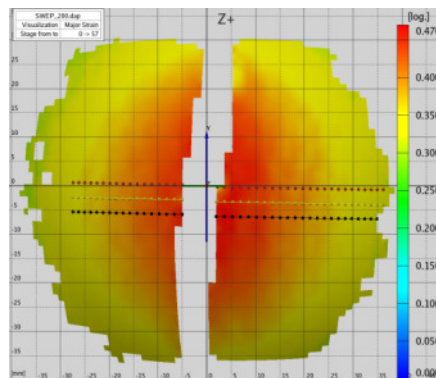


Figure 11. Cross-section

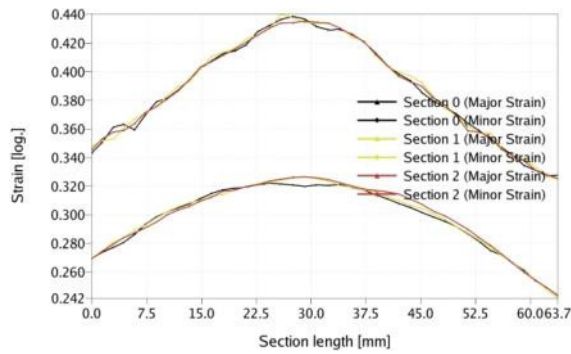


Figure 12. Cross-section for the picture before crack

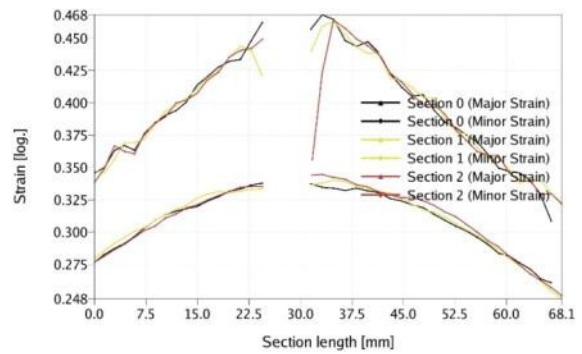


Figure 13. Cross-section for the picture after crack

As shown in picture 12 and 13 there are three curves one for each cross-section an average of the major/minor is then taken on the center of the section. From figure 12 and 13 the major/minor strain is taken. When all seven discs are analysed their major and minor strain is inserted in to a diagram that is shown in figure 14. The curve that represents the FLC is an average between the curves from the cracked and uncracked picture.

This value is for the top surface but if we recalculate the numbers to the mid surface we get a slightly different curve (note this recalculation is done by the software, see figure 15).

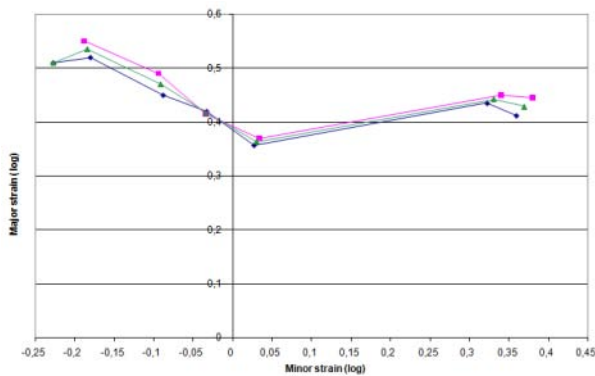


Figure 14. First FLC

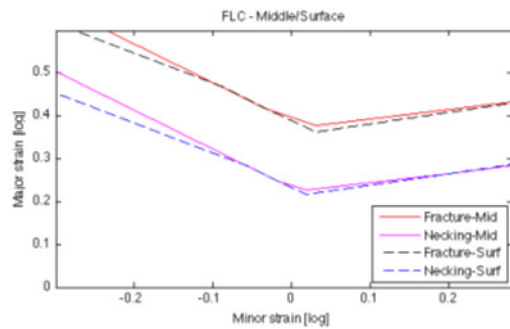


Figure 15. Top and middle surface

Due that SWEP want to see the actual forming window more curves were need, see figure 16. To get the curve for the necking the forming limit curve was offset downwards by 40% (40% is a value that Volvo and IUC has decided together where a safety margin is included). The wrinkling curve is just a curve that is pointed 45° from the axle.

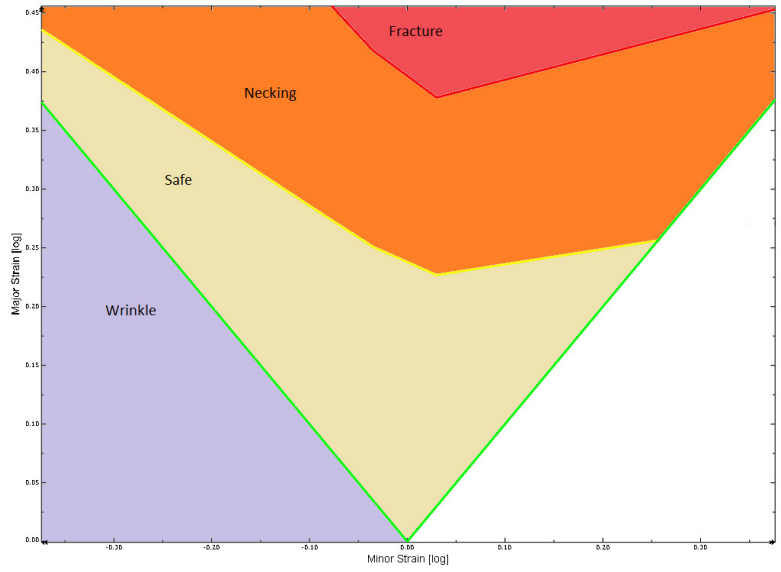


Figure 16. Complete FLC

Forming limit diagram (FLD)

A circular pattern is etched on to the raw plate with a spacing of 1 mm, see figure 17. This is done by applying the etched liquid to a media (in this case a wetex) that then is placed on a film with pre cut holes for the pattern in this case with the earlier mention 1 mm spacing both the film and the media is placed on the raw plate. This is then rolled with a copper roller, see figure 18, which make a current go throw the media and etch the pattern on to the raw plate. The raw plate is then pressed which deforms the circles, see figure 19. To analyze how the circles has deform the BPHE was placed on a rotating magnetic table in a photo cube, see figure 20.

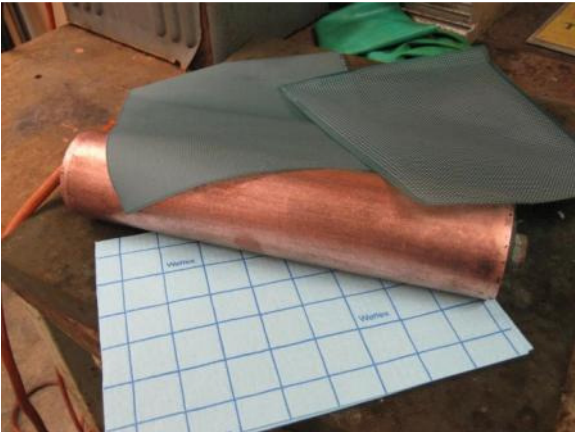


Figure 17. Etching equipment



Figure 18. etched raw plate



Figure 19. The pressed etched channel



Figure 20. Photo cube

A piece of paper was placed over the non interesting part of the BPHE to reduce unnecessary calculation time. Magnets was applied to hold the BPHE plate fixed during the picture taking and different measuring equipment were placed around the BPHE plate, see figure 21. When the part was rigid and ready photos was taken by a regular SLR (Nikon D300) in different angles, see figure 22. This was then sent into a program called ARGUS (by Gom) that analyzed the pictures by measuring the deformation of the circles.

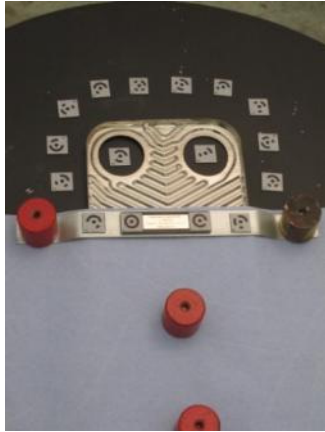


Figure 21. Fixed and cover channel plate



Figure 22. Photographing of the channel plate

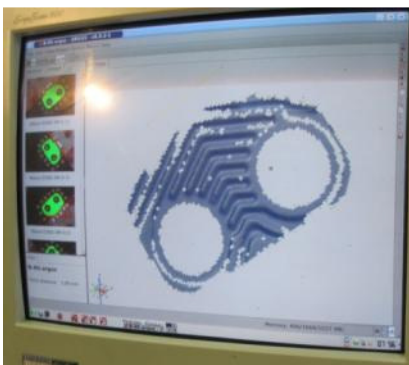


Figure 23. Geometrical analysis of the photos

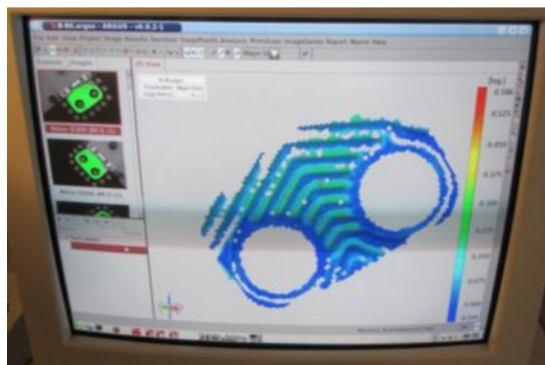


Figure 24. Extracting the major strain

The major and minor strain was calculated and put into the FLD for the material, see figure 23-24. As the volume is considered constant the thickness can be calculated through equation 1-2 Where ϵ_L and ϵ_W are the major and minor respectively. The result is presented in figure 25-28.

$$\epsilon_W + \epsilon_T + \epsilon_L = 0 \quad (1)$$

$$\epsilon_T = \ln\left(\frac{Th}{Th_0}\right) \Rightarrow Th = e^{\epsilon_T} * Th_0 = e^{-(\epsilon_W + \epsilon_L)} * Th_0 \quad (2)$$

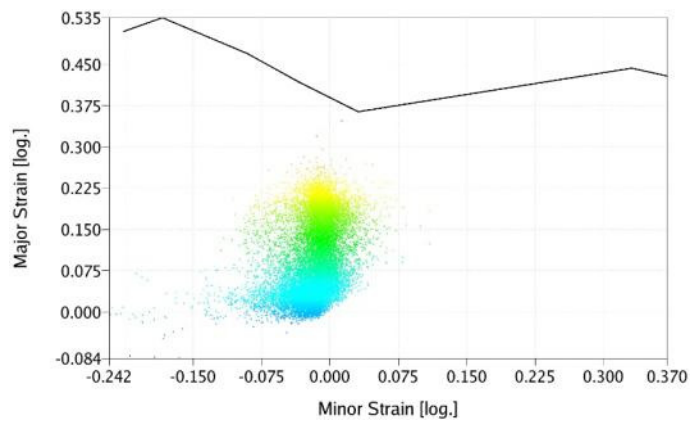


Figure 25. Forming limit diagram (FLD)

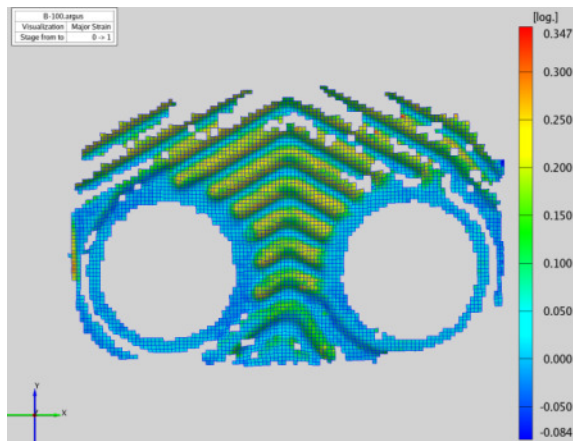


Figure 26. Major strain

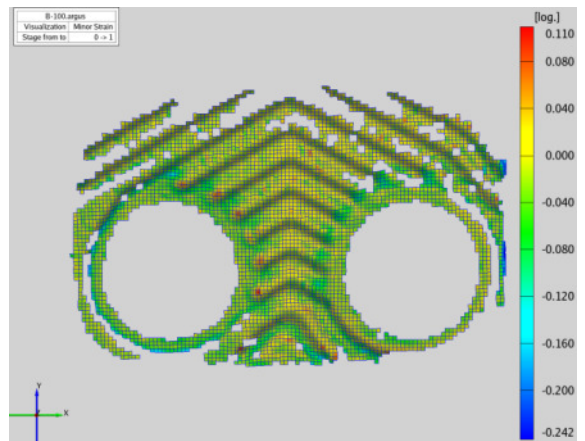


Figure 27. Minor strain

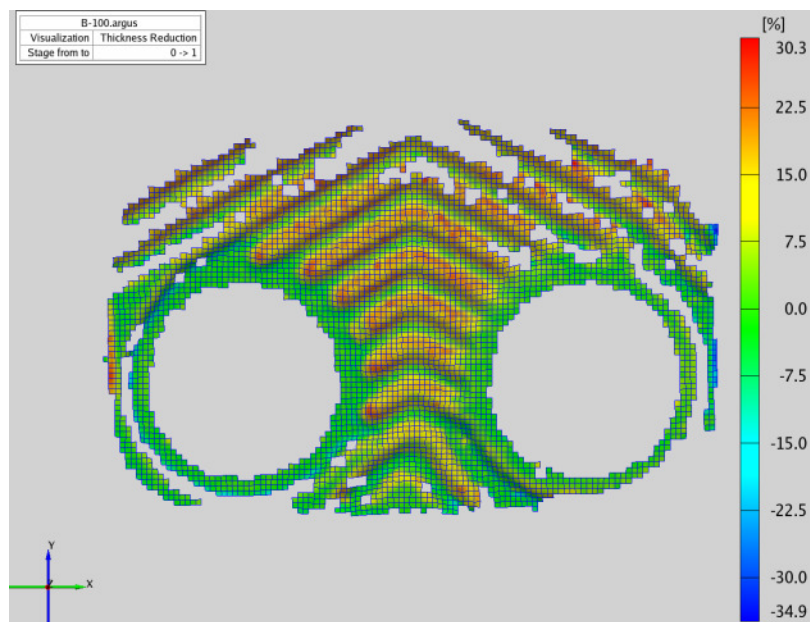


Figure 28. Thickness reduction

Source of errors

In all practical tests there are source of errors, however as this is known they are made to make a small impact as possible.

Forming limit curve (FLC)

The FLD has a number of error margins as this is the first time IUC makes an FLC with steel that is this thin (normal test a made with steel that are 0,7-1,5 mm). Because of the process is made for the thicker material the PVC maybe too thick (3mm) which make the PVC and Teflon slide to the side during the pressing, see figure (29).

Another margin of error is when the FLD is measured through ARAMIS there is a large number of steps that is up to the operators experience to determine the values, which means that the value given at the end isn't exact but approximated.

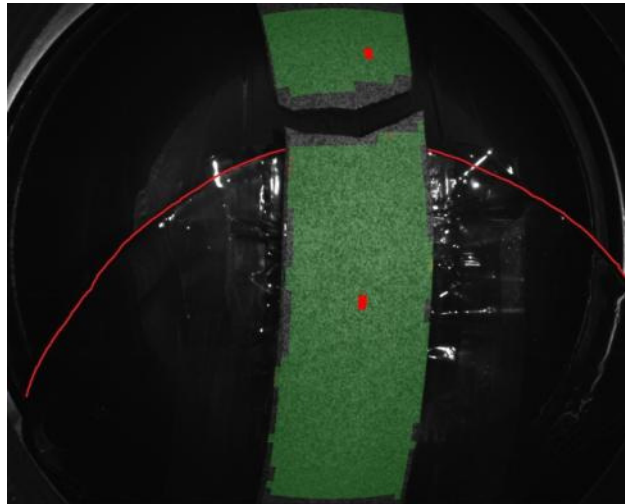


Figure 29. PVC and Teflon disc has slide to the side

Forming limit diagram (FLD)

When making a FLD on an actual product there are different source of errors. When the pattern is etched on the film that makes the pattern can be stretched out during the etching process that gives the circle a deformed look from the beginning, this source of error has been taking into count and makes about 1% of error to the process.

Appendix 3

Metallurgy

A way to physical measure the thickness of the sheet metal is to use metallurgy. The channel plate was cut in to section by using an EDM, see figure 1 and 2 which then was analyzed in SWEPS claim lab. As can be seen in figure 1-4 there was cuts taken on another scallop end as well, this was done for future investigations. For this thesis only piece 2 and 4 are of interest.



Figure 1. cut in 90°



Figure 2. Cut in 0°

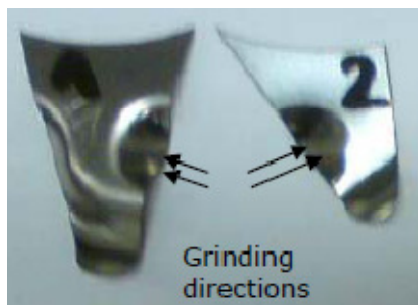


Figure 3. Cut outs in 90°

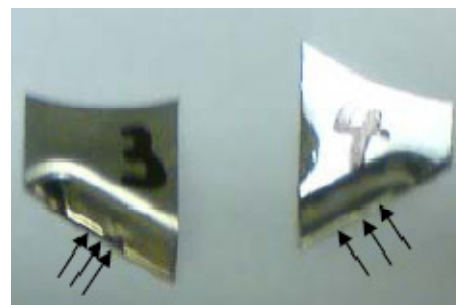


Figure 4. Cut outs in 0°

After the plate was cut the piece was molded into plastic which then was grinded, the final product can be seen in figure 5. The samples were then analyzed using a light optical microscope, see figure 6.



Figure 5. Final sample

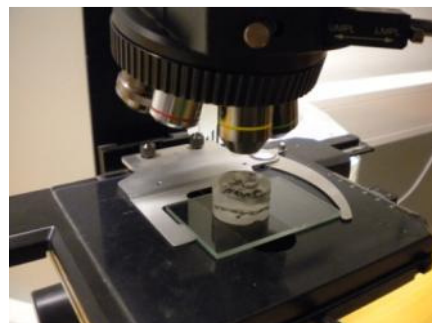


Figure 6. Analysis of the sample

Results

The result of interest for this thesis are cut number 2 and 4 because these are on the same scallop end as the FEA making them direct comparable to the FEA. The amount of material removed was not measured and consequently it is difficult to state exact position of the different polishing.

Cut number 2

The first series of result is referring to cut number 2. Table 1 summarizes the values from the different grindings and an average of the different polishing is presented as well.

Cut number 2				
Grinding	Polishing 1	Polishing 2	Polishing 3	Average
273.45	255.898	247	231	251.837
264.05	248.427	240	227	244.8693
278.29	-	-	-	278.29
285.03	276.435	255	257	268.3663
292.37	294.684	268	-	285.018
306.02	-	-	-	306.02
302.86	301.493	263	267	283.5883
286.66	275.843	249	251	265.6258
276.27	264.754	-	-	270.512
271.87	264.181	267	234	259.2628
268.85	-	-	-	268.85
255.08	246.175	253	232	246.5638

Table 1. 90° in μm

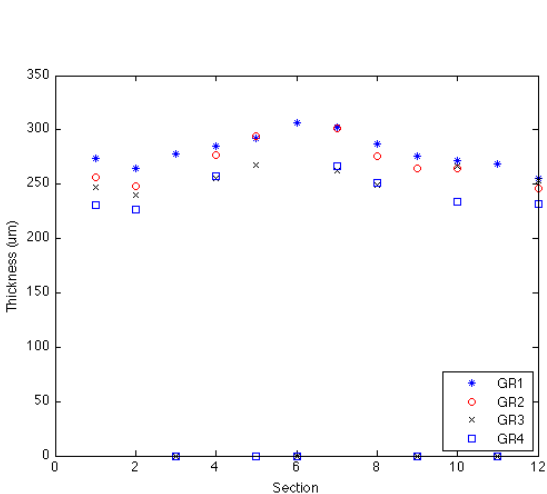


Figure 7. Grinding values

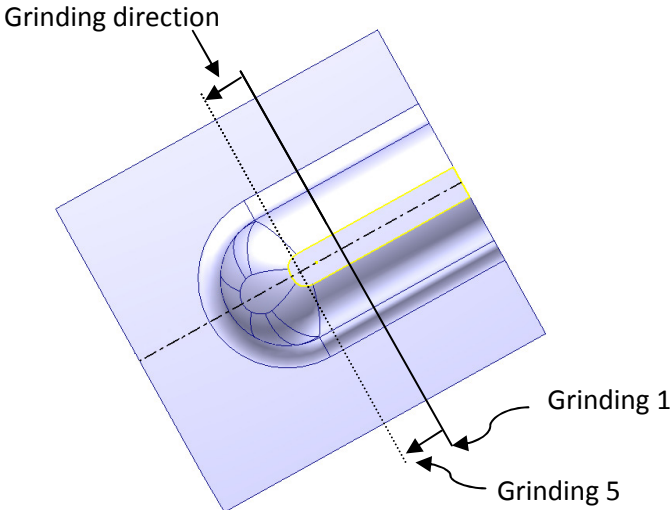


Figure 8. Grinding made in 90°

Cut number 4

Just as for the cut number two cut number four has been grinded five time and this values has been inserted into the table 2 below along with the average.

Cut number 4				
Grinding	Polishing 1	Polishing 2	Polishing 3	Average
266.67	258.459	245	223	248.2823
263.55	250.64	244	214	243.0475
276.15	270.332	-	-	273.241
278.95	-	-	-	278.95
280.81	273.246	271	246	267.764
286.03	280.648	299	314	294.9195
294.45	-	-	-	294.45
317.65	298.531	339	-	318.3937
300.87	-	-	-	300.87
293.79	293.75	339	347	318.385

Table 2. 0° in μm

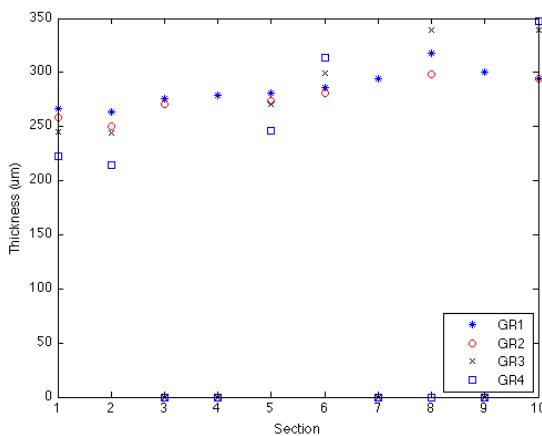


Figure 9. Grinding values

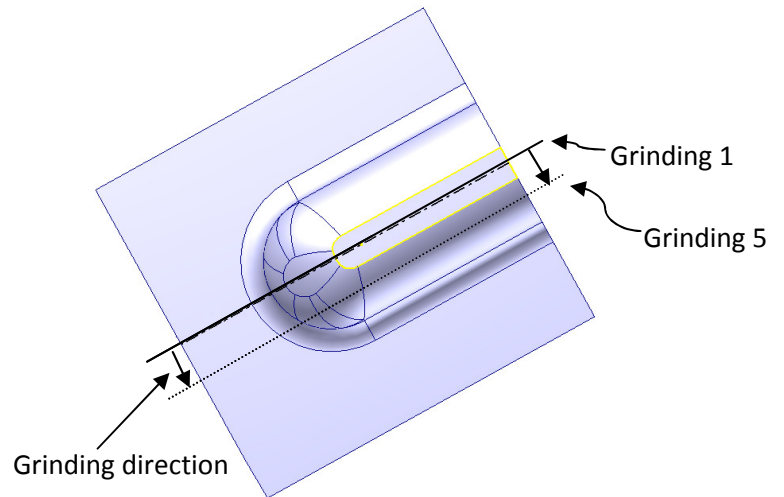


Figure 10. Grinding made in 0°

Source of error

When you need to make measuring in an exact position it is very difficult to make the cut absolutely straight in the middle, see figure 11.

When the metal is molded into the plastic, it's important but very difficult to make it absolutely straight. This will affect the measuring as the sample is grinded down the samples cross section area becomes larger, see figure 13-16. However, if the sample is tilted about 10° the error is only around 1.5 %.

When measuring its not always that it become ortogonal to the surface instead it becomes slightly skew, by this the thickness become a bit larger than the actual thickness,see figur 12.

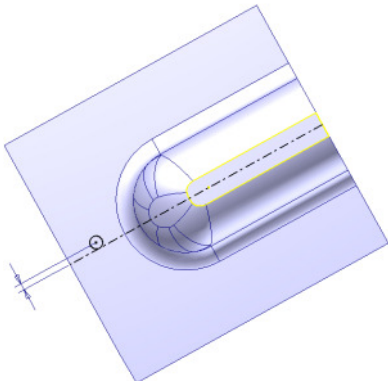


Figure 11. Cut made by EADM thread



Figure 12. Skew measurement

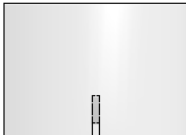
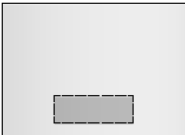


Figure 13. Untilted sample before grinding

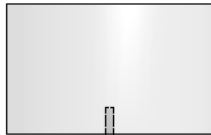
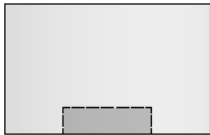


Figure 14. Untilted sample after grinding

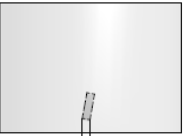
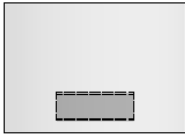


Figure 15. Tilted (10%) sample before grinding

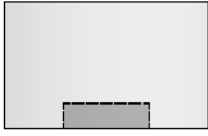
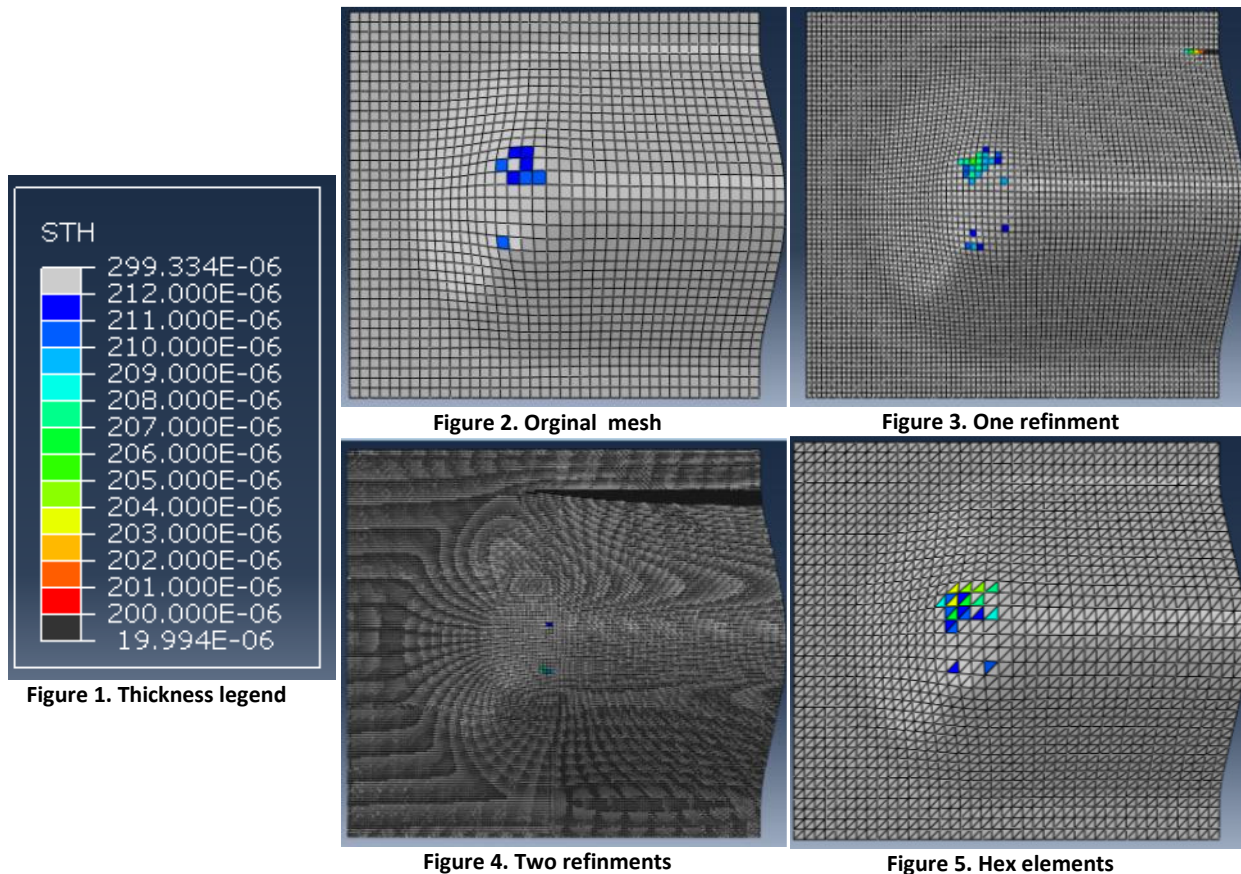


Figure 16. Tilted (10%) sample after grinding

Appendix 4

Mesh Convergence

The mesh that was used was shell elements of the types S4R and S3R. The refinements can be seen in figure 2-5. As can be seen the area are of the thinnest parts are approximately the same for the different mesh sizes.



To more information regarding the difference, the elements with the thinnest section were compared, see figure 6-9. This showed a difference of 1-3% i.e. the original mesh can be used.

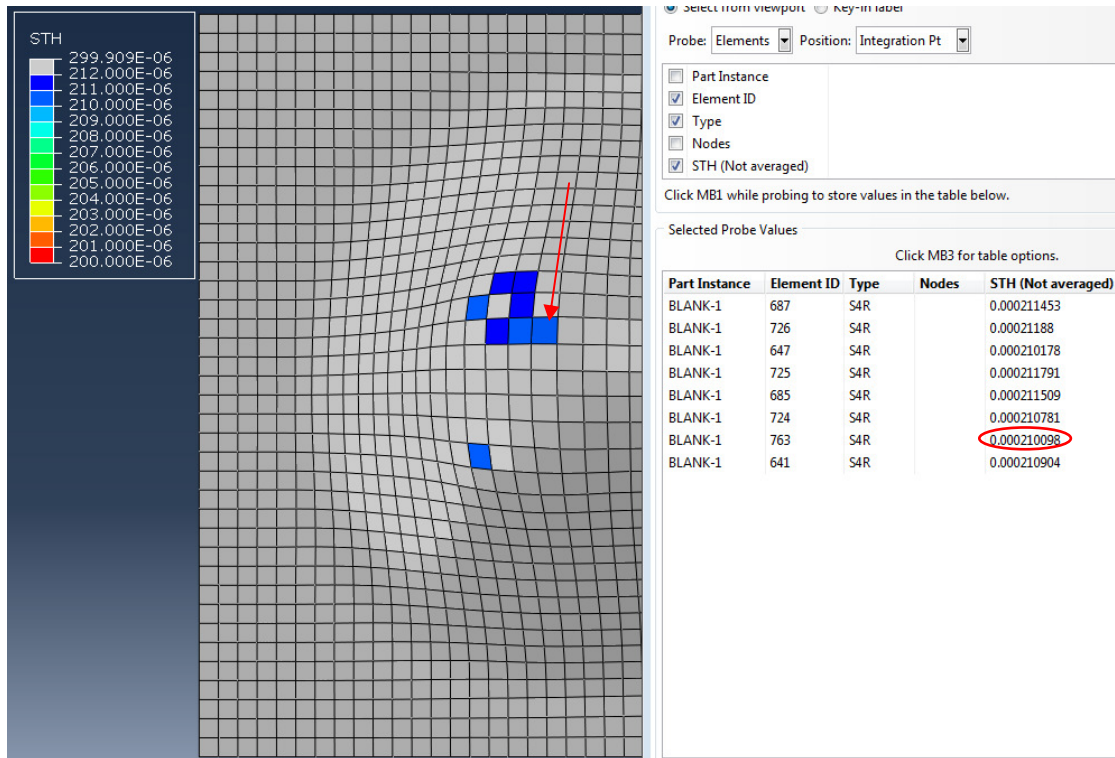


Figure 6. Original mesh

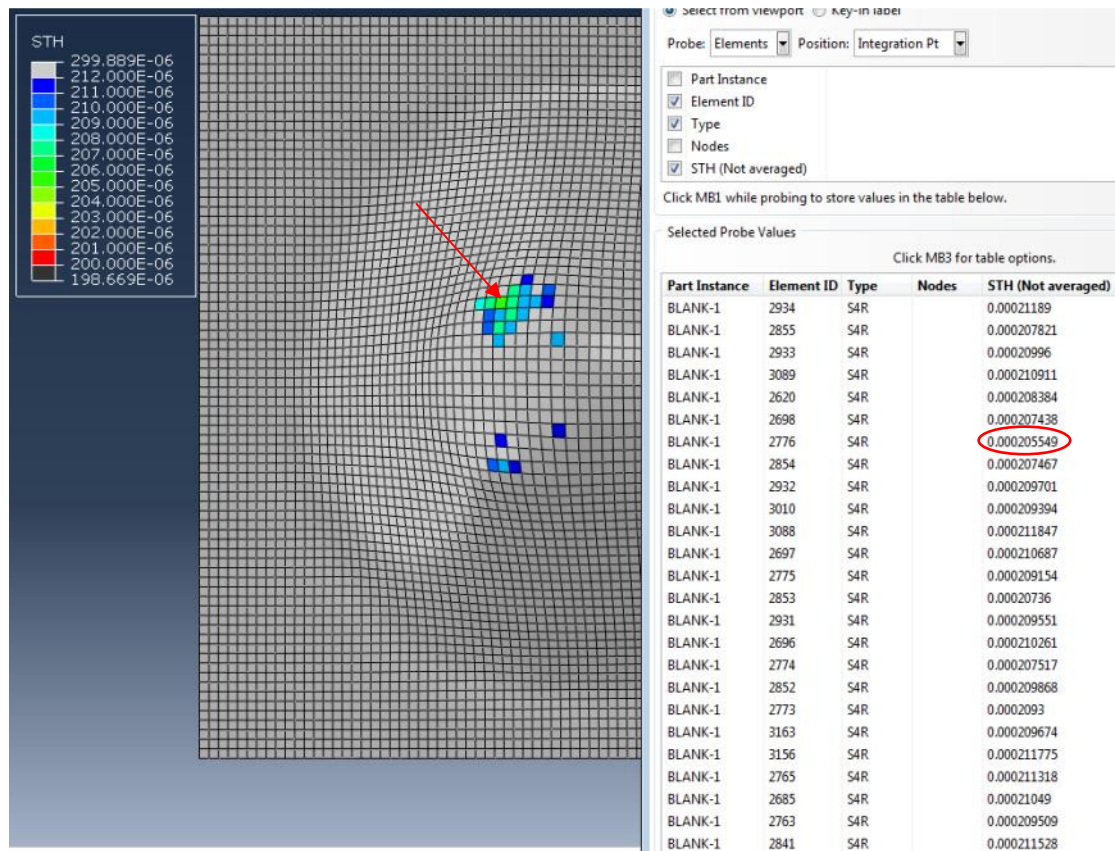


Figure 7. One refinement

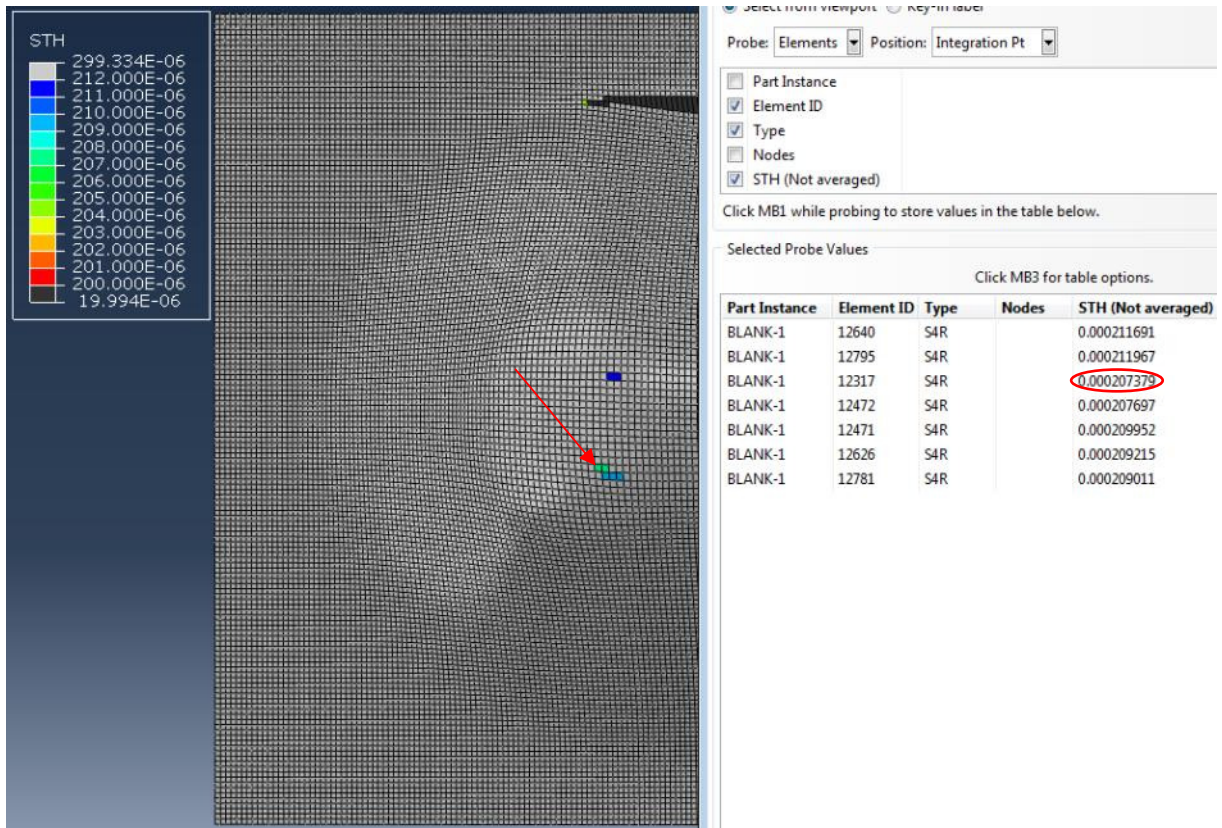


Figure 8. Two refinements

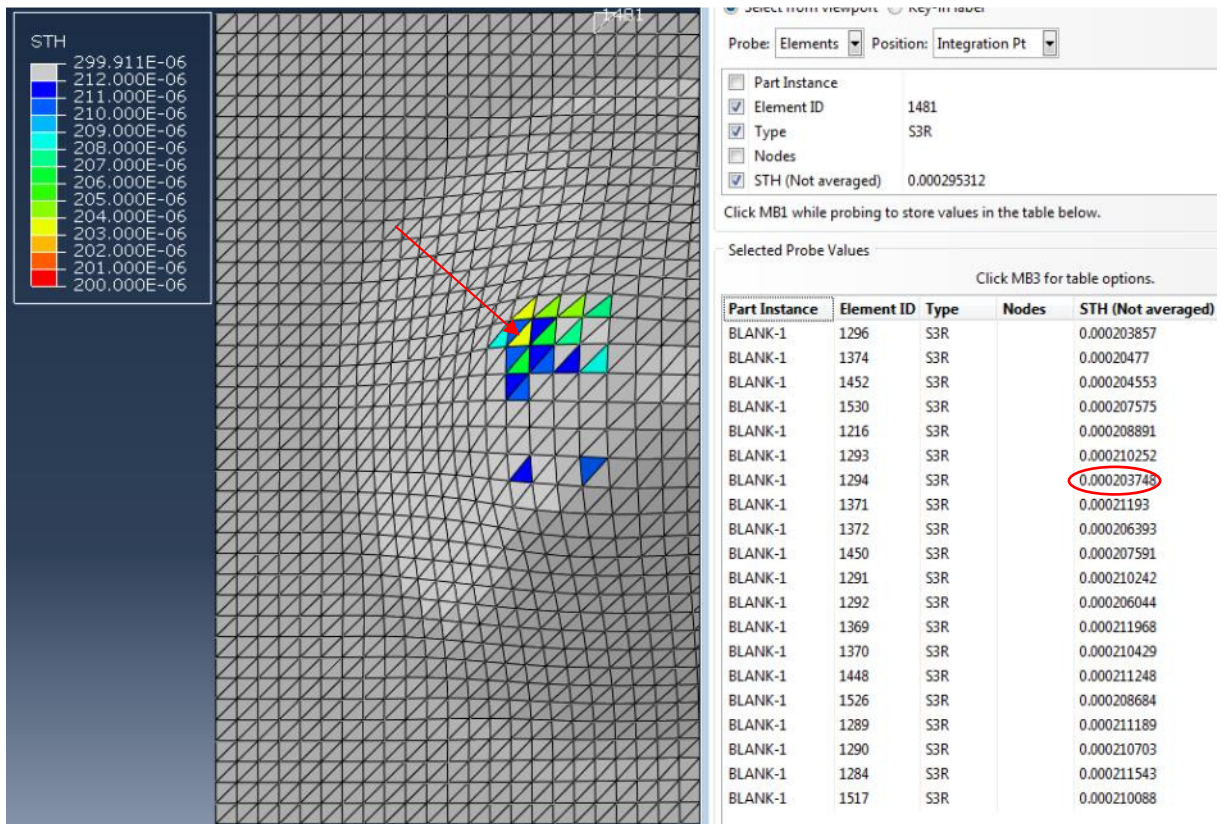


Figure 9. Hex elements

Discontinuities

The discontinuities are shown in figure 10-15. The maximum difference is about 30 μm this is quite alot but after consulting Simulia about this was not considered a problem.

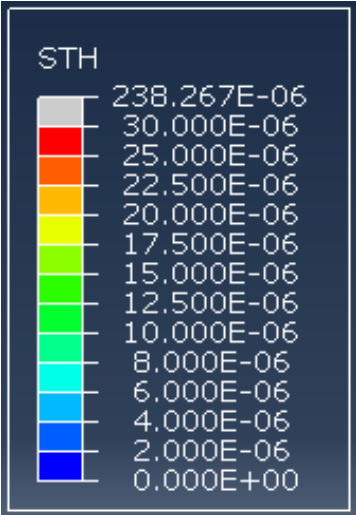


Figure 10. Discontinuities legend

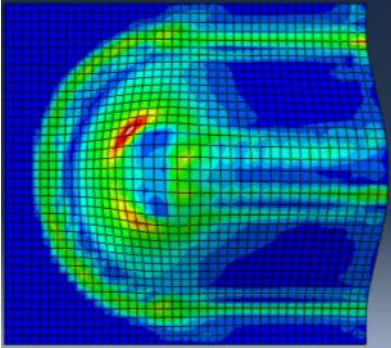


Figure 11. Original mesh

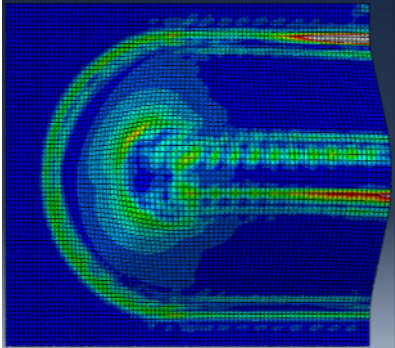


Figure 12. One refinement

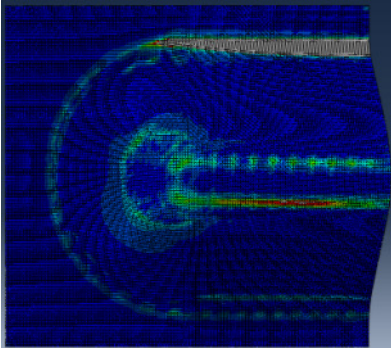


Figure 13. Two refinements

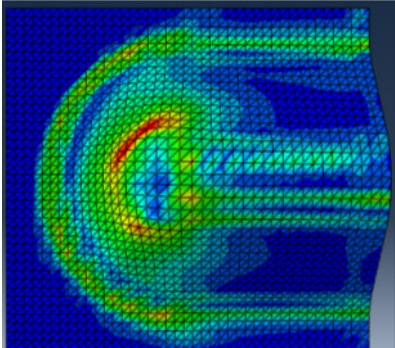


Figure 14. Hex elements